acta physica slovaca vol. 61 No. 5, 483 – 601 **October 2011**

AN INTRODUCTION TO QUANTUM OPTOMECHANICS

G. J. Milburn[1] **and M. J. Woolley**[2,3]
[1] *Centre for Engineered Quantum Systems, University of Queensland, St Lucia QLD 4072, Australia.*
[2] *Department of Physics, McGill University, Montréal, QC, Canada, H3A 2T8.*
[3] *Département de Physique, Université de Sherbrooke, Sherbrooke, QC, Canada, J1K 2R1.*

Received 5 January 2012, accepted 9 January 2012

We provide an introduction to the description of mechanical systems in the quantum regime, and provide a review of the various types of micro-scale and nano-scale optomechanical and electromechanical systems. The aim is to achieve quantum control of micromechanical and nanomechanical resonators using the electromagnetic field. Such control requires the demonstration of state preparation (in particular, cooling to the ground state), coherent control and quantum-limited measurement. These problems are discussed in turn. Some particular problems in force detection, metrology, nonlinear optomechanics and many-body optomechanics are also discussed.

DOI: 10.2478/v10155-011-0005-7

PACS: 42.50.Wk, 42.50.Lc, 42.50.-p, 85.85.+j

KEYWORDS: Quantum optomechanics, Quantum electromechanics, Nanoelectromechanical systems, Microelectromechanical Systems, Quantum optics

Contents

1 Introduction

Quantum optomechanics, and the related field of quantum electromechanics, seek to control the quantum mechanical interaction between electromagnetic radiation and bulk mechanical resonators. The subject has roots in early attempts to develop gravitational radiation detectors using the elastic deformations of large high Q mechanical resonators [1] and optical interferometers with moving end mirrors [2]. Pioneering theoretical work was performed by Braginsky [3], Caves [4] and others. The field has undergone rapid development over the last decade with the separate development of new methods for fabricating small bulk mechanical resonators of various forms; nano-scale beams coupled to microwave cavities [5], photonic-phononic crystals [6], toroidal optical micro-resonators [7], doubly clamped beams with integrated mirrors [8] and drumhead capacitors in superconducting microwave resonators [9]. A variety of optomechanical [10] and electromechanical [11,12] systems have been developed to enable the measurement and control of these mechanical elements, both fitting in to the broader picture of the study of mechanical systems in the quantum regime [13].

Classical optomechanics is an already well developed field of optical engineering and micro-electromechanical systems (MEMS) form an essential component of a great deal of high technology, from iPhones to sensors. The key new element of quantum optomechanics is the ability to prepare one or more bulk flexural modes of a mechanical resonator in a well-defined quantum state (the ground state, for example), to subsequently manipulate this state coherently, and to make quantum-limited measurements of the displacement or energy of the resonator. Typically, this is done by coupling the mechanical resonator to the electromagnetic field either at optical frequencies or at microwave frequencies. This enables both cooling of the mechanical modes of interest, and quantum-limited measurement and control of their motion. These three steps — state preparation, coherent control and quantum measurement — are required of any quantum technology [14], as depicted in Fig. 1.1. The motivation for such work ranges from fundamental tests of quantum mechanics [15] and studies of novel nonlinear and dissipative quantum physics, to extremely precise force and mass sensing [16,17,18,19,20,21,22], and even to applications in quantum information processing [23,24].

Quantum control of vibrational motion was first achieved in ion traps [25]. However, there is a key difference in the theoretical description of trapped ions and the new class of optomechanical and electromechanical systems. In the case of trapped ions, the dynamics is described entirely in terms of Schrödinger's equation for the trapped ions as the elementary mechanical units, coupled by Coulomb forces. In the case of optomechanical systems, however, the description is not given in terms of the quantum dynamics of the atomic constituents of the mechanical resonators. While this would be possible in principle, in practice it is impossible. Instead, an effective quantisation is performed on elastic vibrational modes of the bulk material. As we describe below, we are typically interested only in long-wavelength (low-energy) bulk modes of the material. The theory begins with the wave equation for elastic excitations of the bulk, and by defining a set of orthonormal modes. These are then quantised directly, very much like quantising a scalar field. The implicit assumption is that these collective degrees of freedom factor out of the other microscopic vibrational degrees of freedom (short-wavelength phonon modes, for instance), which are then included in the description as a source of dissipation and decoherence. This approach, typical of the emerging field of engineered quantum systems, has a parallel in the theory of superconducting quantum circuits where the description is not given in terms of BCS

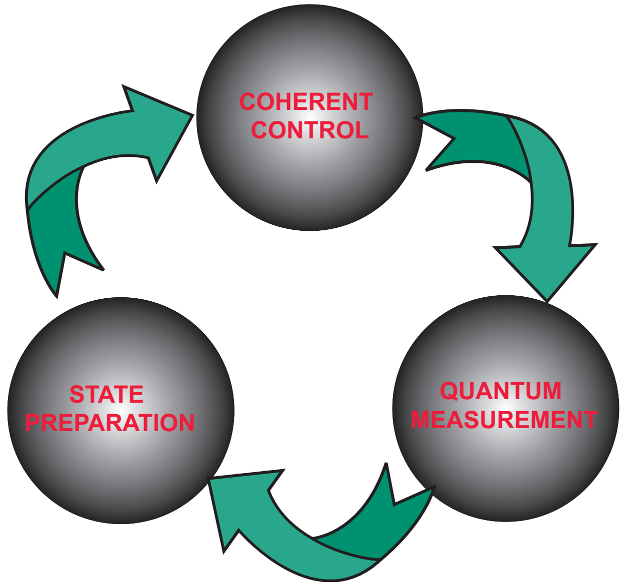

Fig. 1.1. The three elementary enabling steps required for quantum control.

theory and quantum electrodynamics (although again, that is possible in principle), but rather is given by first deriving the classical circuit equations, backing out a Hamiltonian and then directly quantising the relevant collective canonical coordinates (typically charge on an effective capacitor and flux through an effective inductor). This approach goes back to Leggett [26, 27] and is used extensively in the new field of superconducting circuit QED [28].

The study of mechanical systems near the quantum limit encompasses systems having a wide range of size and frequency [13]. In order to study these mechanical resonators, some auxiliary system is required to measure and control them. This auxiliary system may take the form of an electrical circuit ("quantum electromechanics"), an optical cavity ("quantum optomechanics"), or even an atomic system [29]. In the latter case, direct coupling of a BEC to a mechanical oscillator [30], and coupling of cold atoms in an optical lattice to a membrane, mediated by light, has been demonstrated [31]. Experimental realizations of optomechanical and electromechanical systems shall be discussed in Sec. 4 and 5, respectively. Both types of systems face related issues of state preparation (Sec. 6), coherent control (Sec. 7) and quantum-limited measurement (Sec. 8). Beyond this, nonlinear and many-body optomechanics both provide interesting systems to study, and they are described in Sec. 9 and Sec. 10, respectively.

2 Classical *Mechanical* Resonators

2.1 Continuum Mechanics

Before embarking on a quantum description of the dynamics of a mechanical resonator, we shall briefly review how its dynamics would be described classically. The focus shall be on vibrations of a rigid body, rather than on translation or rotation in space. The classical, lossless dynamics of a mechanical resonator is described, within continuum mechanics, by a space- and time-dependent displacement field. Focusing on the lowest-lying (fundamental) mode of the resonator, for small excitation amplitudes the vibration may be described as a linear (harmonic) oscillator, and the motional state may then be described by a single representative position coordinate and a single representative momentum coordinate.

Continuum mechanics is an accurate description of long-wavelength vibrations, and so allows the determination of the fundamental spatial modes of a mechanical system. The description is valid provided that the wavelengths under consideration are large compared with the interatomic spacing of the underlying crystal lattice. In this approach, one often makes the assumption of a linear relationship between the stress and strain fields. We shall focus on translational waves (rotationally-propagating waves have much higher frequencies, and are difficult to detect and actuate). These may be classified as; longitudinal (propagation and displacement in the same direction), transverse (displacements orthogonal to the propagation direction), or torsional (rotational displacements with translational propagation). In three-dimensional structures we are usually interested in longitudinal waves (breathing modes), while in two dimensions and in one dimension we usually focus on transverse waves of low frequency, as these are relatively easy to actuate and detect.

A displacement field $\mathbf{u}(\mathbf{r}, t)$ can be described by the strain tensor [32],

$$S_{\alpha\mu}\left(\mathbf{r}\right) = \frac{1}{2}\left(\frac{\partial u_\alpha}{\partial x_\mu} + \frac{\partial u_\mu}{\partial x_\alpha}\right). \tag{2.1}$$

Assuming linear response, the material may be described by an elastic tensor $E_{\mu\alpha\beta\nu}$, having 36 independent parameters. The elastic tensor can be greatly simplified depending on the symmetries of the underlying crystal lattice. The stress tensor, in terms of the symmetrized elastic tensor $c_{\mu\nu\alpha\beta}$, is then

$$T_{\mu\nu} = \sum_{\alpha,\beta=1}^{3} c_{\mu\nu\alpha\beta} S_{\alpha\beta}. \tag{2.2}$$

The above describes a static scenario; the dynamics are given by,

$$\rho \frac{\partial^2 \mathbf{u}\left(\mathbf{r}, t\right)}{\partial t^2} = \underline{\nabla} \cdot T + \mathbf{f}\left(\mathbf{r}, t\right), \tag{2.3}$$

where **f** describes some externally applied force distribution. In an isotropic solid, one may derive wave equations, describing the possibility of longitudinal, transverse and torsional waves. In an anisotropic solid, assuming wave solutions, we may calculate three phase velocities, corresponding to a longitudinal mode and two transverse modes.

The calculation of wave propagation in restricted geometries with imposed boundary conditions, material anisotropy and material inhomogeneity is complicated, and one must resort to

Oscillation	Equation	Ansatz	Dispersion
Longitudinal	$\rho\frac{\partial^2 u}{\partial t^2} = E\frac{\partial^2 u}{\partial z^2}$	$u(z,t) = u_0 e^{i(qz \pm \omega t + \phi)}$	$\omega = \sqrt{E/\rho}\, q$
Torsional	$\rho\frac{\partial^2 \theta}{\partial t^2} = G\frac{\partial^2 \theta}{\partial z^2}$	$\theta(z,t) = \theta_0 e^{i(qz \pm \omega t + \phi)}$	$\omega = \sqrt{G/\rho}\, q$
Transverse	$\rho A\frac{\partial^2 u}{\partial t^2} = T\frac{\partial^2 u}{\partial z^2} - EI\frac{\partial^4 u}{\partial z^4}$	$u(z,t) = u(z)e^{-i\omega t}$; $u(z) = e^{\pm qz}, e^{\pm iqz}$	$\omega^2 = \frac{T}{\rho A}q^2 + \frac{EI}{\rho A}q^4$

Tab. 2.1. Wave equations for linear elastic one-dimensional structures. The wave equation describing flexural modes applies for a prismatic beam due to bending, neglecting rotational inertia and shear. Setting the time-derivative to zero, this reduces to the well-known beam-bending formula of Euler-Bernoulli theory. Note that u is the translational/rotational displacement of the beam, z is the direction of propagation of the oscillation, ρ is the material density, E is the Young's modulus, G is the shear modulus, A is the cross-sectional area, T is the longitudinal tension, I is the second moment of area about the axis of bending, ω is the angular frequency of oscillation, and q is the wavevector of the oscillation.

numerical techniques. There are also nonlinear effects associated with larger deflections from equilibrium.

However, the equations of motion in simple cases are readily derived from first principles; those for linear one-dimensional structure are summarised in the Table 2.1, and the corresponding allowed spatial modes are given in Table 2.2 [32]. Note that for transverse vibrations there are restoring forces both due to the bending rigidity of the resonator and due to tension. The component due to bending rigidity is dealt with using the Euler-Bernoulli theory of beams. The transverse vibrations of a cantilever or a doubly-clamped beam are particularly important cases, and one may numerically solve for the allowed wavevectors using the equations in Table 2.2, with the results

$$\beta_n \equiv q_n l = 1.875, 4.694, \ldots, \qquad \beta_n \equiv q_n l = 4.730, 7.853, \ldots, \tag{2.4}$$

Wave	Wavevectors	Spatial mode
Longitudinal	$q_n = n\pi/l,\ n = 1, 2, ..$	$u_n(z) = u_{0n}\cos(n\pi z/l)\,,\ n$ odd; $u_n(z) = u_{0n}\sin\left(\frac{n\pi z}{l}\right),\ n$ even.
Torsional	$q_n = n\pi/l,\ n = 1, 2, ..$	$\theta_n(z) = \theta_{0n}\cos(n\pi z/l)\,,\ n$ odd; $\theta_n(z) = \theta_{0n}\sin\left(\frac{n\pi z}{l}\right),\ n$ even.
Transverse	$\cos q_n l \cosh q_n l \mp 1 = 0$ †	$u_n(z) = a_n(\cos q_n z - \cosh q_n z)$ $+b_n(\sin q_n z - \sinh q_n z)$ $b_n = \frac{\cos q_n l + \cosh q_n l}{\sin q_n l - \sinh q_n l}a_n$ for cantilever $b_n = \frac{\cosh q_n l - \cos q_n l}{\sin q_n l - \sinh q_n l}a_n$ for doubly-clamped beam

Tab. 2.2. Spatial modes of linear elastic one-dimensional structures subject to doubly-clamped boundary conditions. The wavevectors are those allowed subject to clamped boundary conditions at $\pm l/2$ for longitudinal and torsional waves, and at $0, l$ for transverse waves. † The minus sign corresponds to doubly-clamped boundary conditions, and the plus sign corresponds to cantilever boundary conditions (clamped at one end and free at the other end).

BC	Force distribution	k_{eff}	m_{eff}
Cantilever	Point load at end	$3EI/l^3$	$0.24m$
	Distributed load	$8EI/l^3$	$0.65m$
Doubly-clamped	Point load at centre	$192EI/l^3$	$0.38m$
	Distributed load	$384EI/l^3$	$0.77m$

Tab. 2.3. Effective spring constants and effective masses for one-dimensional structures.

Shape	Wave equation	Ansatz	Dispersion
Rectangular	$\frac{\partial^2 u}{\partial t^2} = \frac{T}{\rho h}\nabla^2 u - \frac{D}{\rho h}\nabla^4 u$	$u(x, y, t) = X(x)Y(y)e^{i\omega t}$	$\omega^2 = \frac{T}{\rho h}q^2 + \frac{D}{\rho h}q^4$
Circular	$\frac{\partial^2 u}{\partial t^2} = \frac{T}{\rho h}\nabla^2 u - \frac{D}{\rho h}\nabla^4 u$	$u(r, \theta, t) = R(r)\Theta(\theta)e^{i\omega t}$	$\omega^2 = \frac{T}{\rho h}q^2 + \frac{D}{\rho h}q^4$
Cylindrical	$\rho\frac{\partial^2 u}{\partial t^2} = K\nabla^2 u$	$u(r, \theta, z, t) = R(r)\Theta(\theta)Z(z)e^{i\omega t}$	$\omega = \sqrt{K/\rho}q$
Spherical	$\rho\frac{\partial^2 u}{\partial t^2} = K\nabla^2 u$	$u(r, \theta, \phi, t) = R(r)\Theta(\theta)\Phi(\phi)e^{i\omega t}$	$\omega = \sqrt{K/\rho}q$

Tab. 2.4. Wave equations for transverse waves in linear two-dimensional and three-dimensional structures [33]. Note that h is the width of the plate, ∇^4 is the biharmonic operator, $D = Eh^3/12$, and K is the bulk modulus.

respectively. Often, the tensile contribution is negligible, and then one may determine the vibration frequency using the dispersion relation of Table 2.1, with the results

$$\omega_n = \beta_n^2\sqrt{\frac{E}{\rho}}\frac{t}{l^2}, \quad \omega_n = \beta_n^2\sqrt{\frac{E}{\rho}}\frac{r}{2l^2}, \tag{2.5}$$

for a beam of rectangular cross-section (thickness t) and for a beam of circular cross-section (radius r), respectively.

We wish to describe each mode as a simple harmonic oscillator with a single position coordinate and a single momentum coordinate, and with an effective spring constant and an effective mass. The spring constant may be calculated by calculating the static deflection due to a particular force distribution, and the effective mass follows from the known resonance frequency. These are shown in Table 2.3 for the fundamental mode of a flexural resonator, subject to different force distributions.

Two-dimensional and three-dimensional structures of interest include rectangular plates (such as graphene membranes), circular plates (such as microtoroidal resonators), and large cylinders and spheres (such as resonant-mass gravitational wave detectors). The appropriate wave equations are given in Table 2.4, while the corresponding spatial mode solutions may be found in engineering textbooks [33].

We have thus far neglected the role of dissipation. Indeed, in a distributed structure, the problem of dissipation becomes the problem of attenuation; a strain wave propagating with the wave vector q is described by the attenuation constant $A = q/2Q$. However, since we are dealing with standing waves rather than traveling waves, the form of the spatial modes is unaffected. We will discuss dissipation in Sec. 3.4.

2.2 Classical Harmonic Oscillators

We have seen above that, via a continuum mechanics description, a particular vibrational mode may be regarded as a single harmonic oscillator. This may be seen more directly from energetic considerations [32]. We now demonstrate this for the important case of a long, thin doubly-clamped beam. Assume that the neutral axis of the beam is aligned along the z axis, with its ends clamped at $z = 0$ and $z = L$, and that the displacement of the neutral axis is in the x direction. The displacement of the neutral axis is given by $u(z,t) \equiv \mathcal{A}(t)\; u(z)$ where $\mathcal{A}(t)$ is a time-dependent amplitude and $u(z)$ is a dimensionless spatial mode profile defined such that $u(L/2) \equiv 1$. The spatial mode structure and eigenfrequencies of a mechanical resonator may be calculated, as described in Sec. 2.1. The kinetic energy associated with the flexural motion of the beam is given by

$$K = \frac{1}{2}\int_V \rho \left[\frac{\partial u(z,t)}{\partial t}\right]^2 dV = \frac{1}{2}\rho A \dot{\mathcal{A}}^2 \int_0^L [u(z)]^2\, dz = \eta_1 \frac{1}{2} M \dot{\mathcal{A}}^2, \tag{2.6}$$

where V is the volume of the beam, ρ is its density, A is its cross-sectional area, and $M \equiv \rho A L$ is its physical mass. For the fundamental mode of the beam, $\eta_1 \equiv \frac{1}{L}\int_0^L [u(z)]^2\, dz = 0.38$. The strain in the beam is assumed to be along the z axis and has amplitude $\left|x\frac{\partial^2 u(z,t)}{\partial z^2}\right|$. The potential energy associated with this strain is given in terms of a strain field $\epsilon(x,y,z,t)$ as

$$\begin{aligned} U &= \frac{1}{2}\int_V E\,[\epsilon(x,y,z,t)]^2\, dV \\ &= \frac{E}{2}\int_{-t/2}^{+t/2} dx \int_{-w/2}^{+w/2} dy \int_0^L dz\; x^2 \left[\frac{\partial^2 u(z,t)}{\partial z^2}\right]^2 = \eta_1 \frac{1}{2} M \omega_m^2 \mathcal{A}^2, \end{aligned} \tag{2.7}$$

where E is the elastic modulus of the beam, w is the width of the beam and t is the thickness of the beam. Now we consider the representative position coordinate of the beam to be $x \equiv \mathcal{A}(t)$. The Lagrangian equation of motion corresponding to Eqs. (2.6) and (2.7) is then

$$\ddot{x} + \omega_m^2 x = 0. \tag{2.8}$$

This equation describes simple harmonic motion at the resonance frequency $\omega_m \equiv \sqrt{k/m}$, where m is the effective mass of the resonator and k is its effective spring constant. These effective parameters depend upon the force distribution assumed, with two cases quoted in Table 2.3.

The corresponding classical Hamiltonian is

$$H_S = \frac{p^2}{2m} + \frac{1}{2}kx^2, \tag{2.9}$$

where p is a representative momentum coordinate. Such a description is generally valid, though the effective parameters depend on the system considered, and both on the mode under consideration and the nature of the driving.

2.2.1 Damped Harmonic Oscillator

Any macroscopic mechanical resonator will interact with other degrees of freedom, including other particle and quasi-particle modes, and defects. The precise temperature, amplitude and frequency-dependence of dissipation in macroscopic mechanical resonators is not well understood, though it is believed that effective two-level systems associated with fluctuating defects [34] play a significant role [35, 36, 37], as does phonon tunneling through the mechanical supports [38, 39, 40]. As far as the mechanical resonator dynamics are concerned, this results in dissipation and noise. Dissipation results in the mechanical resonator achieving thermodynamic equilibrium with its environment. Because of the associated noise, the representative position coordinate of the fundamental mode, assuming linear damping, obeys a stochastic differential equation known as a Langevin equation,

$$m\ddot{x}(t)+m\omega_m^2 x(t) = -m\int_{-\infty}^{t} dt'\gamma\left(t-t'\right)\dot{x}(t')-\int_{-\infty}^{t} dt'\Delta k(t-t')x(t')+F(t), \tag{2.10}$$

where $\gamma(t-t')$ is the damping kernel, $\Delta k(t-t')$ is the spring constant shift kernel, and $F(t)$ is a force describing both the noise due to the bath and any driving force. We may write $F(t) = F_N(t) + F_D(t)$ where $F_N(t)$ is a zero-mean stochastic force describing the noise due to the environment and $F_D(t)$ is a driving force. The first two terms on the right-hand-side describe the out-of-phase and the in-phase response, respectively, of the environment to the mechanical motion. Assuming a memoryless damping kernel and a negligible frequency shift, we have the more familiar form,

$$m\ddot{x}(t) + m\gamma\dot{x}(t) + kx(t) = F(t). \tag{2.11}$$

In the steady-state, we may take the Fourier transform of both sides of Eq. (2.11) to find $x(\omega) = \chi(\omega)\cdot F(\omega)$ where the so-called mechanical susceptibility is given by

$$\chi(\omega) = \frac{1}{m\left(\omega_m^2-\omega^2-i\gamma\omega\right)}. \tag{2.12}$$

Assuming that the oscillator is undriven, $F_D(t) \equiv 0$, and that it is underdamped, $\gamma^2 < 4mk$, the transient solution for the mean position of the damped harmonic oscillator described by Eq. (2.11) is

$$\langle x(t)\rangle = e^{-\gamma t/2}\left[Ae^{+i\omega_m' t} + Be^{-i\omega_m' t}\right] \quad \text{where} \quad \omega_m' = \sqrt{\omega_m^2 - \frac{\gamma^2}{4}}, \tag{2.13}$$

with A and B determined from the initial conditions. Typically, $\omega_m \gg \gamma$ in systems of interest to us here, and we will often approximate that $\omega_m' \approx \omega_m$. If the oscillator is driven harmonically by $F_D(t) = F_0 \sin\omega_d t$, the steady-state solution to Eq. (2.11) is

$$\langle x(t)\rangle = \frac{F_0}{m\sqrt{\gamma^2\omega_d^2 + \left(\omega_m^2-\omega_d^2\right)^2}}\sin\left(\omega_d t + \phi\right). \tag{2.14}$$

where

$$\phi = \arctan\left(\frac{\gamma\omega_d}{\omega_d^2-\omega_m^2}\right). \tag{2.15}$$

Plots corresponding to Eq. (2.14), in the limit $\omega_m \gg \gamma$, are shown in Fig. 2.1.

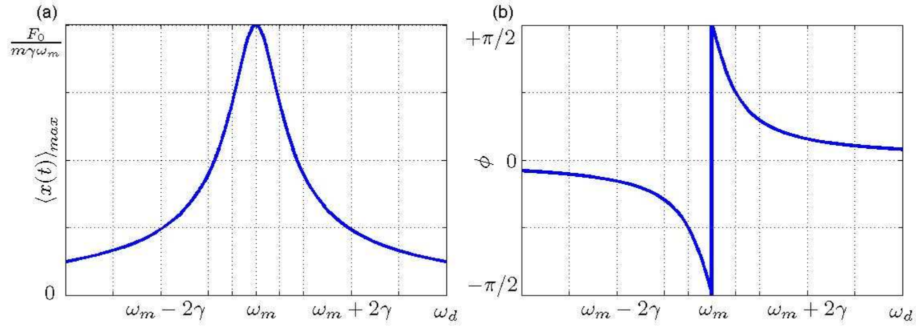

Fig. 2.1. (a) Magnitude and (b) phase response of a classical harmonic oscillator subject to a driving force F_0 at a frequency ω_d, in the limit $\omega_m \gg \gamma$. In this limit (the "high-Q" limit), a plot of $\langle x(t)\rangle^2_{max}$ will be approximately Lorentzian.

2.2.2 Position and Force Noise

In considering mechanical systems near the quantum limit, one is typically more interested in the noise properties of the undriven response than in the driven response. The force and position correlation functions are defined by

$$G_F(\tau) = \lim_{t\to\infty} \langle F(t+\tau), F(t)\rangle\,, \qquad G_x(t) = \lim_{t\to\infty} \langle x(t+\tau), x(t)\rangle\,, \tag{2.16}$$

respectively, where $\langle Q(t+\tau), Q(t)\rangle \equiv \langle Q(t+\tau)Q(t)\rangle - \langle Q(t+\tau)\rangle \langle Q(t)\rangle$. Then the force and position noise spectra are

$$S_F(\omega) \equiv \frac{1}{\sqrt{2\pi}} \int_{-\infty}^{+\infty} dt e^{i\omega t} G_F(t), \qquad S_x(\omega) \equiv \frac{1}{\sqrt{2\pi}} \int_{-\infty}^{+\infty} dt e^{i\omega t} G_x(t), \tag{2.17}$$

respectively. From Eq. (2.11), these noise spectra are related by

$$S_x(\omega) = \frac{S_F(\omega)}{m^2} \frac{1}{(\omega_m^2 - \omega^2)^2 + \gamma^2\omega^2}. \tag{2.18}$$

It is conventional to define the quality factor of a resonator by $Q = \omega_m'/\gamma \approx \omega_m/\gamma$. In the high-Q limit, Eq. (2.18) becomes

$$S_x(\omega) = \frac{S_F(\omega)}{4m^2\omega_m^2} \frac{1}{(\omega_m - \omega)^2 + (\gamma/2)^2}. \tag{2.19}$$

Consider the case where the source of noise is thermal excitation. The classical equipartition theorem gives $m\omega_m^2 \langle x^2\rangle = k_B T$, where $\langle x^2\rangle$ may be calculated by inverting Eq. (2.17). The assumption of a stochastic force delta-correlated in time leads to the force noise spectrum,

$$S_F(\omega) = 2mk_BT\gamma, \tag{2.20}$$

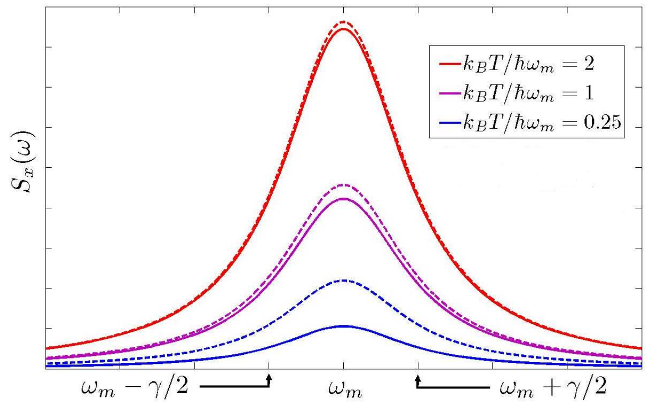

Fig. 2.2. Position noise spectra of classical (unbroken lines) and quantum (dashed lines) harmonic oscillators subject to a white noise force at a variety of temperatures. In the high-temperature limit, $k_BT \gg \hbar\omega_m$, the classical spectrum closely approaches the quantum spectrum. However, in the low-temperature limit, $k_BT \ll \hbar\omega_m$, the quantum spectrum is bounded below by the zero-point fluctuations of the oscillator, while the classical spectrum decreases towards zero.

describing a white noise process [41]. Then Eq. (2.11) describes classical Brownian motion, and the position noise spectrum of the oscillator becomes

$$S_x(\omega) = \frac{k_BT\gamma}{2m\omega_m^2}\frac{1}{(\omega_m-\omega)^2+(\gamma/2)^2}. \tag{2.21}$$

In experiments, one typically measures a spectrum related to $S_x(\omega)$. Hence Eq. (2.21) allows one both to define an effective temperature for a resonator, and may also be used as a basis for calibrating measured position noise spectra. Plots corresponding to Eq. (2.21) are shown in Fig. 2.2; the damping rate γ as defined corresponds to the full-width at half-maximum of the position noise spectrum.

2.2.3 Ensemble of Classical Resonators

Alternatively, a stochastic system may be described by the deterministic evolution of its probability distribution. An ensemble of classical resonators subject to thermal noise may be described by a probability distribution $P(x,p)$ that evolves according to a Fokker-Planck equation,

$$\frac{\partial P}{\partial t} = m\omega_m^2 x\frac{\partial P}{\partial p} - \frac{p}{m}\frac{\partial P}{\partial x} + \frac{\partial}{\partial p}\left[\gamma p P + 2mk_BT\gamma\frac{\partial P}{\partial p}\right]. \tag{2.22}$$

This equation may be obtained from first principles [41]. Alternatively, one can calculate the equations of motion for an arbitrary function of the stochastic position and momentum, using Eqs. (2.11) and (2.20), which can then be used to obtain Eq. (2.22) [42]. The first two terms describe the Hamiltonian dynamics given by Liouville's equation, the third term describes dissipation and the fourth term describes fluctuations. The steady-state solution is Gaussian,

$$P\left(x,p\right)=\frac{\omega_m}{2\pi k_B T}\exp\left[-\frac{1}{2}\left(\frac{m\omega_m^2}{k_B T}x^2+\frac{1}{mk_B T}p^2\right)\right]. \tag{2.23}$$

This distribution has a variance in position of $V(x)=k_B T/m\omega_m^2$, and a variance in momentum of $V(p)=mk_B T$; both being proportional to temperature.

2.3 Nonlinear Classical Oscillators

Nanomechanical resonators also offer the prospect of novel studies of nonlinear dynamics. Even in the classical regime, a variety of phenomena can be explored. One may consider resonators that are nonlinear due to their inherent mechanical nonlinearity [43], or their being subject to nonlinear potentials [44] or nonlinear driving [45].

2.3.1 The Duffing Oscillator

A range of nonlinear mechanical resonators, most notably strongly-driven doubly-clamped beams and clamped membranes, may be described by Duffing or Duffing-like equations. This intrinsic nonlinearity is due to extension of the beam (membrane) under flexure. To account for nonlinear effects in the doubly-clamped beam, one must include a correction due to beam extension in the energies of Eqs. (2.6) and (2.7). One does so by replacing the line element of the neutral axis of the beam, dz, by the element of arc

$$dl=\sqrt{dz^2+[du(z,t)]^2}\approx dz+\frac{1}{2}\left[\frac{\partial u(z,t)}{\partial z}\right]^2 dz. \tag{2.24}$$

The appropriate corrections to the energies of Eqs. (2.6) and (2.7) lead to the corresponding Lagrangian equation of motion acquiring a cubic term,

$$\ddot{x}+\omega_m^2 x+\omega_m^2 k_3 x^3=0. \tag{2.25}$$

Adding driving and linear damping, we have the driven, damped Duffing equation,

$$m\ddot{x}+m\gamma\dot{x}+m\omega_m^2 x+m\omega_m^2 k_3 x^3=F(t). \tag{2.26}$$

For $k_3>0$ ($k_3<0$), the cubic term describes a stiffening (softening) nonlinearity, corresponding to an increase (decrease) in the resonance frequency at large amplitudes. For intrinsic mechanical nonlinearities, one would always expect a stiffening nonlinearity. Since the equation of motion is cubic, the corresponding Hamiltonian is quartic.

One may calculate the quasi-harmonic steady-state response to the drive $F(t)=F_0\cos\omega_d t$ [46]. Assuming a solution of the form $x(t)=\left(\mathcal{A}_0 e^{i\omega_d t}+\mathcal{A}_0^* e^{-i\omega_d t}\right)/2$, where $\mathcal{A}_0\equiv a_0 e^{i\phi_0}$, we can write

$$\left[\omega_m^2-\omega_0^2+\frac{3\omega_m^2 k_3}{4}a_0^2+i\omega_d\gamma\right]a_0=\frac{F_0}{m}e^{-i\phi_0}. \tag{2.27}$$

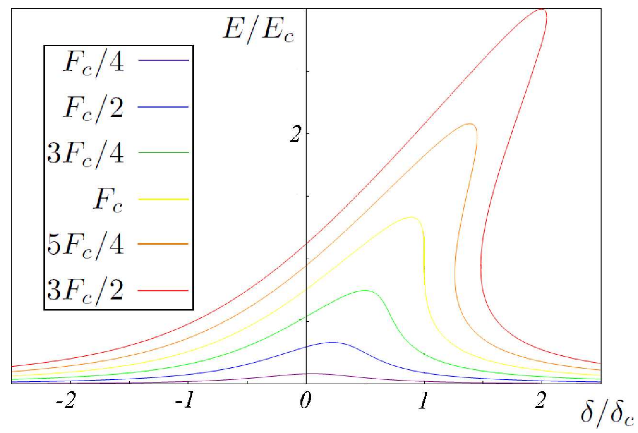

Fig. 2.3. Steady-state response of a damped, driven Duffing oscillator. The steady-state amplitude squared (as a ratio to the critical amplitude squared) is plotted against the scaled detuning (as a ratio to the critical scaled detuning). The response is shown for a range of driving strengths, below, at and above the critical driving strength.

Now approximating $\omega_d = \omega_m(1+\delta)$ where $|\delta| \ll 1$ and writing $E \equiv a_0^2$ and $\kappa = 3k_3/4$, Eq. (2.27) may be decoupled into an amplitude equation and a phase equation as

$$E^3 - \frac{4\delta}{\kappa}E^2 + \left[\frac{1}{Q^2\kappa^2} + \frac{4}{\kappa^2}\delta^2\right]E - \frac{F_0^2}{\kappa^2 m^2 \omega_m^4} = 0, \tag{2.28}$$

$$\tan\phi_0 = \frac{1}{Q}\frac{1+\delta}{2\delta - \kappa E}. \tag{2.29}$$

The critical point, corresponding to $\frac{d\delta}{dE} = 0$, is given by the scaled detuning, amplitude squared and driving strength, respectively,

$$\delta_c = \frac{\sqrt{3}}{2Q}, \qquad E_c = \frac{2}{\sqrt{3}\kappa Q}, \qquad \frac{F_c}{m} = \sqrt{\frac{8\sqrt{3}\omega_m^4}{9\kappa Q^3}}. \tag{2.30}$$

The steady-state response, shown in Fig. 2.3, curve tilts towards higher frequencies at larger drive powers if $k_3 > 0$, a phenomenon known as frequency pulling. Above the critical point, one observes bistability. These stable states are known as attractors or fixed points; and the basins of attraction of each are delineated by a separatrix curve. Noise-induced switching between the basins of attraction is then possible.

2.3.2 The Parametric Oscillator

Another prototypical nonlinear oscillator is the parametric oscillator. A mechanical parametric resonator may be created by modulating the resonator's effective spring constant at some multiple of its mechanical resonance frequency. With the spring constant modulation $\Delta k(t) =$

$\Delta k_0 \sin \omega_p t$ and driving $F_D(t) = F_0 \cos(\omega_d t + \phi)$, the resonator is described by the damped, driven Mathieu equation,

$$m\ddot{x} + m\gamma\dot{x} + (k + \Delta k_0 \sin \omega_p t)\, x = F_0 \cos(\omega_d t + \phi)\,. \tag{2.31}$$

In order to analyse Eq. (2.31), we define the composite position-velocity variable [45], $\alpha \equiv \frac{dx}{dt} + i\Omega^* x$, defined in terms of the generalized frequency, $\Omega \equiv \left[\sqrt{1 - \frac{1}{4Q^2}} + \frac{i}{2Q}\right] \omega_m$. Inverting this definition, we find

$$x = \frac{\alpha - \alpha^*}{i(\Omega + \Omega^*)} \quad \text{and} \quad \dot{x} = \frac{\Omega\alpha + \Omega^*\alpha^*}{\Omega + \Omega^*}. \tag{2.32}$$

Substituting Eq. (2.32) into Eq. (2.31), the result is

$$\frac{d\alpha}{dt} = i\Omega\alpha + i\frac{\Delta k_0}{m} \sin \omega_p t \frac{\alpha - \alpha^*}{\Omega + \Omega^*} + \frac{F_0}{m} \cos(\omega_d t + \phi)\,. \tag{2.33}$$

This equation exhibits resonances at the parametric driving frequencies $\omega_p = 2\omega_m/n$ where n is an integer.

The resonance at $2\omega_p$ is commonly employed for parametric amplification of a drive signal. Assuming that the oscillator is driven on resonance, $\omega_d = \omega_m$, we expect a solution of the form $\alpha = \mathcal{A}_0 e^{i\omega_m t}$. Substituting this into Eq. (2.33) with $\omega_p = 2\omega_m$, retaining terms oscillating at $+\omega_d$, and assuming a high-Q oscillator such that $\Omega + \Omega^* = 2\omega_m$ and $\Omega - \omega_m = \frac{i\omega_m}{2Q}$ to a good approximation, we have

$$\mathcal{A}_0 = F_0 \frac{Q\omega_m}{k} \left[\frac{\cos\phi}{1 + \frac{Q\Delta k_0}{2k}} + i\frac{\sin\phi}{1 - \frac{Q\Delta k_0}{2k}} \right]. \tag{2.34}$$

Using Eq. (2.32), we can write $x(t) = X_1 \cos \omega_m t + X_2 \sin \omega_m t$ where $X_1 = \mathrm{Im}\mathcal{A}_0/\omega_m$ and $X_2 = \mathrm{Re}\mathcal{A}_0/\omega_m$. The parametric gain for quadrature i is then

$$G_i(\phi) \equiv \frac{|X_i|_{\text{pump on}}}{|X_i|_{\text{pump off}}} = \left[\frac{\cos^2\phi}{\left(1 + \frac{Q\Delta k_0}{2k}\right)^2} + \frac{\sin^2\phi}{\left(1 - \frac{Q\Delta k_0}{2k}\right)^2} \right]^{1/2}. \tag{2.35}$$

The gain is phase-sensitive, being a maximum (and greater than one) at $\phi = \pi/2$, and a minimum (and less than one) at $\phi = 0$. At $\Delta k_0 = \frac{2k}{Q}$, the response diverges. Accordingly, one can map out the regions of stable and unstable behaviour over the range of pump frequency ω_p and pumping strength Δk_0 [47].

3 Quantum *Mechanical* Resonators

3.1 Quantum Description

A classical continuum approach provides an accurate description of the vibrational dynamics of a solid in the long-wavelength limit, that is, where the wavelength of the mode of interest is much larger than the lattice spacing. We can give an effective quantum description of the long-wavelength modes by treating the elastic wave as a scalar field and imposing appropriate commutation relations. Alternatively, we can consider the mode of interest as a damped harmonic oscillator with a single representative coordinate pair, and then quantize the representative coordinate.

As an example we will consider the case of the transverse displacement of a doubly-clamped rectangular beam. We will choose coordinates so that z runs along the beam, and the displacement $u(z,t)$ is transverse to the beam, as shown in Fig. 3.1. As given in Table 2.1, the transverse displacement field is described by

$$\rho A \frac{\partial^2 u}{\partial t^2} = T\frac{\partial^2 u}{\partial z^2} - EI\frac{\partial^4 u}{\partial z^4}. \tag{3.1}$$

If we make the harmonic ansatz, $u(z,t) = u(z)e^{-i\omega t}$ and $u(z) = e^{\pm qz}, e^{\pm iqz}$, we get the dispersion relation

$$\omega^2 = \frac{T}{\rho A}q^2 + \frac{EI}{\rho A}q^4. \tag{3.2}$$

The spatial modes of the system are determined by the boundary conditions,

$$\cos q_n l \cosh q_n l \mp 1 = 0, \tag{3.3}$$

and we write them as

$$u_n(z) = a_n\left(\cos q_n z - \cosh q_n z\right) + b_n\left(\sin q_n z - \sinh q_n z\right), \tag{3.4}$$

with the appropriate coefficients given in Table 2.1. The frequency of each spatial mode is then given by Eq. (2.5). The displacement field may then be written as

$$u(z,t) = \sum_n B_n \mathrm{u}_n(z,t) + B_n^\dagger \mathrm{u}_n^*(z,t). \tag{3.5}$$

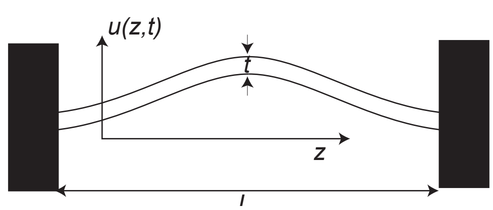

Fig. 3.1. The coordinate system for transverse vibrations of a doubly-clamped mechanical resonator

We now pass to a quantum description by defining the quantum displacement field,

$$\hat{u}(z,t) = \sum_n b_n \mathrm{u}_n(z,t) + b_n^\dagger \mathrm{u}_n^*(z,t), \tag{3.6}$$

with commutation relations, $[b_n, b_m^\dagger] = \delta_{n,m}$. We shall now review some basic features of the quantum harmonic oscillator.

3.2 States of the Quantum Harmonic Oscillator

3.2.1 Quantum Harmonic Oscillator

Much as the electromagnetic field was introduced as a classical field and it was eventually realized that one must quantize the electromagnetic field to explain certain physical phenomena, one might also expect that a quantum description of the dynamics of a macroscopic mechanical resonator would become necessary in particular limits. The displacement field is analogous to the electromagnetic vector potential. Both vector fields obey a wave equation, and the imposition of boundary conditions yields a spectrum of discrete modes. The quanta of our quantized mechanical resonator are, of course, phonons; the quantized normal mode vibrations of the underlying crystal lattice. Near the quantum limit, one is most interested in low-frequency phonons. These lowest-lying vibrational modes have long wavelengths compared with the inter-atomic spacing, and hence a continuum mechanics description is valid.

Nonetheless, assuming that quantum mechanics does indeed apply to a macroscopic mechanical resonator, the fundamental mode may be treated as a quantum harmonic oscillator. Initially we consider just the closed quantum sytem (that is, no dissipation or environment-induced noise); the theory of open quantum systems shall be introduced in Sec. 3.3. The Hamiltonian takes the form of Eq. (2.9),

$$H_S = \frac{\hat{p}^2}{2m} + \frac{1}{2}k\hat{x}^2, \tag{3.7}$$

with the Schrödinger picture canonical commutation relation $[\hat{x}, \hat{p}] = i\hbar$ imposed. Consequently, Heisenberg's uncertainty principle is manifest as the requirement $\Delta x \Delta p \geq \hbar/2$. The uncertainty in an operator is defined in terms of its variance as $\Delta Q \equiv [V(Q)]^{1/2}$, where the variance itself is defined by $V(Q) \equiv \langle \hat{Q}^2 \rangle - \langle \hat{Q} \rangle^2$.

In quantum physics, it is conventional to introduce the lowering and raising operators of the harmonic oscillator as

$$a = \sqrt{\frac{m\omega_m}{2\hbar}}\hat{x} + i\sqrt{\frac{1}{2\hbar m\omega_m}}\hat{p}, \qquad a^\dagger = \sqrt{\frac{m\omega_m}{2\hbar}}\hat{x} - i\sqrt{\frac{1}{2\hbar m\omega_m}}\hat{p}, \tag{3.8}$$

respectively. Eigenvalues of the lowering operator are then given by

$$\alpha \equiv \sqrt{\frac{m\omega_m}{2\hbar}}x + i\sqrt{\frac{1}{2\hbar m\omega_m}}p, \tag{3.9}$$

where x and p correspond to the mean position and momentum, respectively, of the associated eigenstate, termed a coherent state. The corresponding commutation relations are $[a, a^\dagger] = 1$ and $[a, a] = [a^\dagger, a^\dagger] = 0$, and the harmonic oscillator Hamiltonian becomes

$$H_S = \hbar\omega_m \left[a^\dagger a + \frac{1}{2} \right]. \tag{3.10}$$

The offset term, corresponding to the zero-point energy, makes no contribution to the Hamiltonian dynamics, and hence is often omitted.

The Heisenberg picture position and momentum operators are given, in terms of the Schrödinger picture operators considered earlier, by the transformations

$$\hat{x}(t) = e^{-iH_S t/\hbar}\hat{x}e^{+iH_S t/\hbar}, \qquad \hat{p}(t) = e^{-iH_S t/\hbar}\hat{p}e^{+iH_S t/\hbar}. \tag{3.11}$$

The results of these transformations are

$$\hat{x}(t) = \cos\omega_m t\,\hat{x} - \frac{1}{m\omega_m}\sin\omega_m t\,\hat{p}, \qquad \hat{p}(t) = m\omega_m \sin\omega_m t\,\hat{x} + \cos\omega_m t\,\hat{p}, \tag{3.12}$$

and they satisfy the commutation relations

$$[\hat{x}(t), \hat{x}(t')] = \frac{i\hbar}{m\omega_m}\sin\left(\omega_m t' - \omega_m t\right), \tag{3.13}$$

$$[\hat{p}(t), \hat{p}(t')] = i\hbar m\omega_m \sin\left(\omega_m t' - \omega_m t\right), \tag{3.14}$$

$$[\hat{x}(t), \hat{p}(t')] = i\hbar \cos\left(\omega_m t' - \omega_m t\right). \tag{3.15}$$

One may then introduce the dimensionless Heisenberg picture position and momentum quadratures, $\hat{X}(t)$ and $\hat{P}(t)$, as

$$\hat{X}(t) = \frac{\hat{x}(t)}{\sqrt{\hbar/2m\omega_m}}, \qquad \hat{P}(t) = \frac{\hat{p}(t)}{\sqrt{\hbar m\omega_m/2}}, \tag{3.16}$$

with the corresponding commutation relations

$$\begin{aligned}\left[\hat{X}(t), \hat{X}(t')\right] &= \left[\hat{P}(t), \hat{P}(t')\right] = 2i\sin\left(\omega_m t' - \omega_m t\right),\\ \left[\hat{X}(t), \hat{P}(t')\right] &= 2i\cos\left(\omega_m t' - \omega_m t\right).\end{aligned} \tag{3.17}$$

The Hamiltonian for a harmonic oscillator takes the form

$$H_S(t) = \frac{\hbar\omega_m}{4}[\hat{X}^2(t) + \hat{P}^2(t)]. \tag{3.18}$$

Then one can introduce the Heisenberg picture raising and lowering operators, $a(t)$ and $a^\dagger(t)$, in analogy with Eq. (3.8),

$$a(t) = \frac{1}{2}[\hat{X}(t) + i\hat{P}(t)], \qquad a^\dagger(t) = \frac{1}{2}[\hat{X}(t) - i\hat{P}(t)]. \tag{3.19}$$

having the commutation relations

$$[a(t), a^\dagger(t')] = e^{i\omega_m(t'-t)}, \qquad [a(t), a(t')] = [a^\dagger(t), a^\dagger(t')] = 0. \tag{3.20}$$

The Hamiltonian of the harmonic oscillator takes the form of Eq. (3.10), again now with explicitly time-dependent operators. Alternatively, one may obtain all Heisenberg picture operators using transformations of the form of Eq. (3.11). In particular, raising and lowering operators are related as $a = a(t)e^{-i\omega_m t}$ and $a^\dagger = a^\dagger(t)e^{+i\omega_m t}$. Eq. (3.10) and (3.19) demonstrate the equivalence between the position and momentum quadratures defined here, and the amplitude and phase quadratures generally referred to in quantum optics [48].

3.2.2 States of the Quantum Harmonic Oscillator

The energy eigenvalues of the Hamiltonian of Eq. (3.10) are

$$E_n = \hbar\omega_m \left(n + \frac{1}{2}\right), \tag{3.21}$$

with the associated eigenvectors $|n\rangle$ being the so-called number or Fock states. They contain exactly n quanta (in our case, phonons). The operator $\hat{n} = a^\dagger a$ is identified as the number operator; thus $\langle \hat{n} \rangle$ gives the expected number of phonons in a particular mode.

An important class of states of the harmonic oscillator are the so-called coherent states. They are quasi-classical in the sense that they exhibit the minimum uncertainty product allowed by Heisenberg's uncertainty principle, and they are also the eigenstates of a driven harmonic oscillator. In terms of a number state basis, a coherent state is given by

$$|\alpha\rangle = e^{-|\alpha|^2/2} \sum_{n=0}^{\infty} \frac{\alpha^n}{\sqrt{n!}} |n\rangle , \tag{3.22}$$

with number expectation $\langle \hat{n} \rangle = |\alpha|^2$ and number variance $V(n) = |\alpha|^2$.

An undriven harmonic oscillator maintained at some temperature T is said to be in a thermal state, with a density matrix given by

$$\rho = \left(1 - e^{-\hbar\omega_m/k_B T}\right) \sum_{n=0}^{\infty} |n\rangle \langle n| \, e^{-n\hbar\omega_m/k_B T}, \tag{3.23}$$

with the "phonon number" being given by a Bose-Einstein distribution as

$$\bar{n} \equiv \langle \hat{n} \rangle = \frac{1}{e^{\hbar\omega_m/k_B T} - 1} \approx \frac{k_B T}{\hbar\omega_m} \;\; (k_B T \gg \hbar\omega_m), \tag{3.24}$$

and the phonon number variance being given by $V(n) = \bar{n}(1 + \bar{n})$. One could also consider a (coherently) displaced thermal state.

The quantum ground state corresponds to $\bar{n} = 0$ and has a Gaussian wavefunction with a half-width of

$$\Delta x_{\mathrm{ZP}} = \sqrt{\frac{\hbar}{2m\omega_m}}, \tag{3.25}$$

termed the zero-point uncertainty for a harmonic oscillator. The larger the zero-point uncertainty is, the easier it is to detect the quantum fluctuations of the resonator. For this reason, in order to reach the quantum limit, it would appear desirable to have a resonator with a small mass and a small frequency. However, one must consider the thermal occupation given by Eq. (3.24). In the absence of auxiliary cooling mechanisms, one would expect the mode temperature to equilibrate with the ambient temperature. Then to reach the quantum ground state we must require that

$$\hbar\omega_m \gg k_B T. \tag{3.26}$$

This is a very demanding requirement. Typically, bulk refrigeration is inadequate and auxiliary cooling mechanisms are required. Thus, in order to observe quantum states of macroscopic mechanical resonators, we demand that they have low masses and high frequencies.

Once it is possible to cool a mechanical resonator to its quantum ground state and to make quantum-limited measurements of the resonator, one may consider the quantum mechanics of the mechanical resonator itself. The most immediate task is then the generation and detection of quantum states of the resonator. Such experiments are guided by instances of quantum harmonic oscillators in other physical systems; namely, in optical and microwave fields, and the motional states of cold, trapped atoms and ions. In the case of a trapped ion, in contrast with the case of an electromagnetic field, the associated frequencies are not sufficiently high that we may neglect thermal noise, and one must explicitly address the problem of cooling the atom or ion.

Fock, coherent and squeezed states of motion of a harmonically-bound ion have been created [49], as has a Schrödinger cat state [50]. Such states are created by appropriately tuning an incident laser, and the motional state of the ion is reconstructed by tomography. Alternatively, the motion of a single atom may be detected using the spatial variation of the atom-cavity coupling [51]. More recently, motional entangled states of two ions have been demonstrated using internal states [52], as well as the direct, controllable coupling of the quantized motional states through Coulomb coupling [53]. In the case of atomic ensembles, cooling to the motional ground state to form a Bose-Einstein condensate (BEC) has been demonstrated [54], as have squeezed states [55], and measurement back-action from an optical field onto an atomic ensemble has been observed [56]. Recently, high-frequency mechanical resonators have been prepared and measured in their ground states [57,59,58], truly ushering in an age of quantum nanomechanics.

3.2.3 Quantum Phase-Space Distribution Functions

The number states provide a complete basis for the states of the quantum harmonic oscillator. However, alternative representations are often preferable for the analysis and visualization of a wide variety of states. Representations over position and momentum, over position and momentum quadratures, or over complex amplitudes, are referred to as phase-space distribution functions [60]. In the latter case, they are referred to as coherent state representations [48].

The most well-known phase-space distribution is the Wigner function [61], defined in terms of position and momentum by

$$W(x,p,t) = \frac{1}{2\pi^2\hbar}\int d\xi \int d\eta\, \frac{\hbar}{2}\, \chi_S(\xi,\eta) e^{-i\xi x - i\eta p}, \tag{3.27}$$

where $\chi_S(\xi,\eta)$ is the symmetrically-ordered characteristic function,

$$\chi_S(\xi,\eta) = \mathrm{Tr}\, \left[\rho e^{i\xi\hat{x} + i\eta\hat{p}}\right]. \tag{3.28}$$

The Wigner function may be conveniently expressed over position and momentum as

$$W(x,p,t) = \frac{1}{\pi\hbar}\int dx'\, \langle x + x'|\, \rho\, |x - x'\rangle\, e^{-2ix'p/\hbar}, \tag{3.29}$$

where $x' = \eta\hbar/2$, or over position and momentum quadratures as

$$W(X,P,t) = \frac{1}{2\pi}\int dX'\, \langle X + X'|\, \rho\, |X - X'\rangle\, e^{-iX'P}. \tag{3.30}$$

where $X' = (2m\omega_m/\hbar)x'$. The Wigner functions for a number of well-known quantum states are depicted in Fig. 3.2 and tabulated in Table 3.1.

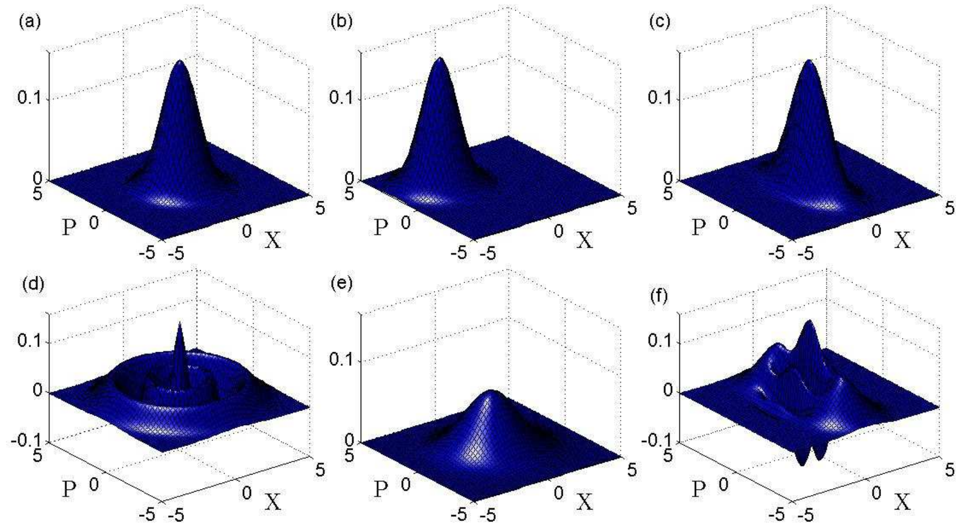

Fig. 3.2. Wigner functions in terms of position and momentum quadratures in a rotating frame, $W(X, P, t)$, for: (a) the quantum ground state of a harmonic oscillator; (b) a coherent state with $X_0 = 2, P_0 = 2$ $(\alpha = 1 + i)$; (c) a squeezed state with squeezing parameter $2r = 0.7$; (d) a Fock ("number") state with 4 quanta; (e) a thermal state with $k_B T = \hbar\omega_m$; (f) a coherent state superposition ("Schrödinger cat" state) with amplitudes $\alpha = \sqrt{2}$ and phase separation of $2\phi = \pi$.

Integrating the Wigner function over different phase-space coordinates, it is seen that the distribution functions over quadratures and complex amplitudes are related to the distribution function over position and momentum of Eq. (3.27) by

$$2\hbar W(x, p, t) = 4W(X, P, t) = W(\alpha, \alpha^*, t). \tag{3.31}$$

Now different conventions for operator ordering in the characteristic functions lead to different

Ground State	Coherent State	Squeezed State
$\frac{1}{2\pi}e^{-\frac{1}{2}\left(X^2+P^2\right)}$	$\frac{1}{2\pi}e^{-\frac{1}{2}\left[(X-X_0)^2+(P-P_0)^2\right]}$	$\frac{1}{2\pi}e^{-\frac{1}{2}\left[X^2e^{2r}+P^2e^{-2r}\right]}$
n^{th} Fock State	Thermal State	"Cat" State
$\frac{1}{2\pi}L_n\left(X^2+P^2\right)e^{-\frac{1}{2}\left(X^2+P^2\right)}$	$\frac{1}{2\pi}\tanh\frac{\hbar\omega_m}{2k_BT}e^{-\frac{1}{2}(X^2+P^2)\tanh\frac{\hbar\omega_m}{2k_BT}}$	$\frac{1}{2}\left(W_{C1}+W_{C2}+W_{int}\right)$

Tab. 3.1. Wigner functions in terms of position and momentum quadratures, $W(X, P, t)$, for the basic quantum states shown in Fig. 3.2. Note that the coherent state is centred at (X_0, P_0), the squeezed state is centred at the origin and the squeezing is of the P quadrature with a magnitude determined by r, L_n is the n^{th} Laguerre polynomial, and T is the temperature of the thermal state. For the cat state, $W_{C1(C2)}$ are coherent states with $X_0 = 2\alpha\cos\phi$ and $P_0 = \pm 2\alpha\sin\phi$, and $W_{int} = \frac{1}{\pi}\cos\left[2\alpha\sin\phi\,(X - \alpha\cos\phi)\right]\exp\left[-\frac{1}{2}\left(X - 2\alpha\cos\phi\right)^2 - \frac{1}{2}P^2\right]$ is an interference term. Note that α is the amplitude of each coherent state and 2ϕ is the phase between them.

distribution functions. The characteristic function corresponding to the Wigner function in a coherent state basis is

$$\chi_S(z,z^*) = \mathrm{Tr}\left[\rho e^{za^\dagger - z^* a}\right], \tag{3.32}$$

where $z = -\eta' + i\xi'$ with $\xi' = \xi\hat{x}/\hat{X}$ and $\eta' = \eta\hat{p}/\hat{P}$. The associated Wigner function directly gives (symmetrically-ordered) position, momentum and quadrature moments,

$$\left\langle a^m a^{\dagger n} + a^{\dagger n} a^m \right\rangle = \int d\alpha\, \alpha^n \alpha^{*m} W(\alpha,\alpha^*,t). \tag{3.33}$$

The P function, also known as the Glauber-Sudarshan or diagonal P representation [62, 63], corresponds to a normally-ordered characteristic function,

$$\chi_N(z,z^*) = \mathrm{Tr}\left[\rho e^{za^\dagger} e^{-z^* a}\right]. \tag{3.34}$$

Accordingly, it directly gives normally-ordered moments.

$$\left\langle a^{\dagger m} a^n \right\rangle = \int d^2\alpha \alpha^{*m} \alpha^n P(\alpha,\alpha^*). \tag{3.35}$$

The P function is a highly singular representation, such that the density operator may be expressed as

$$\rho(t) = \int P(\alpha,\alpha^*,t) \left|\alpha\right\rangle \left\langle\alpha\right| d^2\alpha. \tag{3.36}$$

The Q function [64, 65] corresponds to an anti-normally-ordered characteristic function,

$$\chi_A(z,z^*) = \mathrm{Tr}\left[\rho e^{-z^* a} e^{za^\dagger}\right], \tag{3.37}$$

and is simply given by the matrix elements of the density operator in a coherent state basis,

$$Q(\alpha,\alpha^*,t) = \frac{\left\langle\alpha\right| \rho(t) \left|\alpha\right\rangle}{\pi}. \tag{3.38}$$

The Q function directly gives anti-normally-ordered moments,

$$\left\langle a^m a^{\dagger n} \right\rangle = \int d^2\alpha Q(\alpha,\alpha^*,t) \alpha^m \alpha^{*n}. \tag{3.39}$$

Both the Wigner function and the Q function correspond to Gaussian convolutions of the P function. A complete set of relationships between the distribution functions in different phase-spaces may be derived using Eqs. (3.9) and (3.31).

3.3 Damped Quantum Harmonic Oscillator

To treat dissipation and noise in mechanical systems near the quantum limit, an open quantum systems approach is necessary [66, 67]. Indeed, the ubiquitous thermal state described by Eq. (3.23) arises as the result of coupling an oscillator to an environment at some finite temperature. An open quantum systems approach involves considering our system, with few degrees of freedom, to be coupled to an environment (also known as a “bath” or “reservoir”) composed of many degrees of freedom.

In general, such an approach leads to an understanding of the processes of decoherence and einselection [68, 69], and the ability to describe quantum measurement and control [70]. Decoherence describes the effectively irreversible delocalisation of quantum correlations between components of the system to the environment; it is responsible for the effective suppression of macroscopic quantum superpositions. Decoherence is a ubiquitous phenomenon [71] that occurs very rapidly [72], and is a simple consequence of the principle of superposition and the unitary evolution of the coupled system and environment. Einselection, short for environment-induced superselection, describes the emergence of quasi-classical preferred states, called pointer states, of the system, being those that are least sensitive to becoming entangled with the environment [73]. In the limit of very weak coupling to the environment, energy eigenstates of the system are selected [74], while for a harmonic oscillator weakly coupled to an environment, the coherent states emerge as the pointer states [73].

For the moment, however, we shall simply assume that our system is just the quantum harmonic oscillator and that the effect of the environment is encapsulated by a simple linear momentum damping term. Also, here we shall consider just the evolution of particular system operators, rather than the evolution of the system density matrix.

3.3.1 Quantum Langevin Equation

Combining Heisenberg’s equations corresponding to Eq. (3.7) for the position and momentum operators, and assuming linear momentum damping and a stochastic force $\hat{F}(t)$, we have the coupled system of equations

$$m\dot{\hat{x}}(t) = \hat{p}(t), \tag{3.40}$$

$$\dot{\hat{p}}(t) = -m\omega_m^2\hat{x}(t) - \gamma\hat{p}(t) + \hat{F}(t). \tag{3.41}$$

Combining these, we can write a quantum Langevin equation having the same form as Eq. (2.11),

$$m\ddot{\hat{x}}(t) + m\gamma\dot{\hat{x}}(t) + k\hat{x}(t) = \hat{F}(t). \tag{3.42}$$

Strictly speaking, it is a quantum stochastic differential equation for the position operator in the Heisenberg picture.

3.3.2 Quantum Noise Spectra

Taking the Fourier transform of both sides of Eq. (3.42) yields the mechanical susceptibility of Eq. (2.12). One may define correlation functions and noise spectra as in Eq. (2.16) and (2.17), though the ordering of operators is now significant since, in general, observables at different times will not commute. The unsymmetrized noise spectrum of some observable $\hat{Q}$ is given by

$$S_Q(\omega) = \int_{-\infty}^{+\infty} dt e^{i\omega t} \left\langle \hat{Q}(t)\hat{Q}(0) \right\rangle \equiv \bar{S}_Q(\omega) + \tilde{S}_Q(\omega). \tag{3.43}$$

The symmetrized noise spectrum is

$$\bar{S}_Q(\omega) = \frac{S_Q(+\omega) + S_Q(-\omega)}{2} = \frac{1}{2}\int_{-\infty}^{+\infty} dt e^{i\omega t} \left\langle \left\{ \hat{Q}(t), \hat{Q}(0) \right\} \right\rangle, \tag{3.44}$$

and the anti-symmetrized noise spectrum is

$$\tilde{S}_Q(\omega) \equiv \frac{S_Q(+\omega) - S_Q(-\omega)}{2} = \frac{1}{2}\int_{-\infty}^{+\infty} dt e^{i\omega t} \left\langle \left[\hat{Q}(t), \hat{Q}(0) \right] \right\rangle. \tag{3.45}$$

The position and force noise spectra for a quantum harmonic oscillator are still related as per Eq. (2.18), provided that the spectra are defined consistently.

The force noise spectrum may be expanded in terms of transitions between initial $|i\rangle$ and final $|f\rangle$ environment eigenstates [75],

$$S_F(\omega) = 2\pi \sum_{i,f} p_i \left| \langle f| \hat{F} |i\rangle \right|^2 \delta\left(E_f - E_i - \hbar\omega\right), \tag{3.46}$$

where it is assumed that the environment density matrix is diagonal in its eigenstate basis and p_i is the population of the i^{th} environmental eigenstate. Here $\omega < 0$ corresponds to emission by the environment, and $\omega > 0$ corresponds to absorption by the environment. Note that $S_F(\omega)$ is not symmetric with respect to ω since p_i usually decreases with E_i. Considering two energy eigenstates of the environment in equilibrium, the ratio between the negative and positive frequency noise is set by temperature as

$$\frac{S_F(-\omega)}{S_F(+\omega)} = e^{-\hbar\omega/k_B T}. \tag{3.47}$$

Considering instead transitions between system eigenstates, number states in the case of a quantum harmonic oscillator, Fermi's golden rule gives the upward and downward transition rates in terms of the negative and positive frequency force noise,

$$\Gamma_{n-1\to n} = \frac{n}{2\hbar m\omega_m} S_F(-\omega_m), \quad \Gamma_{n\to n-1} = \frac{n}{2\hbar m\omega_m} S_F(+\omega_m). \tag{3.48}$$

Accordingly, the number state distribution p_n evolves according to the rate equation

$$\dot{p}_n = \Gamma_{n-1\to n} p_{n-1} + \Gamma_{n+1\to n} p_{n+1} - \left(\Gamma_{n\to n+1} + \Gamma_{n\to n-1}\right) p_n. \tag{3.49}$$

The time-evolution of the expected energy of the oscillator, $\langle E(t)\rangle = \sum_{n=0}^{\infty} \hbar\omega_m \left(n + \frac{1}{2}\right) p_n(t)$, is then given by

$$\frac{d}{dt}\langle E(t)\rangle = D - \gamma \langle E(t)\rangle, \tag{3.50}$$

where

$$D = \frac{1}{2m}\bar{S}_F(\omega_m), \quad \gamma = \frac{1}{\hbar m\omega_m}\tilde{S}_F(\omega_m), \tag{3.51}$$

describe momentum diffusion and momentum damping, respectively. The former depends on the symmetrized noise spectrum, while the latter depends on the anti-symmetrized noise spectrum. From Eq. (3.47) and (3.51), one can write down the quantum fluctuation-dissipation theorem [76],

$$\bar{S}_F(\omega) = m\gamma\hbar\omega\coth\frac{\hbar\omega}{2k_BT} = 2m\gamma\left[\frac{\hbar\omega}{2} + \frac{\hbar\omega}{e^{\hbar\omega/k_BT}-1}\right]. \tag{3.52}$$

From Eq. (3.51) and (3.52), it follows that $\bar{S}_F(\omega)/\tilde{S}_F(\omega) = \coth(\hbar\omega/2k_BT)$, such that the environment temperature is a measure of the asymmetry of the quantum noise.

In the high-temperature limit, Eq. (3.52) reduces to the classical white noise spectrum of Eq. (2.20). From Eq. (2.18), the position noise spectrum of a quantum harmonic oscillator is

$$\bar{S}_x(\omega) = \frac{\hbar\omega}{2m\omega_m^2}\frac{\gamma}{(\omega_m-\omega)^2+(\gamma/2)^2}\left[\frac{1}{2} + \frac{1}{e^{\hbar\omega/k_BT}-1}\right]. \tag{3.53}$$

The distinction from the classical case is that Eq. (3.53) enforces a lower limit on the position noise spectrum, as shown in Fig. 2.2, corresponding to the zero-point fluctuations of the oscillator.

3.3.3 Quantum Langevin Equation Revisited

In quantum optics, however, one expects an equation of motion for the damped harmonic oscillator of the form

$$\dot{a}(t) = -i\omega_m a(t) - \frac{\gamma}{2}a(t) + \sqrt{\gamma}a_{in}(t), \tag{3.54}$$

where $a_{in}(t)$ is the input noise operator defined as

$$a_{in}(t) = \frac{1}{\sqrt{2\pi}}\int_{-\infty}^{+\infty} d\omega e^{i\omega(t-t_0)}a_0(\omega). \tag{3.55}$$

Here $a_0(\omega)$ is the input field at some initial time $t = t_0$, defined such that the input noise commutation relation is $[a_{in}(t), a_{in}^\dagger(t')] = \delta(t-t')$. As we shall see in Sec. 3.3.4, Eq. (3.54) corresponds to Eq. (3.42) in the high-Q limit and after a "rotating-wave approximation" has been made. The input ensemble most closely resembling a classical white noise process is described by

$$\langle a_{in}^\dagger(t)a_{in}(t')\rangle = \bar{n}\,\delta(t-t'), \tag{3.56}$$

with $\bar{n}$ being a measurement of the environment temperature as per Eq. (3.24). A quantum Wiener process is then defined by $A(t,t_0) = \int_{t_0}^t a_{in}(t')dt'$, such that $\left[A(t,t_0), A^\dagger(t,t_0)\right] = t - t_0$ and $\left\langle A^\dagger(t,t_0)A(t,t_0)\right\rangle = \bar{n}(t-t_0)$. We also specify that the distribution of $A(t,t_0)$ is Gaussian; that is, the density operator describing the ensemble of input modes is given by the thermal state of Eq. (3.23). Note that Eq. (3.54) may be derived using a microscopic model of the system and its environment [42].

The solution to Eq. (3.54) is

$$a(t) = a(0)e^{-i(\omega_0 - i\gamma/2)t} + \sqrt{\gamma}e^{-i(\omega_0 - i\gamma/2)t}\int_0^t dt' e^{i(\omega_0 - i\gamma/2)t'} a_{in}(t'). \tag{3.57}$$

The average amplitude is clearly then

$$\langle a(t)\rangle = \langle a(0)\rangle e^{-i(\omega_0 - i\gamma/2)t}. \tag{3.58}$$

The mean energy is determined by

$$\begin{aligned}\langle a^\dagger(t)a(t)\rangle \;&=\; \langle a^\dagger(0)a(0)\rangle e^{-\gamma t} \\ &+\; \gamma e^{-\gamma t}\int_0^t dt_1 \int_0^t dt_2 e^{-i(\omega_0 + i\gamma/2)t_1} e^{i(\omega_0 - i\gamma/2)t_2}\langle a_{in}^\dagger(t_1)a_{in}(t_2)\rangle. \end{aligned}\tag{3.59}$$

To proceed further, we need to use the result

$$\int_0^{t_1} dt' \int_0^{t_2} dt'' f^*(t')f(t'')\langle a_{in}^\dagger(t')a_{in}(t'')\rangle = \int_0^{min(t_1,t_2)} dt' |f(t)|^2\, \bar{n}, \tag{3.60}$$

such that

$$\langle a^\dagger(t)a(t)\rangle = \langle a^\dagger(0)a(0)\rangle e^{-\gamma t} + \bar{n}(1 - e^{-\gamma t}) \tag{3.61}$$

In the steady-state, $\langle a^\dagger(t)a(t)\rangle \to \bar{n}$, which indicates the approach to thermal equilibrium.

The position noise spectrum for the quantum optics Langevin equation may be calculated by first taking the Fourier transform of Eq. (3.54),

$$a(\omega) = \frac{\sqrt{\gamma}}{i\,(\omega_m - \omega) + \gamma/2} a_{in}(\omega), \tag{3.62}$$

with operators in the frequency domain being defined by,

$$a(t) = \frac{1}{2\pi}\int_{-\infty}^{\infty} d\omega e^{-i\omega t}\tilde{a}(\omega). \tag{3.63}$$

and input noise correlations in the frequency domain being

$$\langle a_{in}^\dagger(\omega')a_{in}(\omega)\rangle \;=\; \bar{n}\delta(\omega - \omega'), \tag{3.64}$$

$$\langle a_{in}(\omega')a_{in}^\dagger(\omega)\rangle \;=\; (\bar{n}+1)\delta(\omega - \omega'). \tag{3.65}$$

The analysis of the steady-state of quantum Langevin equations in the frequency domain leads to the input-output formalism of open quantum systems [77, 78]. The position noise spectrum may then be calculated using Eq. (3.62), as

$$\bar{S}_x(\omega) = \frac{\hbar}{2m\omega}\frac{\gamma}{(\gamma/2)^2 + (\omega_m - \omega)^2}\left[\frac{1}{2} + \frac{1}{e^{\hbar\omega/k_B T} - 1}\right]. \tag{3.66}$$

Comparison with Eq. (3.53) shows that the noise spectrum is the same in the vicinity of the resonance frequency.

In terms of the Heisenberg picture position operator of Eq. (3.12), Eq. (3.54) and its Hermitian conjugate may be written as the coupled system of equations,

$$m\dot{\hat{x}}(t) = \hat{p}(t) - \frac{\gamma}{2}m\hat{x}(t) + \sqrt{\gamma}m\hat{x}_{in}(t), \tag{3.67}$$

$$\dot{\hat{p}}(t) = -m\omega_m^2\hat{x}(t) - \frac{\gamma}{2}\hat{p}(t) + \sqrt{\gamma}\hat{p}_{in}(t). \tag{3.68}$$

Comparing Eq. (3.68) with Eq. (3.41), it is clear that the damped harmonic oscillator of quantum optics has position damping (and the associated noise) in addition to the momentum damping of Eq. (3.41). Combining Eqs. (3.67) and (3.68), one finds

$$m\ddot{\hat{x}}(t) + \gamma m\dot{\hat{x}}(t) + m\omega_m^2\hat{x}(t) + \frac{\gamma^2}{4}m\hat{x}(t) = \sqrt{\gamma}\left[\frac{m\gamma}{2}\hat{x}_{in}(t) + 2\hat{p}_{in}(t)\right]. \tag{3.69}$$

The position and momentum damping combine to give the same effective momentum damping as in Eq. (3.42), and there is an additional frequency shift. The noise spectrum of the input noise terms on the right-hand-side of Eq. (3.68) may be calculated as

$$\bar{S}_F(\omega) = 4m\gamma\left[\frac{\hbar\omega}{2} + \frac{\hbar\omega}{e^{\hbar\omega/k_BT} - 1}\right] + \frac{m\gamma^3}{4\omega^2}\left[\frac{\hbar\omega}{2} + \frac{\hbar\omega}{e^{\hbar\omega/k_BT} - 1}\right]. \tag{3.70}$$

In the high-Q limit, this is the result we have in Eq. (3.52) with the replacement $\gamma \to \gamma/2$. This is due to the factor of two difference between the damping rate as conventionally defined in a Brownian motion Langevin equation, as compared with a quantum optical Langevin equation. One may numerically verify that, in the high-Q limit, the dynamics described by Eq. (3.69) approach those described by Eq. (3.42).

3.3.4 Master Equations

In general, to reproduce the full quantum dynamics of a system using the quantum Langevin equation approach, one must solve a hierarcy of moment equations to all orders. An alternative is to write down an equation describing the evolution of the system density operator, and we now consider approaches for doing this.

Formally, an open quantum system evolves on the composite Hilbert space of the system and environment, $\mathcal{H} = \mathcal{H}_S \otimes \mathcal{H}_E$, and we denote the density operator defined on this space by $\rho(t)$. Given a separable initial state, $\rho(0) = \rho_S(0) \otimes \rho_E(0)$, the exact evolution of the reduced density operator of the system, $\rho_S(t) = \mathrm{Tr_E}\ \rho(t)$ where $\mathrm{Tr_E}[\ldots]$ denotes the trace over the environmental degrees of freedom, is given by

$$\rho_S(t) = \mathrm{Tr_E}\left\{\mathrm{U(t)}\left[\rho_\mathrm{S}(0) \otimes \rho_\mathrm{E}(0)\right]\mathrm{U}^\dagger(\mathrm{t})\right\}, \tag{3.71}$$

where $U(t) = e^{-iHt/\hbar}$ is the unitary evolution operator corresponding to the composite system-environment Hamiltonian H.

In general, it is not possible to calculate the exact dynamics according to Eq. (3.71), and we must approximate to make the problem tractable. There are two common approaches, one being based on the Liouville-von Neumann equation and the other based on the use of path integrals.

In the former approach, one obtains a time-local, first-order differential equation for the reduced density operator of the system, known as a master equation. This is the quantum analogue of a classical Fokker-Planck equation. Indeed, under certain conditions, a master equation can be mapped onto a Fokker-Planck equation for a corresponding quantum phase-space distribution function of the type discussed in Sec. 3.2.3.

In the latter approach, the evolution of the system is expressed in terms of a path integral, or propagator [79]. The evolution of the reduced density matrix of the system may be expressed as a path integral in terms of the so-called Feynman-Vernon influence functional. Historically, the path integral approach was widely used in the development of the theory of open quantum systems: prominent examples include the mapping between different environment models [80], the formulation of quantum Brownian motion [81] and of macroscopic quantum tunneling [82], and the discussion of continuous measurement [83]. However, due to the greater generality, the calculations tend to be more complicated than those required in the master equation approach.

3.3.5 Born-Markov Master Equation

The Born-Markov master equation is an equation that is both widely applicable and mathematically tractable, and its derivation is now outlined [67]. Both the well-known quantum Brownian motion master equation and the quantum optics master equation shall emerge as special cases. Suppose that the system is described by the Hamiltonian H_S, the environment is described by H_E, and the system-environment interaction is described by H_I. Moving to an interaction picture with respect to $H_S + H_E$, the time-evolution of the density matrix is described by the Liouville-von Neumann equation,

$$\frac{d}{dt}\rho(t) = -\frac{i}{\hbar}\left[H_I(t), \rho(t)\right]. \tag{3.72}$$

This equation may be formally integrated iteratively, and then by tracing over the environmental variables and assuming, without loss of generality, that $\mathrm{Tr_E}\left[H_I(t), \rho(0)\right] = 0$,

$$\frac{d}{dt}\rho_S(t) = -\frac{1}{\hbar^2}\int_0^t dt' \mathrm{Tr_E}\left[H_I(t), \left[H_I(t), \rho(t')\right]\right]. \tag{3.73}$$

The assumptions of weak coupling to the environment, a "large" environment and an initial product state justify the so-called Born approximation, that the system and the environment do not become entangled and that the environmental state is unaffected by its interaction with the system, $\rho(t) = \rho_S(t) \otimes \rho_E(0)$.

It is possible to now make the Markov approximation without the form of the system-environment interaction being specified [66], but it shall prove more useful to do so. Assuming that the interaction takes the bilinear form

$$H_I = \sum_i S_i \otimes E_i, \tag{3.74}$$

where S_i are system operators and E_i are environment operators, with environmental correlation functions

$$\mathcal{C}_{ij}(t - t') \equiv \mathrm{Tr_E}\left[E_i(t - t')E_j\rho_E(0)\right], \tag{3.75}$$

then Eq. (3.73) leads to

$$\begin{aligned}\frac{d}{dt}\rho_S(t) &= -\frac{1}{\hbar^2}\int_0^t dt' \sum_{i,j}\{\mathcal{C}_{ij}(t-t')\left[S_i(t)S_j(t')\rho_S(t') - S_j(t')\rho_S(t')S_i(t)\right] \\ &\quad + \mathcal{C}_{ji}(t'-t)\left[\rho_S(t')S_j(t')S_i(t) - S_i(t)\rho_S(t')S_j(t')\right]\}\,. \quad (3.76)\end{aligned}$$

The Markov approximation is that the environment operators are correlated over time-scales short compared with the time-scale for the decay of the system [84]. Accordingly we make the replacement $\rho_S(t') \to \rho_S(t)$ in Eq. (3.76), extend the lower limit on the integral to minus infinity, and make the replacement $t' \to \tau \equiv t - t'$. Then transforming back to the Schrödinger picture, the Born-Markov master equation is

$$\frac{d}{dt}\rho_S(t) = -\frac{i}{\hbar}\left[H_S, \rho_S(t)\right] - \frac{1}{\hbar^2}\sum_i \{[S_i, B_i\rho_S(t)] + [\rho_S(t)C_i, S_i]\}\,, \quad (3.77)$$

where

$$B_i = \int_0^\infty d\tau \sum_j \mathcal{C}_{ij}(\tau)S_j(-\tau), \quad \mathcal{C}_i = \int_0^\infty d\tau \sum_j \mathcal{C}_{ji}(-\tau)S_j(-\tau), \quad (3.78)$$

and $\mathcal{C}_{ij}(\tau)$ are sharply-peaked environmental correlation functions. Henceforth, we shall only be interested in the reduced density operator of the system, and so the "S" subscript shall be dropped.

The so-called Lindblad form of the master equation ensures the positivity of the density matrix [85], and it may be derived from a Born-Markov master equation by making a rotating-wave approximation [66]. The rotating-wave approximation means that we neglect dynamics fast compared with system dynamics. In its most general form, a Lindblad master equation is given by

$$\frac{d}{dt}\rho(t) = -\frac{i}{\hbar}\left[H_S, \rho(t)\right] + \frac{1}{2}\sum_{i,j}\gamma_{ij}\left\{\left[S_i, \rho(t)S_j^\dagger\right] + \left[S_i\rho(t), S_j^\dagger\right]\right\}, \quad (3.79)$$

where γ_{ij} forms the decoherence matrix. Diagonalizing this matrix leads to

$$\frac{d}{dt}\rho(t) = -\frac{i}{\hbar}\left[H_S', \rho(t)\right] + \frac{1}{2}\sum_k \gamma_k\left[2L_k\rho(t)L_k^\dagger - L_k^\dagger L_k\rho(t) - \rho(t)L_k^\dagger L_k\right], \quad (3.80)$$

where L_k are called Lindblad operators and H_S' is the renormalized system Hamiltonian. When the Lindblad operators are Hermitian they correspond to physical observables, and Eq. (3.80) can be written as

$$\frac{d}{dt}\rho(t) = -\frac{i}{\hbar}\left[H_S', \rho(t)\right] - \frac{1}{2}\sum_k \gamma_k\left[L_k, \left[L_k, \rho(t)\right]\right]. \quad (3.81)$$

The second term on the right-hand-side then describes decoherence without dissipation.

Typically, the environment of an open quantum system is modeled as a thermal ensemble of non-interacting harmonic oscillators, $\rho_E(0) = e^{-\beta H_E}/\mathrm{Tr}\left[e^{-\beta H_E}\right]$ where

$$H_E = \sum_i\left(\frac{\hat{p}_i^2}{2m_i} + \frac{1}{2}m_i\omega_i^2\hat{q}_i^2\right), \quad (3.82)$$

with $\hat{q}_i$ and $\hat{p}_i$ denoting the position and momentum, respectively, of the i^{th} environmental oscillator. This provides a good generic model for a dissipative environment; indeed, in the limit of weak coupling to the environment it may be shown that any environment may be mapped onto an oscillator environment [80]. It is also tractable; in the path integral approach the Feynman-Vernon influence functional may be explicitly evaluated, and in the master equation approach, the correlation functions may be evaluated.

Eq. (3.82) describes the environment for the two types of master equation of particular interest, corresponding to quantum Brownian motion and quantum optical systems. These equations differ in the form of the system-environment interaction due to the fact that a rotating-wave approximation is made in the latter case. It is often said that the quantum optical master equation is derived in the weak damping limit, while the quantum Brownian motion master equation is derived in the slow system limit. Although this is true, these regimes can certainly overlap, and both approximations will often be valid.

3.3.6 Quantum Brownian Motion Master Equation

In the case of quantum Brownian motion, it is assumed that a single system position coordinate couples linearly to the position of each environmental oscillator, such that

$$H_I = \hat{x} \otimes \sum_i c_i \hat{q}_i \equiv \hat{x} \otimes E, \tag{3.83}$$

where E is an effective environment operator. The effective environmental correlation function is $\mathcal{C}(\tau) = \nu(\tau) - i\eta(\tau)$, where the so-called noise and dissipation kernels are

$$\nu(\tau) = \hbar \int_0^\infty d\omega J(\omega) \coth \frac{\hbar\omega}{2k_B T} \cos\omega\tau, \qquad \eta(\tau) = \hbar \int_0^\infty d\omega J(\omega) \sin\omega\tau, \tag{3.84}$$

respectively, and the spectral density of the environment is

$$J(\omega) = \sum_i \frac{c_i^2}{2m_i\omega_i} \delta\left(\omega - \omega_i\right). \tag{3.85}$$

Substituting Eq. (3.84) and (3.85) into Eq. (3.77) and (3.78), transforming all operators back to the Schrödinger picture, and assuming that our "system" under consideration is a harmonic oscillator with the Hamiltonian of Eq. (3.10), the master equation describing quantum Brownian motion with a harmonic oscillator system is

$$\begin{aligned} \frac{d}{dt}\rho(t) \;=\; & -\frac{i}{\hbar}\left[\frac{\hat{p}^2}{2m} + \frac{1}{2}k\hat{x}^2 + \frac{1}{2}m\tilde{\omega}^2\hat{x}^2, \rho(t)\right] \\ & - \frac{i\gamma}{\hbar}\left[\hat{x}, \{\hat{p}, \rho(t)\}\right] - \frac{D}{\hbar^2}\left[\hat{x}, [\hat{x}, \rho(t)]\right] - \frac{f}{\hbar}\left[\hat{x}, [\hat{p}, \rho(t)]\right], \end{aligned} \tag{3.86}$$

where the frequency shift and momentum damping are given by

$$\tilde{\omega}^2 = -\frac{2}{\hbar m}\int_0^\infty d\tau \eta(\tau) \cos\omega_m\tau, \qquad \gamma = -\frac{1}{\hbar m\omega_m}\int_0^\infty d\tau\eta(\tau)\sin\omega_m\tau, \tag{3.87}$$

respectively, and the momentum normal-diffusion and anomalous-diffusion coefficients, are

$$D = \int_0^\infty d\tau \nu(\tau) \cos \omega_m \tau, \qquad f = \frac{1}{\hbar m \omega_m} \int_0^\infty d\tau \nu(\tau) \sin \omega_m \tau, \tag{3.88}$$

respectively. The momentum normal-diffusion coefficient describes the monitoring of $\hat{x}$ and so decoherence in the position basis. Note that Eq. (3.87) is not completely positive on short time-scales, though this is not problematic provided that one does not attempt to interpret the equation on such time-scales.

In order to evaluate the coefficients in Eq. (3.87), one must assume some form for the spectral density of Eq. (3.85). An ohmic spectral density, $J(\omega) \propto \omega$, with a high-frequency cut-off, $\Lambda \gg \omega_m$, of the Lorentz-Drude form is often assumed,

$$J(\omega) = \frac{2m\gamma_0}{\pi} \frac{\omega \Lambda^2}{\Lambda^2 + \omega^2}. \tag{3.89}$$

The coefficients may then be evaluated as $\gamma = \gamma_0 \Lambda^2 / \left(\Lambda^2 + \omega_m^2\right)$, $D = \hbar m \gamma \omega_m \coth\left(\hbar\omega_m / 2k_B T\right)$ and $\tilde{\omega}^2 = -2\gamma\Lambda$, while f is assumed to be negligibly small. Considering the high-temperature limit, $k_B T \gg \hbar\omega_m$, one obtains the famous Caldeira-Leggett master equation [81],

$$\begin{aligned} \frac{d}{dt}\rho(t) \; &= \; -\frac{i}{\hbar}\left[\frac{\hat{p}^2}{2m} + \frac{1}{2}m\left(\omega_m^2 - 2\gamma\Lambda\right)\hat{x}^2, \rho(t)\right] \\ &- \; \frac{i\gamma}{\hbar}\left[\hat{x}, \{\hat{p}, \rho(t)\}\right] - \frac{2m\gamma k_B T}{\hbar^2}\left[\hat{x}, \left[\hat{x}, \rho(t)\right]\right]. \end{aligned} \tag{3.90}$$

In the limit of very weak damping, one may write down a Fokker-Planck equation for the corresponding Wigner function [86], $W \equiv W(x,p,t)$, as

$$\begin{aligned} \frac{\partial W}{\partial t} \; &= \; -\frac{\partial}{\partial x}\left(pW\right) + m\omega_m^2 \frac{\partial}{\partial p}\left(xW\right) \\ &+ \; 2\gamma \frac{\partial}{\partial p}\left(pW\right) + m\gamma\omega_m \hbar \coth\frac{\hbar\omega_m}{2k_B T}\frac{\partial^2 W}{\partial p^2}. \end{aligned} \tag{3.91}$$

3.3.7 Quantum Optical Master Equation

In the quantum optical case, it is again assumed that a single system position coordinate couples linearly to the position of each environmental oscillator, though one additionally makes a rotating-wave approximation on this coupling,

$$\begin{aligned} H_I = \hat{x} \otimes \sum_i c_i \hat{q}_i \quad \stackrel{\text{RWA}}{\longrightarrow} \quad H_I \quad &= \quad \frac{\hbar}{2m}\sum_i \frac{c_i}{\sqrt{\omega_m \omega_i}}\left(a \otimes b_i^\dagger + a^\dagger \otimes b_i\right) \\ &= \quad \sum_i \frac{c_i}{2}\left(\hat{x} \otimes \hat{q}_i + \frac{1}{m^2 \omega_m \omega_i}\hat{p} \otimes \hat{p}_i\right), \end{aligned} \tag{3.92}$$

where a and b_i are the annihilation operators corresponding to the system oscillator and the i^{th} environmental oscillator, respectively. The approximation is that we may neglect dynamics fast on the time-scale of system dynamics. Generally speaking, this approximation is not as well justified in the description of a mechanical resonator as it is in an optical setting, though discrepancies become negligible in the high-Q limit.

One may proceed with the derivation of the master equation from Eq. (3.92), by comparing Eq. (3.92) with Eq. (3.74), calculating the environment correlation functions according to Eq. (3.75), and substituting into the Born-Markov master equation of Eq. (3.77). Alternatively, we could simply use the Lindblad form of Eq. (3.79), or make a rotating-wave approximation directly on Eq. (3.87) and neglect the level shift and anomalous diffusion terms. Then the Schrödinger picture quantum optics master equation is

$$\begin{aligned}\frac{d}{dt}\rho(t) &= -\frac{i}{\hbar}\left[\frac{\hat{p}^2}{2m}+\frac{1}{2}k\hat{x}^2,\rho\right]-\frac{\gamma m\omega_m}{4\hbar}\coth\frac{\hbar\omega_m}{2k_BT}\left[\hat{x},\left[\hat{x},\rho(t)\right]\right]-i\frac{\gamma}{4\hbar}\left[\hat{x},\{\hat{p},\rho(t)\}\right]\\ &- \frac{\gamma}{4\hbar m\omega_m}\coth\frac{\hbar\omega_m}{2k_BT}\left[\hat{p},\left[\hat{p},\rho(t)\right]\right]+i\frac{\gamma}{4\hbar}\left[\hat{p},\{\hat{x},\rho(t)\}\right]. \qquad (3.93)\end{aligned}$$

The second and third terms describe momentum diffusion and damping, while the fourth and fifth terms (not present in quantum Brownian motion) describe position diffusion and damping. The additional terms are sufficient to ensure the positivity of Eq. (3.93). The corresponding Fokker-Planck equation for the Wigner function is that of Eq. (3.92), but with the added position damping and diffusion,

$$\begin{aligned}\frac{\partial W}{\partial t} &= -\frac{\partial}{\partial x}(pW)+m\omega_m^2\frac{\partial}{\partial p}(xW)+2\gamma\frac{\partial}{\partial p}(pW)+m\gamma\omega_m\hbar\coth\frac{\hbar\omega_m}{2k_BT}\frac{\partial^2 W}{\partial p^2}\\ &+ 2\gamma\frac{\partial}{\partial x}(xW)+\frac{\hbar\gamma}{m\omega_m}\coth\frac{\hbar\omega_m}{2k_BT}\frac{\partial^2 W}{\partial x^2}. \qquad (3.94)\end{aligned}$$

In terms of the (Heisenberg picture) quadratures of Eq. (3.16), Eq. (3.93) is

$$\begin{aligned}\frac{d}{dt}\rho(t) &= -\frac{i}{\hbar}\left[\frac{\hbar\omega_m}{4}\left(\hat{X}^2+\hat{P}^2\right),\rho\right]\\ &- \frac{\gamma}{4}(\bar{n}+1/2)\left[\hat{X}(t),\left[\hat{X}(t),\rho\right]\right]-\frac{\gamma}{4}(\bar{n}+1/2)\left[\hat{P}(t),\left[\hat{P}(t),\rho\right]\right]\\ &- i\frac{\gamma}{8}\left[\hat{X}(t),\left\{\hat{P}(t),\rho\right\}\right]+i\frac{\gamma}{8}\left[\hat{P}(t),\left\{\hat{X}(t),\rho\right\}\right], \qquad (3.95)\end{aligned}$$

where $\bar{n}$ is the thermal occupation of the environment, given by a Bose-Einstein distribution evaluated at the frequency of the system harmonic oscillator. In terms of the Schrödinger picture raising and lowering operators of Eq. (3.8), it takes the familiar form

$$\begin{aligned}\frac{d}{dt}\rho(t) &= -\frac{i}{\hbar}\left[\hbar\omega_m a^\dagger a,\rho\right] \qquad (3.96)\\ &+ \gamma(\bar{n}+1)\left(a\rho a^\dagger-\frac{1}{2}a^\dagger a\rho-\frac{1}{2}\rho a^\dagger a\right)+\gamma\bar{n}\left(a^\dagger\rho a-\frac{1}{2}aa^\dagger\rho-\frac{1}{2}\rho aa^\dagger\right).\end{aligned}$$

Using Eq. (3.47) and (3.52), this may be expressed as

$$\begin{aligned}\frac{d}{dt}\rho(t) &= -\frac{i}{\hbar}\left[\hbar\omega_m a^\dagger a,\rho\right]+\mathrm{Re}\left[S_F(+\omega_m)\right]\left(a\rho a^\dagger-\frac{1}{2}a^\dagger a\rho-\frac{1}{2}\rho a^\dagger a\right)\\ &+ \mathrm{Re}\left[S_F(-\omega_m)\right]\left(a^\dagger\rho a-\frac{1}{2}\rho aa^\dagger-\frac{1}{2}aa^\dagger\rho\right). \qquad (3.97)\end{aligned}$$

More general forms of quantum optics master equation are sometimes quoted, accounting for level shifts and/or a phase-dependent bath [48]. Also, one may rewrite the master equations of Eq. (3.93) and (3.97) in the interaction picture by replacing each Schrödinger picture system operator with its Heisenberg picture equivalent, and by removing the harmonic oscillator Hamiltonian terms.

3.4 Dissipation via Phonon Tunneling

Nanomechanical resonators are primarily damped by excitation of short-wavelength phonon modes in bulk material that provides the support for the beam [87]. This may be treated using standard methods for bosonic baths. For very small beams, with large surface area to volume ratios, the low temperature dissipation may also be influenced by two-level systems corresponding to elastic defects in the beam [88]. We will neglect this source of dissipation and focus on the dissipation due to the supports, following the phonon-tunnelling model of Wilson-Rae [87]. Experiments have verified the validity of this theory [39, 40].

The elastic energy of the flexural mode decays through inducing stresses in the bulk material at the supports of the beam. This can be treated as weak phonon tunnelling in the limit that $k_0 d \ll 1$ where k_0 is the wavevector of the flexural mode and d is the length scale for the contact area between the beam and the support. In this limit we can approximate the Hamiltonian for the system by

$$H = \hbar\omega_0 b_0^\dagger b_0 + \hbar(b_0 + b_0^\dagger) \int dq\, \xi(q)\ \left[b(q) + b^\dagger(q)\right] + \int dq\, \hbar\omega(q) b^\dagger(q) b(q), \tag{3.98}$$

where b_0 annihilates a phonon in the mechanical resonator flexural mode with mode function $u_0(r) = u(q_0, r)$ and the coupling constant determines the bath spectral density function,

$$J(\omega) = 2\pi \int dq |\xi(q)|^2 \delta\left[\omega - \omega(q)\right]. \tag{3.99}$$

Under the weak tunnelling approximation this is given by

$$J(\omega) \approx \frac{\pi}{2\rho_s^2 \omega_0 \omega} \int dq \left| \int_S dr^2 \left[\underline{u}_0(\underline{r}) \cdot \underline{\sigma}_q(\underline{r}) - \underline{u}_q(\underline{r}) \cdot \underline{\sigma}_0(\underline{r})\right] \cdot \hat{n} \right|^2 \times \delta[\omega - \omega(q)], \tag{3.100}$$

where $\underline{u}_q(\underline{r})$ and $\underline{\sigma}_q(\underline{r})$ are the displacement and stress fields associated with bulk phonon modes while $\underline{u}_0(\underline{r})$ and $\underline{\sigma}_0(\underline{r})$ are the corresponding fields for the beam resonator mode, S is the contact area between the beam and the support while ρ_s is the density of the support substrate. Careful fabrication can be used to engineer this spectral density to a considerable degree [89].

If we further assume that the mechanical frequency is very high compared to the typical time scale of the tunnelling interaction, we may assume a master equation taking the form of Eq. (3.97) with $\gamma = J(\omega_0)$.

4 Quantum Optomechanical Systems

In optomechanical systems, an optical field is used for the measurement and control of the mechanical resonator. The optical field is usually confined within a cavity, providing resonant enhancement of the field strength and sensitivity to mechanical displacements.

4.1 Optomechanical Couplings

An optical field may couple to a mechanical resonator through the effects of radiation pressure, via optical gradient forces, via the Doppler effect, or via photothermal forces. Radiation pressure is a scattering force that arises due to the reflection of light, which of course, has some momentum associated with it. Optical gradient forces (also known as dipole forces) arise from the spatial variation of optical intensity. The Doppler effect is typically very weak [90], requiring a mirror with a strong dependence of reflectivity on wavelength [91]. Further, photothermal effects, arising from temperature gradients induced by the uneven absorption of light, are inherently dissipative [92]. Thus, for the consideration of quantum optomechanical systems, we shall focus on radiation pressure and optical gradient forces.

Radiation pressure was first demonstrated experimentally over one hundred years ago [93, 94]. The static effect of radiation pressure on an optomechanical cavity is bistability [95]. The dynamic effect of radiation pressure, associated with a finite cavity lifetime, is a frequency shift and a modified damping of the mechanical resonator [96, 97].

The simplest optomechanical system in which radiation pressure provides the dominant optomechanical coupling is a Fabry-Pérot cavity in which one of the mirrors is mechanically compliant, as depicted in Fig. 4.1(a). This coupling is typically dispersive, meaning that the primary effect of the mechanical motion is to shift the resonance frequency of the optical cavity. A micromechanical cavity or waveguide, in which the optical field is confined within the structure having the mechanical degree of freedom, also leads to the same type of radiation pressure coupling. Within dielectric waveguides, an optomechanical coupling can arise from photoelastic scattering and electrostriction. This coupling may also be employed for excitation [98] or for cooling [99].

The other type of forces that we shall consider are optical gradient forces. They have long been utilized for the manipulation of small particles via optical tweezers [101]. Large optical intensity gradients often exist outside the tightly confined field of a microcavity. This field is known

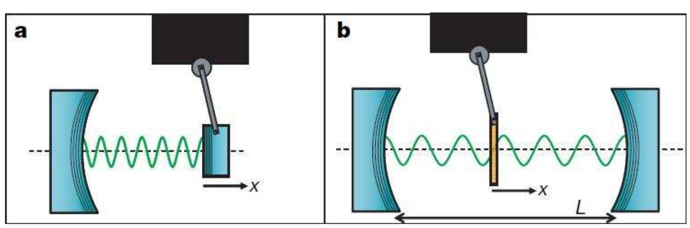

Fig. 4.1. (a) An optomechanical Fabry-Pérot cavity. (b) An optomechanical "membrane-in-the-middle" cavity. Reprinted by permission from McMillan Publishers Ltd: Nature [100], copyright 2008.

as an evanescent field, and placing a mechanical resonator in this field leads to the possibility of large optical gradient forces [102]. These evanescently-coupled optomechanical systems typically exhibit both a dispersive and reactive coupling. The primary effect of the reactive coupling is to modify the cavity damping rate.

4.1.1 Dispersive Coupling

We first consider the optomechanical coupling in the simplest case, a Fabry-Pérot cavity in which one of the mirrors is mechanically compliant. The motion of the mechanical resonator will change the length of the optical cavity, and so change the cavity's resonance frequency. Thus, the coupling is readily calculated by determining the dependence of the cavity resonance frequency on the displacement of the mechanical component [103, 104]. It will turn out that the same form of Hamiltonian coupling can emerge for a nanomechanical resonator coupled to a microwave circuit, or for a membrane in a cavity that couples to an optical field by spatial modulation of the cavity's refractive index.

Suppose that the Hamiltonian of the coupled system is

$$H = \hbar\omega_c(x)a^\dagger a + \hbar\omega_m b^\dagger b, \tag{4.1}$$

where a and b are the annihilation operators for the cavity mode and the mechanical mode, respectively, and x is the displacement of the mechanical mode. A resonant cavity mode must have $n\lambda_n = 2L$ for some integer n, where λ_n is the wavelength of the relevant optical mode and L is the length of the cavity. Then the resonance frequency of the cavity is $\omega_c = n\pi c/L$. Now allowing some displacement such that the new cavity length is $L + x$, the resonance frequency of the cavity is

$$\omega_c(x) = \frac{n\pi c}{L + x} = \omega_c\left[1 - \frac{x}{L}\right], \tag{4.2}$$

and the Hamiltonian of Eq. (4.1) becomes

$$H = \hbar\omega_c a^\dagger a + \hbar\omega_m b^\dagger b - \hbar\kappa a^\dagger a x \qquad \text{where} \qquad \kappa = \frac{\omega_c}{L}. \tag{4.3}$$

This coupling has units of $\mathrm{s}^{-1}\mathrm{m}^{-1}$. One can write $x = \Delta x\left(b + b^\dagger\right)$, to get the single photon optomechanical coupling,

$$\kappa_0 = \omega_c \frac{\Delta x}{L}, \tag{4.4}$$

with the associated Hamiltonian being

$$H = \hbar\omega_c a^\dagger a + \hbar\omega_m b^\dagger b - \hbar\kappa_0 a^\dagger a\left(b + b^\dagger\right). \tag{4.5}$$

Alternatively, this radiation pressure coupling may be rigorously derived by quantizing an electromagnetic field with time-varying boundary conditions [105]. A Hamiltonian of this form applies not only to optomechanical Fabry-Pérot cavities, but also to micromechanical cavities, such as a microtoroidal cavity where the length L may be identified as the circumference of the microtoroid. Evanescently-coupled optomechanical systems will also give rise to a dispersive shift of the cavity resonance frequency. Indeed, such couplings can be made very large as the effective length in the coupling κ can be much smaller than the physical dimensions of the cavity involved.

As the cavity must be of the order of the wavelength the coupling has a natural upper bound. The micro-mechanical resonator in the optomechanical Fabry-Perot experiment of Aspelmeyer [106] had an effective mass of $m = 145$ng and a resonant frequency of $\omega_m = 2\pi \times 947$kHz. The ground state uncertainty is then $\Delta_0 = 2.4 \times 10^{-16}$m. The cavity length was $L = 2.5$mm and the optical cavity resonance frequency was $\omega_c = 2\pi \times 2.82 \times 10^{14}$ giving an effective vacuum coupling strength of about $\kappa_0 = 2\pi \times 2.7$ Hz. Stronger couplings have been obtained in other systems, such as by the Painter group at Caltech using optomechanical crystal structures [107]. They obtained a coupling as high as $\kappa_0 = 2\pi \times 4 \times 10^5$ Hz.

A situation commonly encountered is where the cavity is strongly driven to some large coherent amplitude $\alpha \equiv \langle a \rangle$. Suppose that the cavity is driven at a frequency ω_d, detuned from the cavity resonance by $\delta_d \equiv \omega_c - \omega_d$ and with an input power P_{in}. It is assumed that the optomechanical coupling is sufficiently weak that $|\kappa x| \ll \delta_d$ or $\gamma_c/2$ at all times. Then if the cavity damping is given by γ_c, the number of photons in the cavity in the steady-state is

$$n_c \equiv |\alpha|^2 = \frac{P_{in}}{\hbar\omega_d} \frac{\gamma_c}{\gamma_c^2 + 4\delta_d^2}. \tag{4.6}$$

Assuming that the phase of the drive is set such that the steady-state amplitude α is real, then in a rotating frame and a displaced picture with $a \to \alpha + \hat{a}$, the Hamiltonian is

$$H = \hbar\delta_d \hat{a}^\dagger \hat{a} + \hbar\omega_m b^\dagger b - \hbar\kappa |\alpha|^2 x + \hbar g \left(\hat{a} + \hat{a}^\dagger\right) x, \tag{4.7}$$

where the effective optomechanical coupling is now written as

$$g \equiv \kappa\alpha = \frac{\omega_c}{L} \sqrt{\frac{P_{in}}{\hbar\omega_d}} \sqrt{\frac{\gamma_c}{\gamma_c^2 + 4\delta_d^2}}. \tag{4.8}$$

The regime of strong optomechanical coupling $(g > \gamma_c, \gamma_m)$ leads to the emergence of optomechanical normal-mode splitting [108].

It shall prove useful to distinguish two distinct regimes of operation of optomechanical systems: the adiabatic regime (also known as the "bad-cavity" limit) where $\gamma_c \gg \omega_m$, and the resolved-sideband regime (also known as the "good-cavity" limit) where $\omega_m \gg \gamma_c$. In the latter case, the effects of dynamical back-action (associated with the finite cavity lifetime) are more pronounced.

An alternative system consists of a partially transparent dielectric membrane between the mirrors of a rigid Fabry-Pérot cavity; a "membrane-in-the-middle" setup [100]. This is depicted in Fig. 4.1(b). In this case, the resonance frequency of the cavity depends periodically on the position of the membrane x as [109]

$$\omega_c(x) = \frac{c}{L} \cos^{-1}\left[|r| \cos\frac{4\pi x}{\lambda_d}\right], \tag{4.9}$$

where r is the reflectivity of the membrane. Most importantly, at an extremum of $\omega_c(x)$, the optomechanical coupling is proportional to the position squared, as $\hbar\frac{1}{2}\omega_c''(0) x^2 a^\dagger a$. In the rotating-wave approximation, the coupling is proportional to the phonon number operator, such that the Hamiltonian is

$$H = \hbar\omega_c(0) a^\dagger a + \hbar\omega_m b^\dagger b + \hbar\omega_c''(0)(\Delta x)^2 \left(b^\dagger b + \frac{1}{2}\right) a^\dagger a. \tag{4.10}$$

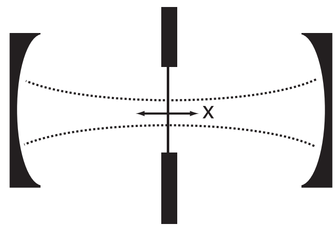

Fig. 4.2. A “membrane-in-the-middle” optomechanical system based on an intracavity dielectric membrane. The cavity frequency, $\omega(x)$, varies as the membrane is displaced from equilibrium [110].

Then the possibility of the measurement and conditional generation of Fock states, and the observation of quantum jumps, emerges in these systems.

4.1.2 Coupling via Refractive Index Modulation

The third implementation we will consider, pioneered by the Harris group [110], is based on the spatial modulation of the refractive index of the cavity using a suspended SiN membrane, which vibrates like a drum head, in the middle of a Fabry-Perot cavity, see Fig. 4.2.

The dielectric membrane displacement modulates the cavity frequency $\omega(x)$. We again expand this to lowest non-zero order in x. This gives an interaction which is linear in x if $\omega(x)$ has a maximum slope at $x = x_0$ or quadratic in x if $\omega(x)$ corresponds to an extremum at $x = x_0$. The linear case gives the standard radiation pressure coupling with $G_0 \sim 10^{-3}$Hz. The quadratic case gives an interaction Hamiltonian of the form

$$H = \hbar\omega_c a^\dagger a + \hbar\omega_m b^\dagger b + \hbar\frac{\chi}{2}a^\dagger a(b + b^\dagger)^2. \tag{4.11}$$

In [111] the optomechanical coupling is $\chi = 10$Hz for an incident power of 10μW. In the interaction picture, we neglect rapidly oscillating terms and write

$$H_I = \hbar\omega_c a^\dagger a + \hbar\omega_m b^\dagger b + \hbar\chi a^\dagger a b^\dagger b. \tag{4.12}$$

The important point here is that the interaction commutes with the phonon number operator, $b^\dagger b$, suggesting that one can use this to make a quantum nondemolition (QND)measurement [112] of the energy of the mechanical resonator. We will discuss this in more detail in Sec. 8.5.

4.1.3 Dispersive Coupling: Sideband Transitions

From a semi-classical perspective, the cavity field experiences a periodic modulation of the detuning (frequency modulation). To see this, we can move to an interaction picture for the mechanical resonator to obtain the Hamiltonian,

$$H_{om} = \hbar G_0 a^\dagger a(be^{-i\omega_m t} + b^\dagger e^{i\omega t}). \tag{4.13}$$

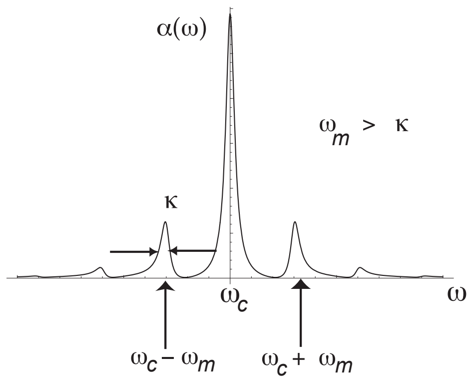

Fig. 4.3. The cavity spectrum due to a periodic modulation of the cavity detuning by the mechanical resonator results in sidebands at multiples of the mechanical frequency, ω_m. Each peak has the same linewidth as the cavity (κ) and an amplitude determined by Bessel functions.

If the mechanical resonator is driven into a steady-state oscillation with amplitude $\beta(t) = \beta_0 e^{-i\omega_m t}$, we can make the semi-classical replacement $b \to \beta$. The semi-classical cavity Hamiltonian is then

$$H_{sc} = \hbar\omega_c a^\dagger a + \hbar\Delta(t) a^\dagger a, \tag{4.14}$$

where

$$\Delta(t) = G_0(\beta e^{-i\omega_m t} + \beta^* e^{i\omega t}) \equiv D\cos(\omega_m t), \tag{4.15}$$

where we have taken β to be real for convenience and define $D = 2G_0\beta$ as the modulation amplitude. We can solve the Heisenberg equation of motion for the classical field amplitude $\alpha(t)$ to obtain,

$$\alpha(t) = \alpha(0) e^{-i\omega_c t - i(D/\omega_m)\sin(\omega_m t)}. \tag{4.16}$$

This periodic function can be expanded as a Fourier series in terms of Bessel functions. Using a Jacobi-Anger expansion, we find

$$a(t) = a(0) e^{-i\omega_c t} \sum_{n=-\infty}^{\infty} J_n(D/\omega_m)\, e^{in\omega_m t}. \tag{4.17}$$

:make Thus if we now weakly drive the cavity we should expect to see a spectrum that has peaks at $\omega = \omega_c \pm n\omega_m$; that is, the cavity acquires sidebands at multiples of ω_m. These peaks will have the width of the cavity decay rate κ. If $\omega_m > \kappa$ the sidebands can be resolved as distinct sidebands, as shown in Fig. 4.3. This is called the "resolved sideband" or "good cavity" limit.

Another way to increase the optomechanical coupling is to drive the cavity so that a large steady state amplitude can build up. The small phase shift induced by the optomechanical coupling then appears as a displacement of the cavity field amplitude. We can describe this by linearising the quadratic radiation pressure interaction, resulting in an interaction that is linear in the cavity field amplitude.

The master equation of a driven cavity, in the interaction picture at the cavity driving frequency, is given by

$$\frac{d\rho}{dt} = -i\delta[a^\dagger a, \rho] - i\epsilon[a + a^\dagger, \rho] + \kappa\mathcal{D}[\rho], \tag{4.18}$$

where $\mathcal{D}[A]\rho = A\rho A^\dagger + A^\dagger A\rho/2 + \rho A^\dagger A/2$ and $\delta = \omega_c - \omega_D$. The steady-state amplitude of the cavity field is the coherent state with amplitude

$$\alpha_0 = -\frac{i\epsilon}{\kappa/2 + i\delta}. \tag{4.19}$$

If we now include a weak optomechanical radiation pressure coupling, we expect the cavity field to remain near a coherent state. Accordingly, we make the canonical transformation to a displaced picture by $a \to \alpha_0 + \bar{a}$ and expand the Hamiltonian of Eq. (4.5) (now in an interaction picture) to linear order in $a, a^\dagger$. We find

$$H = \hbar\delta\bar{a}^\dagger\bar{a} + \hbar\omega_m b^\dagger b - \hbar G_0(\alpha_0\bar{a}^\dagger + \bar{a}\alpha_0^*)(b + b^\dagger) - \hbar G_0|\alpha_0|^2(b + b^\dagger). \tag{4.20}$$

The last terms is a linear constant force acting on the mechanics and will impart a small displacement of the mechanical resonator's equilibrium position. It shall be ignored, and we will work with the quadratic interaction, $\hbar g(a + a^\dagger)(b + b^\dagger)$, where we have fixed the phase of the driving field to make α_0 real and dropped the bars for convenience. The new coupling rate $g = -G_0\alpha_0$ is now enhanced by a factor that is the square root of the steady-state photon number inside the cavity.

The sideband spectrum motivates an approximation scheme based on driving the system with a laser detuned exactly to one or the other sideband, in the resolved-sideband limit. Starting with linearised interaction Hamiltonian,

$$H = \hbar\delta a^\dagger a + \hbar\omega_m b^\dagger b + \hbar g(a^\dagger + a)(b + b^\dagger), \tag{4.21}$$

we move to (another) interaction picture for both the cavity and the mechanics,

$$H = \hbar g(ae^{-i\delta t} + a^\dagger e^{i\delta t})(be^{-i\omega_m t} + b^\dagger e^{i\omega_m t}). \tag{4.22}$$

If we now drive the cavity on the blue sideband $\delta = -\omega_m$, such that $\omega_D = \omega_c + \omega_m$, and make the rotating-wave approximation (assuming $g < \omega_m$), we can approximate the interaction via the *blue sideband* Hamiltonian,

$$H_b = \hbar g(ba + b^\dagger a^\dagger). \tag{4.23}$$

Such a Hamiltonian excites both the cavity and the mechanics via Raman transitions that down convert laser pump photons to the cavity resonance and simultaneously emits a phonon into the mechanics. Quadratic Hamiltonians of this kind are known as two-mode squeezing interactions [113].

If we tune the laser to the red sideband such that $\delta = \omega_m$, and then $\omega_D = \omega_c - \omega_m$, the approximate Hamiltonian under the same assumptions as above is

$$H_r = \hbar g(ba^\dagger + b^\dagger a). \tag{4.24}$$

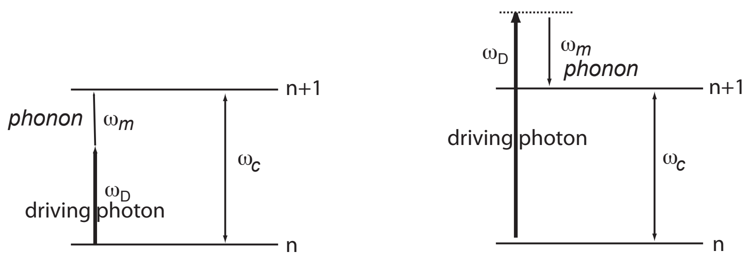

Fig. 4.4. A diagram representing the red (left) and blue (right) sideband transitions.

This process excites cavity photons by a Raman process that absorbs a mechanical phonon and a laser photon. This kind of process can cool the mechanics. A diagrammatic representation of the red and blue sideband processes is given in Fig. 4.4.

Finally, we could choose "two-tone" driving, simultaneously exciting the red and blue transitions [114]. In that case the effective Hamiltonian is

$$H_{rb} = \hbar g(a + a^\dagger)(be^{-i\phi} + b^\dagger e^{i\phi}) \tag{4.25}$$

where ϕ is the relative phase of two driving fields. This Hamiltonian commutes with a quadrature of the mechanical position operator, and thus implements a quantum nondemolition measurement of such a quadrature. Which quadrature is measured is determined by the choice of ϕ.

4.1.4 Dissipative Coupling

One can also consider the situation in which the motion of the mechanical resonator modulates the damping rate of the cavity, instead of or in addition to, modulating the resonance frequency of the cavity. Accounting for both, the Hamiltonian coupling is [115]

$$H = -\hbar\kappa a^\dagger a x - i\hbar\left[\frac{1}{2\gamma_c}\sqrt{\frac{\gamma_c}{2\pi\rho}}\sum_i\left(a^\dagger b_i - b_i^\dagger a\right)\right]\frac{d\gamma_c}{dx}\,x, \tag{4.26}$$

where ρ is an environmental density of states, and b_i is the annihilation operator of the i$^{\text{th}}$ environmental mode. Such couplings have been investigated experimentally in evanescently-coupled optomechanical systems [116].

4.2 Macro-optomechanical Systems

Optomechanical systems have a long history, dating back to early attempts at gravitational wave detection. An interferometric gravitational wave detector is formed from a Michelson interferometer, with a resonant Fabry-Pérot cavity in each arm, as shown in Fig. 4.5. The end-mirrors are suspended from wires and, in the absence of optical fields, behave as free masses. The field of a gravitational wave produces tidal forces, and so should change the interferometer arm-length difference. The recombined light output from the interferometer is proportional to the arm-length difference as a fraction of the interferometer length, referred to as the gravitational wave strain. Clearly, the suspended end-mirrors and the cavity field form a very large optomechanical system.

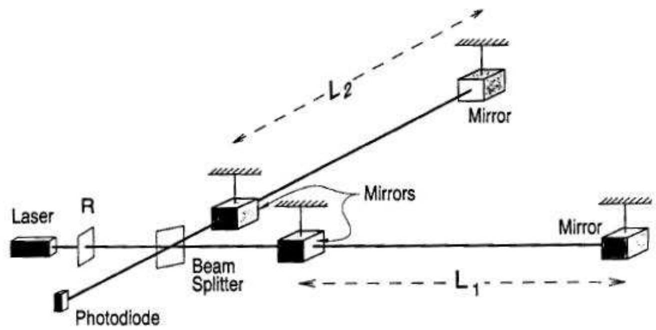

Fig. 4.5. Schematic of the setup of an interferometric gravitational wave detector. Figure reproduced from [117].

The interferometers of LIGO [118] have reached an astounding displacement sensitivity of $10^{-18}\mathrm{m}$ [119]. Beyond searches for gravitational waves, feedback cooling of the suspended end-mirrors of LIGO has been demonstrated [120]. The enhancement of the gravitational wave observatory GEO600 using squeezed light has been demonstrated [121]. A number of experiments have been conducted on small-scale optomechanical systems formed from a suspended free mass. In general, the optical field will provide a harmonic potential and a damping of the mechanical mode; forming a so-called optical spring. The direct observation of an optical spring effect in a detuned Fabry-Pérot cavity has been achieved [122]. A stable radiation-pressure dominated trap for a macroscopic mirror has been created from two frequency offset laser fields [123], and feedback cooling of a suspended gram-scale mirror has been demonstrated [124, 125].

4.3 Micro-optomechanical Systems

As for electromechanical systems, to enter the quantum regime, we need to consider smaller and faster mechanical systems. Here, we consider micro-optomechanical systems. Again, experimental progress in this field is largely driven by applications, particularly in sensing technology.

Micro-optomechanical Fabry-Pérot cavities have incorporated silicon mechanical resonators [126, 127] or commercial micro-cantilever probes with mirror coatings applied [128]. Mechanical resonators have also been formed from free-standing Bragg mirrors [129], or Bragg mirrors coated onto silicon nitride resonators [130]. Membrane-in-the-middle systems have employed both commerical [100] and stoichiometric [131] membranes. Micromechanical waveguides and cavities are usually formed from silica, silicon [132] or silicon nitride [133].

Actuation of the mechanical component of a micro-optomechanical system may be required for calibration of the optical displacement transducer or for cooling of the mechanical resonator. Actuation to higher amplitudes is required to create an oscillator for sensing applications, or to observe nonlinear dynamics. Optical actuation is typically achieved by frequency-modulation of an optical field at near the mechanical resonance frequency. In general, both photothermal effects and radiation pressure effects will contribute to the actuation, though typically one wishes to engineer the system such that the contribution from dissipative photothermal processes is neg-

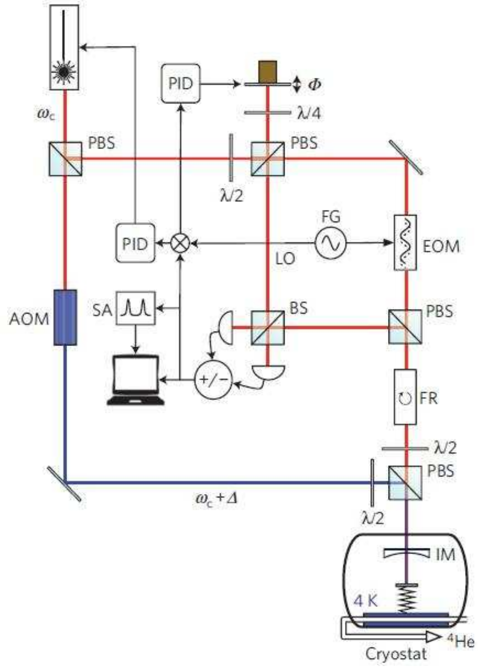

Fig. 4.6. Experimental setup for the back-action cooling of a micromechanical resonator in a cryogenic environment. The Fabry-Pérot cavity is driven on its red-detuned sideband for cooling, with the detuning provided by an acousto-optic modulator. The displacement is independently monitored by a resonant probe of the cavity, locked to a reference cavity by the Pound-Drever-Hall technique. The reflection of the resonant probe is monitored via homodyne detection. Reprinted by permission from McMillan Publishers Ltd: Nature Physics [130], copyright 2009.

ligible. In low-frequency applications, the use of a piezoelectric drive is feasible [134]. Optical gradient forces in evanescent fields have also been used for actuation [133, 132, 135]. A variation of this technique has used gradients produced by electric fields [136].

4.3.1 Fabry-Pérot Cavities

In optomechanical Fabry-Pérot cavities, shot-noise-limited displacement sensing based on homodyne detection [137] or on frequency-modulation detection [138] have been demonstrated. An experimental setup for such a system is depicted in Fig. 4.6. Feedback cooling with actuation via modulation of the radiation pressure of light [126, 128], via electrostatic actuation [139], and via piezoelectric actuation [134] have all been demonstrated. Back-action cooling of a micromechanical cantilever via photothermal pressure [140], and of a micro-mirror via radiation pressure [127, 129] have been achieved. Resolved-sideband radiation pressure back-action cooling has been achieved in a cryogenic environment [130]. The same group has demonstrated strong optomechanical coupling, and the associated normal-mode splitting [108].

Strong dispersive optomechanical coupling and cooling has also been demonstrated in the

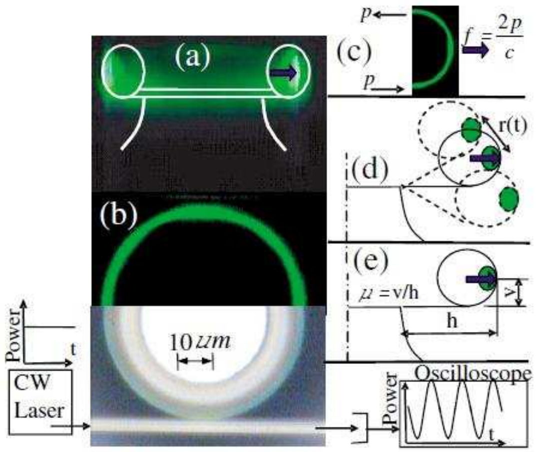

Fig. 4.7. A microtoroid optomechanical system. (a) An optical field is confined in the microtoroid cavity. (b) Light is coupled into and out of the cavity using a tapered fiber. The radiation pressure of light in a whispering gallery mode of the microtoroid exerts a radiation pressure force on the structure (c), and so can amplify or damp the oscillation of a mechanical mode (d). Reprinted figure with permission from [149]. Copyright 2005 by the American Physical Society.

membrane-in-the-middle system [100]. A subsequent experiment exploited avoided crossings of the transverse optical modes of the cavity to realize couplings linear, quadratic and quartic in the membrane displacement [141]. The tunability is attained in situ by adjusting the tilt and position of the membrane. This technique allowed much stronger quadratic coupling. Membrane-in-the-middle systems with stoichiometric silicon nitride membranes have also been created, with higher-order mechanical modes cooled by selectively probing individual antinodes using the field of a Fabry-Pérot cavity [131]. A related group of experiments uses centre-of-mass motional modes of an ensemble of cold atoms as the mechanical resonator. Sub-wavelenght positioning of the ensemble has facilitated tunable linear and quadratic couplings [142]. Ponderomotive light squeezing [143] and motional sideband spectroscopy have also been demonstrated in this system [144].

Taking these systems to their limit, one can imagine that the mechanical oscillator be supported optically rather than mechanically [146, 145]. Indeed, millikelvin feedback cooling of the high-frequency centre-of-mass motion of an optically trapped microsphere in vacuum was recently demonstrated [147]. One could even imagine extending such experiments to the domain of living organisms [148].

4.3.2 Micromechanical Cavities and Waveguides

Another class of optomechanical systems is formed by micromechanical cavities and waveguides. Here the optical field is confined within the structure that possesses the mechanical degree of freedom. Perhaps the most well-known example is the microtoroidal cavity [150, 151], with the optical component being the whispering gallery mode of the toroid and the mechanical modes being formed by the breathing modes or crown modes of the microtoroid surface. This is depicted in Fig. 4.7. A tapered optical fiber is used to excite the optical modes in the microtoroid through evanescent coupling. Then the radiation pressure of the confined light exerts a force on the toroid which may be used to drive mechanical motion. Radiation-pressure-induced oscillations [149, 152] and back-action cooling have both been demonstrated [153]. The motion of the microtoroid can be transduced through intensity modulation of the input optical field that is operated at the full-width at half-maximum of the cavity transmission spectrum, or by phase modulation of a resonant optical probe. Subsequent experiments demonstrated resolved-sideband cooling of the mechanical mode, starting from room temperature [154], and then with cryogenic pre-cooling [156] down close to the quantum ground state [155]. A modified, spoked design has facilitated cooling to 1.7 quanta, with pulsed optical excitation revealing coherent state swapping between the mechanical and the optical mode. Mechanical nonlinearities have been observed [157], optomechanically induced transparency has been demonstrated [158], and crystalline microtoroid cavities have been studied [159].

Resolved-sideband cooling of a microspherical cavity mode has also been demonstrated [160]. The mechanical oscillations of a deformed silica microsphere are coupled to optical whispering-gallery modes that can be excited and detected by free-space evanescent coupling. An extension of these experiments would be to an optically levitated nanosphere [161].

An electrically-controlled microtoroid has been created, with electrical control via a sharp electrode above the microtoroid and a grounded flat electrode beneath it [136]. The microtoroid is polarized by a dc voltage, and a radio-frequency voltage creates a gradient force for driving. Feedback cooling has been demonstrated in this system. Regenerative amplification and linewidth narrowing via delayed electrical feedback has been achieved [162], as has feedback-enhanced sensitivity [163] and amplification via optical backaction [164].

Mechanical oscillation and cooling actuated by optical gradient forces has been demonstrated in a strongly-coupled pair of concentric silica disks with a nano-scale gap [165]. The possibility of phonon laser action in a coupled microtoroid system has been studied [166]. Here, the system consists of two evanescently-coupled microtoroids, driven and monitored via a common tapered fiber.

A variation on these systems is where the micromechanical element is an optical waveguide rather than a cavity. One example of such a micromechanical waveguide is a single-mode beam that may be driven by evanescent coupling to the substrate and transduced by monitoring the transmission through it [132, 167]. High-amplitude operation of a bistable mechanical resonator that forms part of a ring resonator has been demonstrated, along with its demonstration as a non-volatile mechanical memory [168].

Evanescently-coupled pairs of micromechanical waveguides have also been demonstrated, taking the form of adjacent beams [169, 170] or rings [171]. If the waveguides are patterned with an array of etched holes, the optical modes can be localized, forming a so-called zipper cavity [172]. The in-plane differential motion of the beams is strongly coupled to the optical cavity field. Coherent mixing of mechanical excitations has been demonstrated in the zipper cavity and the double-microdisk resonator [173].

Further, a planar, doubly-clamped silicon "optomechanical crystal" has been demonstrated that is capable of co-localizing and strongly dispersively coupling photons and phonons [174]. Again, a tapered fiber allows actuation and detection of the motion of the resonators in these experiments. Although photonic crystals are well-known, phononic crystals have also been developed recently [175]. More recently, laser cooling of a mechanical mode in such an op-

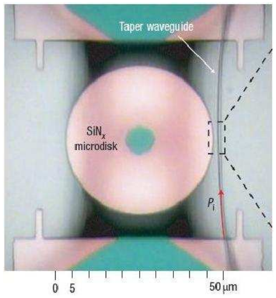

Fig. 4.8. Microdisk cavity evanescently coupled to micromechanical waveguide. Reprinted by permission from McMillan Publishers Ltd: Nature Photonics [133], copyright 2007.

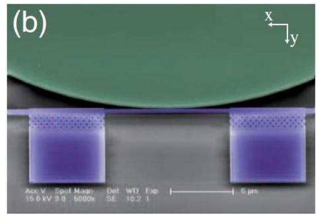

Fig. 4.9. Microtoroid cavity evanescently coupled to nanomechanical waveguide. Reprinted figure with permission from [116]. Copyright 2009 by the American Physical Society.

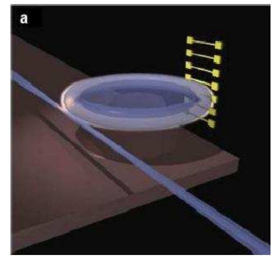

Fig. 4.10. Microtoroid evanescently coupled to nanomechanical resonators. Reprinted by permission from McMillan Publishers Ltd: Nature Physics [135], copyright 2009.

tomechanical crystal, surrounded by a "phononic shield", to its quantum ground state has been achieved [58]. An occoupancy of 0.85 quanta was observed for a 3.68 GHz mode. The same group has demonstrated electromagnetically-induced transparency [176] and motional sideband spectroscopy [177] in these systems. Experiments have also been performed with two-dimensional optomechanical crystals [178], and with electrically-controllable cavity optomechanical systems formed by a suspended photonic crystal defect cavity [180]. The latter system potentially provides a platform for the interconversion of weak microwave and optical signals.

4.3.3 Evanescently-Coupled Optomechanical Systems

Yet another type of optomechanical system is formed by those devices in which the optical field is evanescently coupled to the mechanical resonator. A dielectric mechanical resonator in an electric field will experience a polarization. Thus, in a non-uniform electric field, it will experience a dipole force. In the case where the electric field is provided by the evanescent field of an optical microcavity, the dielectric will experience a time-averaged polarization, and so an optical dipole force. It is then attracted to the high field of the cavity. The subsequent mechanical motion changes the optomechanical coupling. In general, this leads to a dispersive and a reactive optomechanical coupling, resulting in a frequency shift and a modified damping, respectively, of the mechanical motion.

The spatial variation of this force has been measured in a system composed of a movable, tapered fiber waveguide evanescently-coupled to an optical microdisk resonator [133]. Both dispersive and reactive optomechanical couplings have been demonstrated in a smaller system composed of a microdisk separated from a vibrating nanomechanical waveguide [116]. An array of silicon nitride nanomechanical resonators has been evanescently-coupled to a microtoroid, with strong dispersive coupling demonstrated [135]. In such a similar system, but with a single nanomechanical resonator, transduction with an imprecision far below the standard quantum limit has been achieved [181]. Images of these devices are shown in Figs. 4.8-4.10.

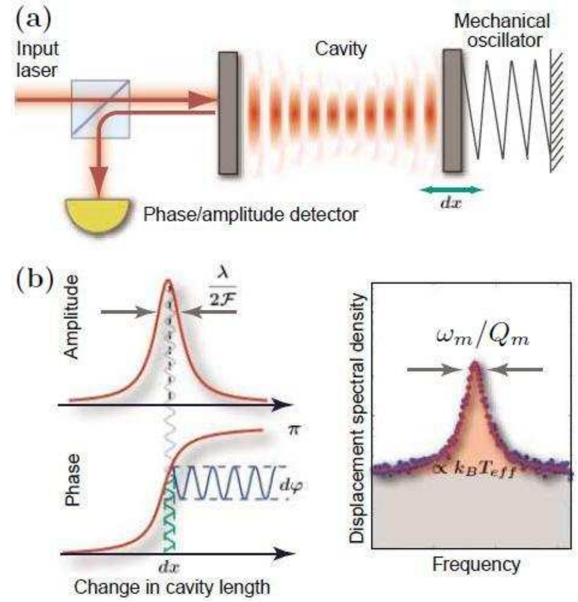

Fig. 4.11. (a) Schematic of resonant optical detection scheme for mechanical oscillator in optomechanical Fabry-Pérot cavity. (b) Amplitude and phase response of resonant input light to changes in cavity length. For a resonant input laser, the phase response is optimally sensitive to cavity length changes, while the amplitude response is insensitive to first-order. Optimal sensitivity of the amplitude response to changes in cavity length is obtained by probing with the laser tuned to the half-maximum of the amplitude response. The resulting displacement spectral density allows one to determine the effective temperature of the mechanical oscillator, as well as its resonance frequency and quality factor. Figure adapted from [187]. Reprinted with permission from AAAS.

4.4 Transduction of Optomechanical Systems

Mechanical motion may be detected through the amplitude or phase modulation of the probe light transmitted through, or reflected by, the cavity. This is depicted schematically in Fig. 4.11(a). As seen in Fig. 4.11(b), the optimal sensitivity to phase modulation is attained by probing the cavity on resonance. Optimal sensitivity to amplitude modulation is attained by probing the cavity at the full-width at half-maximum of its resonance peak. The output is typically a Lorentzian noise spectral density of the type shown in Fig. 4.11(b), which may be converted to a displacement noise spectral density by careful calibration. Such calibration may be performed using a frequency-modulated drive or by temperature control.

These transduction techniques require that the probe light is locked to a stable frequency with respect to the equilibrium cavity resonance frequency. Such locking may be achieved by locking the laser to an adjustable, but stable, Fabry-Pérot reference cavity. A locking technique commonly used is the Pound-Drever-Hall technique [182].

Perhaps the simplest possible detection technique involves monitoring the intensity transmitted or reflected by an optomechanical Fabry-Pérot cavity; this detects the amplitude modulation

System	Optomechanical Fabry-Pérot	Optomechanical Fabry-Pérot	Membrane-in-the-middle	Microtoroid
Ref.	[127]	[130]	[100]	[156]
$\omega_m/2\pi$	814kHz	945kHz	134kHz	65.1MHz
Δx (m)	7.37×10^{-18}	4.55×10^{-16}	1.25×10^{-15}	1.14×10^{-16}
$\sqrt{S_x}$ (mHz$^{-1/2}$)	4.0×10^{-19}	2.6×10^{-17}	5.5×10^{-16}	1.5×10^{-18}
$\sqrt{S_x}/\sqrt{S_x^{\mathrm{SQL}}}$	0.87	0.48	1.0	5.5
$\sqrt{S_x S_F}$	Unobserved	Unobserved	Unobserved	$220\frac{\hbar}{2}$

System	Micromechanical waveguide	Optomechanical crystal	Evanescently coupled nanomechanics
Ref.	[132]	[174]	[181]
$\omega_m/2\pi$	8.87MHz	2.25GHz	8.3MHz
Δx (m)	3.28×10^{-14}	3.36×10^{-15}	1.65×10^{-14}
$\sqrt{S_x}$ (mHz$^{-1/2}$)	1.8×10^{-14}	1.1×10^{-17}	2.5×10^{-16}
$\sqrt{S_x}/\sqrt{S_x^{\mathrm{SQL}}}$	67.4	7.5	0.08
$\sqrt{S_x S_F}$	Unobserved	Unobserved	Unobserved

Tab. 4.1. Comparison of experiments demonstrating sensitive displacement detection in nano- and micro-optomechanical systems. Note that Δx is the standard quantum limit as given by Eq. (8.7), S_x is the measurement imprecision of the transducer, S_x^{SQL} is the standard quantum limit on the noise added by the measurement given by Eq. (8.6), and $S_x S_F$ is the imprecision-back-action product of Eq. (8.4).

of the probe light. Several experiments have used this detection technique [183, 140, 128, 134, 100]. However, this technique requires an off-resonant probe, and is surpassed in detection sensitivity by phase-sensitive schemes. However, an interesting variation of this technique, by detecting the non-uniform optical intensity produced by an illuminated resonator above a Schottky contact has allowed transduction of a very small resonator [184].

The majority of experiments on optomechanical systems near the quantum limit employ phase-sensitive displacement detection schemes. A comparison of these experiments is provided in Table 4.1. Recently, transduction using multiple cavity modes has also been considered theoretically [185].

Phase-sensitive detection may be achieved using the error signal from the Pound-Drever-Hall locking technique [123], or more commonly, via homodyne detection of the reflected or transmitted probe light [126, 137, 130]. The input light is split at a beamsplitter into a local oscillator and a probe beam. The probe beam enters the optomechanical cavity, and the reflected optical field experiences a phase shift related to the displacement of the mechanical degree of freedom. This reflected field is then mixed with the local oscillator field at a balanced beamsplitter, photon counting is performed at each output and the intensity difference is monitored. If the local oscillator is strong and the probe field is weak, then the output is proportional to a quadrature of the reflected optical field. This is simply optical homodyne detection.

We now consider quantum limits to the continuous measurement of the position of a mechanical resonator using an optical field. Obviously, the precision of the measurement is limited by photon shot noise. The measurement imprecision due to this noise can be reduced by increasing the intensity of the probe light. However, there is another fundamental source of noise in this measurement, the back-action of the probe light on the resonator being measured. This may be attributed to radiation pressure fluctuations, and at sufficiently high probe powers, the total position measurement uncertainty will be dominated by this back-action [186]. Note that this quantum back-action has not been directly observed since this uncertainty is masked by thermal fluctuations in existing experiments. The standard quantum limit for position measurement arises when the uncertainties due to the imprecision and the back-action are equal, subject to the requirements specified in Sec. 8.1.

The position measurement imprecision due to photon shot noise in an optomechanical system is readily derived. We assume that the the probe is resonant with the cavity at its equilibrium length, and we consider phase-sensitive detection. The phase shift of the reflected probe, at a detuning ω from the equilibrium cavity resonance (attributed to the mechanical motion), is given by

$$\delta\phi(\omega) = 2\pi\mathcal{F}\frac{\delta x(\omega)}{\lambda_d}, \tag{4.27}$$

where $\delta x(\omega)$ is the component of mechanical motion at ω, λ_d is the wavelength of the light used to probe the motion and $\mathcal{F}$ is the cavity finesse, giving the number of reflections in the cavity before a photon escapes. The shot noise of the light at the detuning ω is

$$\delta\phi(\omega) = \frac{1}{\sqrt{n_c(\omega)}} \qquad \text{where} \qquad n_c(\omega) = \frac{P_{in}}{\hbar\omega_d}\frac{\gamma_c^2}{\gamma_c^2 + 4\omega^2} \tag{4.28}$$

is the rate of photons exiting the cavity at the detuning ω, with P_{in} being the laser input power. Now the cavity damping rate, in terms of the finesse, is $\gamma_c = (1/\mathcal{F})(c/L)$, and the optomechanical coupling is $\kappa = \omega_d/L$. A signal-to-noise ratio of one between Eqs. (4.27) and (4.28) leads to the position measurement imprecision [188],

$$S_x(\omega) = 4\frac{\hbar\omega_d}{P_{in}}\left(\frac{\gamma_c/2}{\kappa}\right)^2\left[\frac{(\gamma_c/2)^2 + \omega^2}{(\gamma_c/2)^2}\right]. \tag{4.29}$$

Heisenberg's uncertainty principle demands that there is an associated back-action force, and that the spectral density of this force satisfies the inequality of Eq. (8.4). Thus the back-action force noise spectral density must satisfy

$$S_F(\omega) \geq \frac{\hbar^2}{16}\frac{P_{in}}{\hbar\omega_d}\left(\frac{\kappa}{\gamma_c/2}\right)^2\left[\frac{(\gamma_c/2)^2}{(\gamma_c/2)^2 + \omega^2}\right]. \tag{4.30}$$

The total added noise, referred back to the mechanical resonator, is given by the measurement imprecision noise and the contribution due to back-action fluctuations,

$$S_x^{\mathrm{tot}}(\omega) = S_x(\omega) + |\chi(\omega)|^2\, S_F(\omega), \tag{4.31}$$

where $\chi(\omega)$ is the mechanical susceptibility given in Eq. (2.12). The total measurement uncertainty is minimized at a particular input power. Assuming that the detector satisfies the criteria

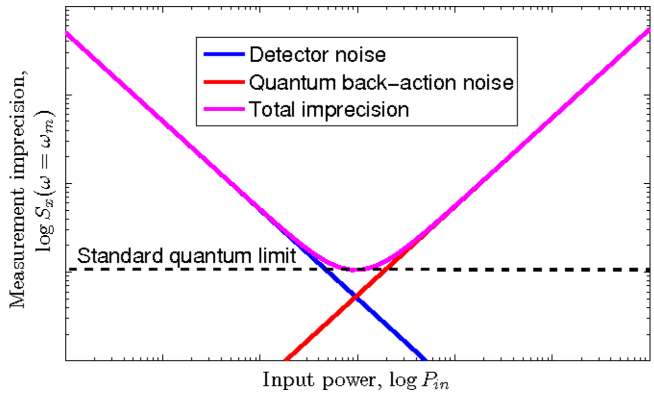

Fig. 4.12. Measurement uncertainties versus input power in an optical displacement detection scheme. The total added noise (purple curve) of the transducer has a contribution from both the intrinsic noise of the detector (blue curve) and the added noise due to the back-action of transducer fluctuations on the measured system (red curve). The detector noise decreases with increasing input power, while the back-action noise increases with increasing input power. There is an optimal input power at which the contribution from the detector noise and the back-action noise are equal, and this gives rise to the standard quantum limit on position detection.

discussed in Sec. 8.1, the total added noise at this input power is referred to as the standard quantum limit for the measurement of position of a harmonic oscillator,

$$S_x^{\mathrm{SQL}}(\omega) = \frac{\hbar}{m\sqrt{(\omega_m^2 - \omega^2)^2 + \gamma_m^2\omega^2}}. \tag{4.32}$$

This function attains its maximum value at the mechanical resonance frequency, at which we have

$$S_x^{\mathrm{SQL}}(\omega_m) = \frac{\hbar}{m\gamma_m\omega_m}. \tag{4.33}$$

The detector imprecision noise, quantum back-action noise, and total added noise are plotted in Fig. 4.12, as a function of the input power.

It is important to note that, by injecting a squeezed state into the unused port of an interferometer, one can decrease the shot noise uncertainty at the expense of increasing the radiation pressure uncertainty, or vice versa [186]. This allows the power required to reach the standard quantum limit to be lowered. Furthermore, squeezed states can in fact be used to beat the standard quantum limit [189]. In this sense, the standard quantum limit is not a fundamental limit, though quantum tricks are required to circumvent it.

5 Quantum Electromechanical Systems

5.1 Macro-electromechanical Systems

Resonant-mass gravitational wave detectors [190] typically take the form of large cylinders weighing up to several tonnes and operated cryogenically [191, 192]. The normal-mode oscillations of these masses are usually detected electrically, and so they form macro-electromechanical systems.

One class of transducers, often referred to as parametric transducers [193], employs capacitive or inductive coupling to radio-frequency circuits [194] or microwave cavities [195, 196]. Another class of transducers employ capacitive or inductive coupling to a SQUID-based circuit [197], with the SQUID functioning as a linear amplifier. SQUID-based detectors became the most widely used on operating resonant-mass gravitational wave detectors [198, 199, 200]. In a related series of experiments on prototype systems, back-action evading measurement of a mechanically compliant capacitance bridge was demonstrated [201, 202, 203].

Beyond measurement, back-action cooling [196] and feedback cooling have been achieved [204] on full-scale systems. However, it is unlikely that resonators on this scale could be cooled to the quantum ground state. Much smaller and higher frequency mechanical resonators are required.

5.2 Nano-electromechanical Systems

Indeed, small mechanical structures have been long been fabricated using semiconductor processing techniques [205], though technological progress has allowed a gradual scaling down of feature sizes achievable, culminating in the fabrication of high-frequency, high-quality-factor, doubly-clamped nanomechanical resonators from silicon [206]. Such small resonators may be integrated with electrical circuits for measurement and control, resulting in nano-electromechanical systems.

A variety of more exotic nanoelectromechanical systems were soon created [207], and subsequent studies of doubly-clamped nanomechanical resonators were performed in silicon carbide [208, 209], aluminium nitride [210], silicon nitride [211], aluminium [212], diamond [213] and gold [214]. Scaling down further, individual platinum and silicon [215] nanowires could be fabricated. The ability to tune mechanical resonance frequencies (and to some extent, quality factors) through tension has been demonstrated using capacitive coupling [216] and chip-bending [217].

In the domain of molecular materials, doubly-clamped carbon nanotube resonators have been fabricated [218]. Subsequently, tunable slack [219] and taut [220] resonators were created. More recently, carbon nanotube resonators having high quality factors [221] and graphene electromechanical resonators have been demonstrated [222]. A torsional pendulum based on an individual carbon nanotube has also been fabricated [223].

In order to drive the mechanical resonator, magnetomotive, electrostatic or piezoelectric effects may be utilised. In magnetomotive actuation [224], the axis of the beam is oriented perpendicular to the magnetic field generated by a solenoid. Applying an alternating electrical current along the beam, generates a Lorentz force $\underline{F} = I\underline{L} \times \underline{B}$ on it that is proportional to the current and the magnetic field strength. Thus the beam is driven transverse to both its axis and to the field direction.

For electrostatic actuation, a gate electrode drives the nanoresonator into motion [225, 219]. One applies a dc voltage V_g and an ac voltage V_g^{ac} at the frequency ω_m to the gate electrode, which induces a driving force due to the displacement-dependent gate capacitance C_g. The external force is given by $F(t) = \frac{1}{2}\frac{dC_g}{dx}\left[V_g^2 + \frac{1}{2}V_g^{ac^2} + 2V_gV_g^{ac}\cos\omega_m t + \frac{1}{2}V_g^{ac^2}\cos 2\omega_m t\right]$. Electrical field gradients may also be used for the actuation of a dielectric mechanical resonator [226]. A static voltage polarizes the dielectric resonator and subjects it to an attractive force towards maximum field strength that can be modulated at high frequency.

The piezoelectric effect is the generation of mechanical strain in response to an applied electric field. The piezoelectric actuation of a mechanical resonator by a voltage applied across integrated semiconductor junction has been demonstrated [227]. A dc voltage tunes the depletion region width, and so allows tuning of the mechanical resonance.

5.2.1 Transduction

Perhaps the simplest method for sensitively detecting the motion of a nanomechanical resonator is magnetomotive detection [224]. In magnetomotive detection, the motion of the nanomechanical resonator through a transverse magnetic field generates an electromotive force across the ends of the resonator that is readily detected. Magnetomotive detection has recently been extended to an array of uncoupled mechanical resonators [228]. However, this technique is inherently dissipative, and so inappropriate for experiments close to the quantum regime.

Alternative approaches include monitoring the modulation of a capacitively-coupled radio-frequency circuit or microwave cavity, or monitoring the modulation of the transport through a coupled quantum transport device. Coupling to, or integration with, Josephson junction circuits has also been employed for displacement detection. Mechanical resonances may also be observed directly by microscopy; examples include scanning probe microscopy [233] and radio-frequency scanning tunneling microscopy [234]. Very recently, the mechanical motion of a nanowire cantilever has been measured via time-resolved fluorescence and photon-correlation measurements of the emission from an embedded nitrogen-vacancy defect [179]. The most successful techniques for near quantum-limited detection employ coupling to quantum transport devices, microwave circuits or Josephson-junction devices, and they shall be discussed in the following sections.

5.2.2 Coupling to Quantum Transport Devices

Quantum transport devices may be used for ultra-sensitive displacement detection since the nanoresonator's motion typically induces a change in the transport device's conductance that can be directly measured. The transport device may be capacitively-coupled to, or integrated into, the mechanical resonator. If the transport device is capacitively-coupled, the nanoresonator must be held at some non-zero voltage with respect to the gate. If the transport device is integrated into it, the resonator must be capacitively-coupled to an electrode at some non-zero voltage with respect to it. A comparison of experimental achievements is given in Table 5.1.

Alternatively, such transducers may function via a displacement-dependent tunneling to the nanoresonator. Completely self-sensing nanomechanical resonators can be operated on the basis

System	Ultracryogenic RF-SSET	Ultracryogenic integrated DC SQUID	Ultracryogenic tunnel junction	Cryogenic off-board QPC	Cryogenic self-sensing QPC
Ref.	[229]	[230]	[214]	[231]	[232]
$\omega_m/2\pi$	21.8MHz	2.0MHz	43.1MHz	5.2kHz	1.5MHz
Δx (m)	24×10^{-15}	133×10^{-15}	9×10^{-15}	284×10^{-15}	10×10^{-15}
$\sqrt{S_x}$ ($\mathrm{mHz}^{-1/2}$)	3×10^{-16}	10^{-14}	2.3×10^{-15}	3×10^{-16}	3×10^{-12}
$\sqrt{S_x}/\sqrt{S_x^{\mathrm{SQL}}}$	3.9	36	42	> 100	$> 10^4$
$\sqrt{S_x S_F}$	$15\frac{\hbar}{2}$	Unobserved	$3400\frac{\hbar}{2}$	Unobserved	Unobserved

Tab. 5.1. Comparison of experiments demonstrating sensitive displacement detection using quantum transport devices or circuits based on Josephson junctions. Note that Δx is the standard quantum limit as given by Eq. (8.7), S_x is the measurement imprecision of the transducer, S_x^{SQL} is the standard quantum limit on the noise added by the measurement given by Eq. (8.6), and $S_x S_F$ is the imprecision-back-action product of Eq. (8.4).

of piezoresistive or piezoelectric effects. In low-frequency mechanical resonators, the modulation of the conductance may be monitored directly. For high-frequency mechanical devices, one may either configure the transport device as a mixer or use a radio-frequency device.

Capacitively-coupled single-electron transistors (SETs) have been used for sensitive displacement detection. High-frequency detection has been demonstrated using a normal-state SET configured as a mixer [235] and by a radio-frequency superconducting SET (RF-SSET) [236]. Operation as a mixer is obtained by modulating the SET conductance at a frequency offset from the mechanical drive frequency, such that there is a signal at the difference frequency. The nanomechanical resonator is held at a fixed voltage, and its motion changes the local potential at the island of the SET, and so modulates the transport through it. As the nanomechanical resonator voltage is increased, the SET becomes more sensitive to displacements, ultimately being limited by its shot noise, but the back-action on the nanomechanical resonator is increased. One must find an optimal compromise between the two. The back-action of a SSET has also been measured and used to cool the nanoresonator, with the system shown in Fig. 5.1 [229]. A variation of this scheme uses an off-board quantum point contact (QPC) capacitively-coupled to the tip of a cantilever [231].

The displacement of carbon nanotube resonators has been detected by the modulation of the current through it. High-frequency transduction is achieved by operating the nanotube as a mixer [219], though recent experiments have transduced the motion using the dc current through it [237]. Similar experiments have been performed on nanowires with integrated field-effect transistors [238]. This transduction is possible by capacitively-coupling the nanotube to a gate electrode held at a constant voltage. The motion of the nanotube modifies its capacitance to the gate electrode, giving rise to a change in the gate-induced charge on the nanotube, and modifying its conductance.

A completely different approach uses the displacement-dependent tunneling of electrons to the nanomechanical resonator itself in order to transduce its motion. High-frequency displacement detection has been demonstrated in this manner using a radio-frequency circuit [214].

Fully self-sensing integrated transduction of nanomechanical resonators has been demon-

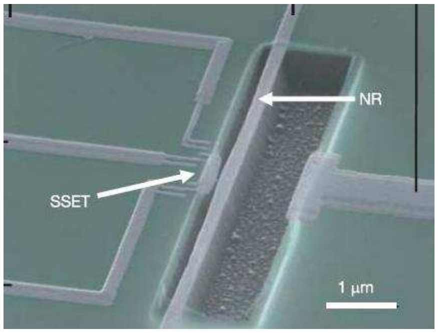

Fig. 5.1. Displacement detection of a nanomechanical resonator via a capacitively-coupled superconducting single-electron transistor. Reprinted by permission from McMillan Publishers Ltd: Nature [229], copyright 2006.

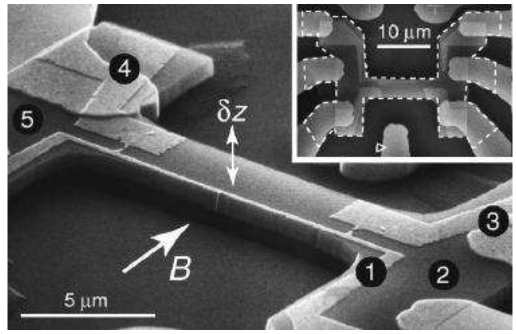

Fig. 5.2. Piezoelectric displacement detection of a micromechanical resonator with an integrated, piezoelectric quantum point contact. Reprinted with permission from [232]. Copyright 2002, American Institute of Physics.

strated using piezoresistive [239] and piezoelectric effects [240]. The piezoresistive effect describes the change in the resistance of a material due to an applied strain. Thus, displacement detection may be performed by monitoring the modulation of resistance associated with the strain induced by oscillation of a mechanical resonator. Again, this is achieved at high-frequency by operating the mechanical resonator as a mixer [241, 242].

The piezoelectric effect is the generation of electrical fields in response to an applied strain, again leading to modulation of the conductance throught the resonator. Piezoelectric transduction was demonstrated at low-frequency using micromechanical resonators with integrated field-effect transistors [243], and at high-frequency using a resonator with an integrated quantum point contact operated as a mixer, as depicted in Fig. 5.2 [232]. A macroscopic mechanical resonator, driven by electrical back-action due to the piezoelectric effect has also been demonstrated [244]. The back-action of electrons tunneling through a radio-frequency quantum point contact, leading to vibrations of the host crystal, was observed. The transport through the quantum point contact couples to vibrational modes via the piezoelectric effect, modifying the current. High-frequency motion was transduced by embedding the quantum point contact in an RF circuit.

5.2.3 Coupling to Microwave Circuits

Capacitively coupling a moving mechanical resonator to a radio-frequency or microwave circuit changes the total capacitance of the circuit, and so modulates its resonance frequency. An input electrical signal will also be modulated, and the reflected or transmitted signal may be used to acquire information about the mechanical motion. Such systems are essentially equivalent to the optomechanical Fabry-Pérot cavities to be discussed in Sec. 4. However, displacement detection is also possible here using a DC electrical circuit [226], and this technique has been extended to an array of mechanical resonators [248].

Sensitive displacement detection has been demonstrated using a nanomechanical resonator integrated into a superconducting coplanar microwave cavity [245], of a micromechanical res-

System	Resonant-mass GWD with cavity	Nanomechanics supercond. μwave cavity	Nanomechanics with microwave cavity and JPA	Nanomechanics with microwave cavity (BAE)	Micromechanical membrane with LC and JPA
Ref.	[196]	[245]	[246]	[247]	[59]
m	0.45kg	2pg	11pg	2.2pg	48pg
$\omega_m/2\pi$	700Hz	240kHz	1.04MHz	5.57MHz	10.56MHz
Δx (m)	1.6×10^{-19}	4.2×10^{-15}	8.6×10^{-16}	2.6×10^{-14}	4.1×10^{-15}
$\sqrt{S_x}$	3×10^{-17}	2×10^{-13}	4.8×10^{-15}	8.1×10^{-15}	?
$\sqrt{S_x}/\sqrt{S_x^{SQL}}$	29.7	27.4	0.41	1.3*	?
$\sqrt{S_xS_F}$	Unobserved	$3000\frac{\hbar}{2}$	Unobserved	$180\frac{\hbar}{2}$	$10\ \frac{\hbar}{2}$

Tab. 5.2. Comparison of experiments demonstrating sensitive displacement detection of a mechanical resonator using a microwave or radio-frequency electrical circuit. JPA denotes Josephson parametric amplifier, BAE denotes a back-action evading measurement. *The measurement sensitivity quoted for the BAE scheme refers to the detector imprecision for the measurement of a quadrature. Note that Δx is the standard quantum limit as given by Eq. (8.7), $\sqrt{S_x}$ in $\mathrm{mHz}^{-1/2}$) is the measurement imprecision of the transducer, S_x^{SQL} in is the standard quantum limit on the noise added by the measurement given by Eq. (8.6), and S_xS_F is the imprecision-back-action product of Eq. (8.4).

onator coupled to a radio-frequency electrical circuit [249], and a micromechanical membrane as one plate of a capacitor in a lumped-element superconducting LC resonator [9]. Experimental achievements are compared in Tab. 5.2. Typically, transduction via phase-sensitive electrical detection is best achieved by probing the cavity on resonance. The Hamiltonian electromechanical coupling takes the form $-\hbar\kappa a^\dagger ax$, where $\kappa = -\partial\omega_c/\partial x$, analogous to the dispersive radiation pressure coupling of cavity optomechanics. In some circumstances, there may also be a significant coupling to the position squared. A variation on this approach is to place a dielectric mechanical resonator between the plates of a capacitor in a lumped-element microwave circuit [250].

The measurement imprecision can be reduced by measuring with a larger input power, stronger coupling and minimal added noise. The last issue may be addressed using a Josephson parametric amplifier to measure the output microwave field [246]. Continuous, broadband back-action evading measurement of a quadrature of the nanomechanical motion has been demonstrated, using the setup depicted in Fig. 5.3 [247]. This is achieved by probing the cavity on two resolved sidebands. The sensitivity of the back-action evading measurement is limited by the power handling of the stripline resonator and the noise floor of the microwave detector circuit. Beyond monitoring mechanical motion, low-noise amplification of weak microwave signals has been demonstrated in these systems [251].

The quantum description of these systems is obtained using an equivalent circuit to capture the dynamics of collective circuit variables; the charge Q on the capacitor and the flux Φ through the inductor. The effective Hamiltonian is

$$H = \frac{\hat{p}^2}{2m} + \frac{m\omega_m^2}{2}\hat{x}^2 + \frac{\hat{\Phi}^2}{2L} + \frac{\hat{Q}^2}{2C(\hat{x})} + e(t)\hat{Q}, \tag{5.1}$$

where $\hat{x}, \hat{p}$ are the effective canonical displacement and momentum coordinates for the mechanical resonator mode of interest, m is the effective mass, L is the circuit inductance and $C(\hat{x})$ is

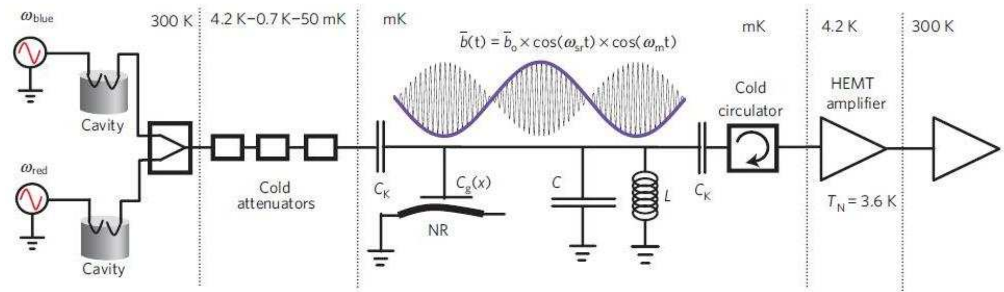

Fig. 5.3. Experimental setup for back-action evading measurement of a quadrature of a nanomechanical resonator using a superconducting microwave cavity. The microwave cavity (here represented by an LC tank circuit) is driven at two tones, corresponding to driving on the blue- and red-detuned sidebands of the cavity. The detuning corresponds to the mechanical resonance frequency. Reprinted by permission from McMillan Publishers Ltd: Nature Physics [247], copyright 2010.

the position-dependent circuit capacitance. Driving of the circuit has been is included as the last term. Driving with an AC voltage is described by writing $e(t) = e_0 \cos(\omega_D t)$.

We now expand the capacitance to linear order around its equilibrium position (taken to be $x = 0$) for the mechanical displacement,

$$H = \frac{\hat{p}^2}{2m} + \frac{m\omega_m^2}{2}\hat{x}^2 + \frac{\hat{\Phi}^2}{2L} + \frac{\hat{Q}^2}{2C_0} - \frac{\beta}{2C_0}\hat{Q}^2\hat{x} + e(t)\hat{Q}, \tag{5.2}$$

where

$$\beta = \frac{1}{C_0}\left.\frac{dC(x)}{dx}\right|_{x=0}, \tag{5.3}$$

which has units of inverse length. We now define bosonic annihilation operators for the circuit resonator and the mechanical resonator by

$$a = \sqrt{\frac{\omega_c L}{2\hbar}}\hat{Q} + \frac{i}{\sqrt{2\hbar\omega_c L}}\hat{\Phi}, \tag{5.4}$$

$$b = \sqrt{\frac{m\omega_m}{2\hbar}}\hat{x} + \frac{i}{\sqrt{2\hbar m\omega_m}}\hat{p}, \tag{5.5}$$

respectively, and write the Hamiltonian of Eq. (5.2) as

$$H = \hbar\omega_c a^\dagger a + \hbar\omega_m b^\dagger b + \hbar\frac{G_0}{2}(b + b^\dagger)(a + a^\dagger)^2 + \hbar\epsilon(e^{i\omega_D t} + e^{-i\omega_D t})(a + a^\dagger), \tag{5.6}$$

with

$$G_0 = \frac{\beta\omega_c}{2}\Delta x, \tag{5.7}$$

where Δx is given by Eq. (3.25). If we now go into an interaction picture at the driving frequency and neglect rapidly rotating terms in the interaction we find that

$$H = \hbar\Delta a^\dagger a + \hbar\omega_m b^\dagger b - \hbar G_0 a^\dagger a(b + b^\dagger) + \hbar\epsilon(a + a^\dagger), \tag{5.8}$$

where $\Delta = \omega_c - \omega_D$. The interaction thus has the same form as the radiation pressure interaction in Eq. (4.5).

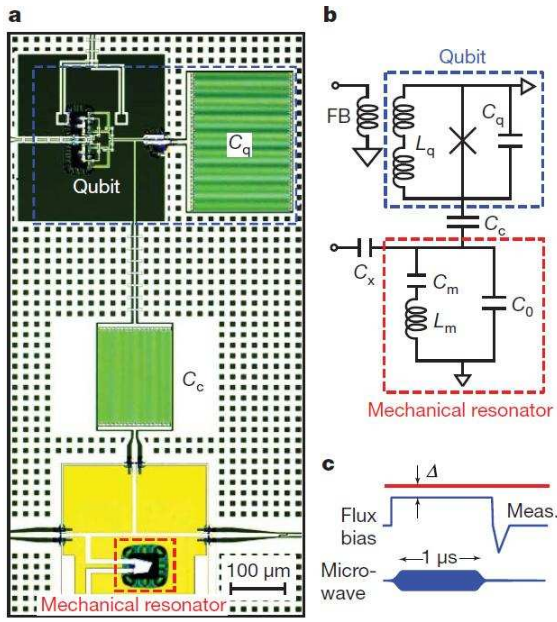

Fig. 5.4. A phase qubit coupled to a suspended film bulk acoustic resonator. (a) The coupling is mediated by a capacitive coupling C_c and piezoelectric voltages induced by the mechanical motion. (b) Schematic of the system, with an electrical circuit used to model the mechanical resonator. (c) Pulse sequence used to bring the qubit into resonance with the mechanical mode. Reprinted by permission from McMillan Publishers Ltd: Nature [57], copyright 2010.

5.2.4 Coupling to Josephson Junction Devices

Another class of electromechanical systems is formed by coupling a nanomechanical resonator to, or integrating a nanomechanical resonator into, a nonlinear circuit based on the Josephson junction. One such device consists of a micromechanical resonator integrated into one arm of a dc SQUID [230]. The current through the SQUID loop depends on the magnetic flux through it, such that it is possible to detect small changes in the area of a loop due to the motion of a flexural resonator in a static magnetic field. The backaction of the SQUID on the mechanical resonator, and so its frequency and quality factor, may be tuned via the bias current and applied magnetic flux [252].

Coupling of a nanomechanical resonator to a superconducting qubit, in the form of a Cooper pair box charge qubit, has also been demonstrated [253]. The coupling results in a dispersive shift of the nanomechanical frequency, and the magnitude of this shift allows mechanical spectroscopy of the superconducting qubit, including the observation of Landau-Zener interference effects. Parametric amplification of a nanoresonator, mediated by a Cooper pair box qubit, has also been achieved [254].

Conversely, a mechanical resonator has been resonantly coupled to a superconducting qubit, in the form of a phase qubit, in which the qubit has been used to read-out the mechanical resonator [57]. Here, the mechanical component is an aluminium nitride film bulk acoustic resonator sandwiched between aluminium electrodes, as shown in Fig. 5.4. The resonator expands and contracts in the direction perpendicular to the electrodes, and in so doing generates a piezoelectric signal that capacitively couples it to an adjacent phase qubit. In order to probe the mechanical resonator, the qubit was prepared in its ground state, and then tuned into resonance with the mechanical resonator for a short interval. In this experiment, the qubit was observed to remain in its ground state, providing evidence that the mechanical resonator is in its quantum ground state. Time-domain control allows one to coherently transfer quanta the mechanical resonator, resulting in the creation of an entangled qubit-mechanical state and a single-phonon mechanical state. This achievement was chosen as *Science* magazine's "Breakthrough of the Year" in 2010 [255].

6 State Preparation

6.1 Cooling of Mechanical Systems

The first step in a quantum control protocol is to prepare the system, here a simple harmonic oscillator, in a 'known' state. If a quantum state is indeed perfectly known it is a state of zero entropy, that is to say, a pure state. In practice no state can be known with total certainty and we need to give some figure of merit for how well we can do. In the case of a simple harmonic oscillator the target state is typically the ground state from which other states can be reached by unitary control, displacement and squeezing. A good figure of merit is either the occupation probability for the ground state or, more usually, the average number of excitations present in the mode, $\bar{n}$. For a simple harmonic oscillator with fundamental frequency ω_0 in thermal equilibrium at temperature T, the average number of excitations is given by a Bose-Einstein distribution,

$$\bar{n} = \left(e^{\hbar\omega/k_B T} - 1\right)^{-1}. \tag{6.1}$$

For example, a 10 MHz resonator at a temperature of 4K has $\bar{n} = 5.5 \times 10^4$, while at a temperature of 10mK it would have $\bar{n} = 136$. A 1 GHz resonator at 4 K will have $\bar{n} = 550$, and at 10 mK it would have $\bar{n} = 0.9$. Mechanical resonator frequencies typically scale inversely with the size of the resonator (see Sec. 2.1), so to get very high frequencies we typically need to move to nano-scale systems. In a land mark experiment, O'Connell *et al.* [256], using a dilatational micromechanical resonator with a frequency of 6 GHz at 25 mK achieved $\bar{n} = 0.07$; we describe below how this was measured. Typical mechanical resonators have fundamental frequencies between $1 - 100$MHz, such that passive cooling in a dilution fridge is inadequate for preparing them near the ground state.

Clearly cooling must be an irreversible process. The key is to use a laser to drive transitions to remove a phonon and dump the energy into a spontaneously emitted optical or microwave photon. As the electromagnetic field at optical frequencies is essentially at zero temperature at laboratory temperatures, this process can be very efficient. This idea is the basis of laser cooling and has led to many important discoveries in atomic physics over the last four decades, including the ability to create a Bose Einstein condensate in a dilute atomic gas [257], and prepare single trapped ions in a vibrational ground state of the trap [25]. Optical cooling of a bulk mechanical resonator was first reported in three separate papers in the same issue of Nature in 2006 [106, 258, 259].

An important variation on the idea is to use a resonator for the electromagnetic field. A coherent pump field can then be used to drive Raman transitions that absorb one pump photon and one phonon to excite the cavity mode at its resonance frequency. This photon can then be rapidly damped from the cavity field, see Fig. 4.4. The process is called red side-band cooling as the pump field is detuned below the cavity resonance by an amount equal to the mechanical frequency. We describe the process in some detail below. Teufel et al. [9] used this process to cool a micro-mechanical resonator using a microwave cavity. At mK temperatures the microwave cavity has a mean thermal photon occupation of the order of $\bar{n}_c \sim 0.09$, providing the low temperature heat bath required for cooling. Before we describe this process in detail we need to make briefly review the quantum description of a weakly damped simple harmonic oscillator.

A macroscopic mechanical resonator, in the absence of driving, will tend to a thermal state. By virtue of typical mechanical resonator frequencies, typical cryogenic temperatures are ususally

System	Ultracryogenic resonant-mass GWD	Cryogenic micromechanical Fabry-Pérot	Cryogenic microtoroid	Ultracryogenic nanoresonator	Ultracryogenic FBAR
Ref.	[192]	[130]	[156]	[229]	[57]
m	2260kg	4.3ng	10ng	0.68pg	0.66ng
$\omega_m/2\pi$	923Hz	945kHz	65.3MHz	21.9MHz	6.175GHz
n_f	2.3×10^6	1.2×10^5	770	25	0.07

Tab. 6.1. Comparison of experiments demonstrating cooling of a mechanical mode by bulk refrigeration. Note that n_f denotes the lowest achieved occupation of the mechanical mode.

insufficient to achieve quantum ground-state cooling. A notable exception is the suspended film-bulk acoustic resonator recently demonstrated [57]. The observed occupancies achievable in a variety of systems are shown in Table 6.1. Thus, in general, auxiliary cooling mechanisms are required; such mechanisms may be classified as active feedback or passive back-action cooling schemes.

In feedback cooling, the motion of the resonator is measured, and a feedback force is applied in opposition to the motion. Feedback cooling of a small mechanical resonator was first demonstrated over fifty years ago [260, 261]. If the feedback force is proportional to the velocity as $F(t) = -gm\dot{x}(t)$, then the modified mechanical susceptibility is, c.f. Eq. (2.12),

$$\chi(\omega) = \frac{1}{m\left[\omega_m^2 - \omega^2 - i\left(\gamma + g\right)\right]}. \tag{6.2}$$

The associated reduction in effective temperature is $\frac{T_{fb}}{T} = \frac{\gamma}{\gamma+g}$. This mechanism is sometimes referred to as cold damping, since it effectively introduces an additional viscous force without the associated thermal noise. Naturally, the achievable cooling is diminished by noise in the feedback loop, and is potentially limited by measurement back-action.

Back-action cooling describes the cooling of a system by simply allowing it to interact with some auxiliary system in a controlled manner. The auxiliary system is biased or driven such that it preferentially absorbs energy from the system to which it is coupled. This technique is analogous to the Doppler cooling [262] or resolved sideband cooling [263, 264] of trapped atoms and ions. No explicit measurement process is involved, though the auxiliary system must be damped into a heat bath at a lower temperature, such that the process is irreversible. Cooling of a mechanical resonator via the back-action of a coupled transport device [229] and via the back-action of a driven microwave or optical cavity have been demonstrated [140, 129, 127, 153, 154, 265]. The latter approach, in particular, appears to be a promising route to ground-state cooling [156, 130, 266].

6.2 Cooling in Optomechanical Systems

The other key issue for the development of quantum optomechanics is cooling. There have been many demonstrations of cooling in optomechanical systems, using both active feedback and passive back-action cooling. The relevant experiments are compared in Tables 6.2 and 6.3. The

System	Cryogenic resonant-mass GWD	kg-scale pendulum in optical spring	gram-scale pendulum in optical spring	Micromechanical Fabry-Pérot	Cryogenic nanomechanical cantilever
Ref.	[204]	[120]	[124]	[126]	[134]
Feedback	Electrical	EM	RP	RP	Piezo
m	1100kg	2.7kg	1g	190μg	322pg
$\omega_m/2\pi$	900Hz	140Hz	1.018kHz	1.859MHz	2.6kHz
n_f	4000	234	1.4×10^5	8.3×10^4	2.3×10^4

Tab. 6.2. Comparison of experimental demonstrations of feedback cooling in electromechanical and optomechanical systems. Note that "Feedback" refers to the actuation mechanism: "EM" = Electromagnetic, "RP" = Radiation pressure. Further, n_f denotes the final occupation of the cooled mechanical mode.

most successful approach has been back-action cooling based on radiation pressure [267], and the theory underlying this technique is also discussed here.

6.2.1 Active Feedback Cooling

A variety of feedback cooling experiments are compared in Table 6.2. The cooling may be actuated using the radiation pressure of a modulated laser [126, 124]. At low-frequency, piezoelectric [134] or electromagnetic [120] actuation may be employed. For the optomechanical case [268, 269], in principle, quantum ground-state cooling is achievable in the limit of large feedback gain, ideal homodyne detection and very large input power. These are demanding requirements, however. Nonetheless, it is believed that optomechanical feedback cooling may still be more effective than back-action cooling in the bad-cavity limit [270].

6.2.2 Passive Back-Action Cooling

A variety of back-action cooling experiments using radiation pressure are compared in Table 6.3. These experiments are closely related to the experiments demonstrating back-action cooling of nanomechanical resonator using resonant microwave circuits. Back-action cooling based on radiation pressure allows, in principle, cooling to the quantum ground state if one is in the resolved-sideband regime [271,272]. Table 6.3 includes systems that are in the resolved-sideband and adiabatic regimes. As is to be expected, the most effective cooling has been achieved with systems operating in the resolved-sideband regime. It should be noted that back-action cooling based on photothermal pressure has also been demonstrated [140]. An alternative approach to radiation pressure cooling based on a dispersive couplings, is to cool using a reactive coupling [115]. There, it has been shown that ground-state cooling is possible, in principle, even when one is not in the resolved-sideband regime.

6.2.3 Radiation Pressure Back-action Cooling: Classical Picture

The origin of radiation pressure back-action cooling may be understood in a classical framework. In an optomechanical cavity, the light moves the mirror, which alters the optical resonance fre-

System	gram-scale pendulum in optical spring	Micromech. Fabry-Pérot	Microtoroid	Micromech. membrane-in--the-middle	Cryogenic microtoroid
Ref.	[123]	[127]	[154]	[100]	[156]
m	1g	190μg	10ng	40ng	10ng
$\omega_m/2\pi$	172Hz	814kHz	73.5MHz	134kHz	65.1MHz
ω_m/γ_c	0.016	0.775	22.97	2.86	3.43
n_f	10^8	2.6×10^5	5900	1100	63

System	Cryogenic microsphere	Cryogenic micromech. Fabry-Pérot	Ultracryogenic spoked microtoroid	Cryogenic optomechanical crystal
Ref.	[160]	[130]	[273]	[58]
m	41ng	43ng	10ng	311fg
$\omega_m/2\pi$	118.6MHz	945kHz	78MHz	3.68GHz
ω_m/γ_c	4.0	0.8	11	1.05×10^5
n_f	37	32	1.7	0.85

Tab. 6.3. Comparison of experiments demonstrating radiation pressure back-action cooling in cavity optomechanics. The ratio ω_m/γ_c determines whether or not the system is in the resolved-sideband regime. Note that n_f denotes the final thermal occupation of the mechanical mode.

quency of the cavity, and so the circulating intensity, leading back to a change in the radiation pressure force on the mirror. The radiation pressure force responds to the mirror motion with some time lag due to the time taken for photons to leak out of the cavity, meaning that the optical field can perform some net work on the mirror.

In a detuned cavity, a static radiation pressure force arises from the dependence of the stored energy on the cavity length. The number of photons in a cavity driven at a frequency ω_d at a power P_i, with a damping rate γ_c, and detuned from a nearby resonance by $\delta_d \equiv \omega_d - \omega_c(L)$, is

$$n_c = \frac{P_i}{\hbar\omega_d}\frac{\gamma_c}{\gamma_c^2 + 4\delta_d^2}. \tag{6.3}$$

The half-maxima of this peak are at $\delta_d = \pm\gamma/2$. Suppose that the nearest resonance frequency is ω_0, corresponding to the cavity length L_0, such that $\omega_0 = n\pi c/L_0$. The detuning due to a change in the cavity length is then $\delta_L = \omega_0 - \omega_c(L) = \omega_0\left(1 - \frac{L_0}{L}\right)$. The corresponding intracavity power is $P_{cav} = n_c\hbar\omega_d c/L$. Thus, from Eq. (6.3), we have

$$P_{cav} = P_{in}\frac{c}{L}\frac{\gamma}{\gamma^2 + 4\left[\omega_d - \frac{L_0}{L}\omega_0\right]^2}. \tag{6.4}$$

This is plotted in Fig. 6.1, as a function of the cavity length L, centred on the length corresponding to the cavity being on resonance with the drive. About some detuned operating point, the linearized force is proportional to $\left(\frac{dP_{\text{cav}}}{dL}\right)x$, where x is the displacement from the operating point.

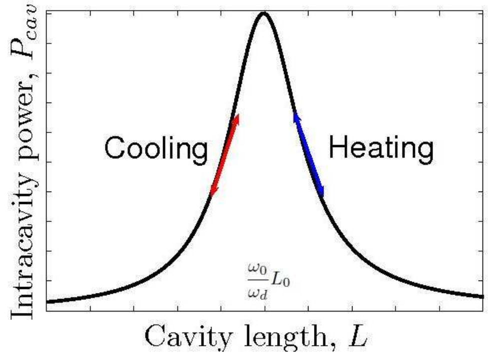

Fig. 6.1. Intracavity optical power as a function of cavity length L. It is assumed that the cavity is driven at a frequency ω_d, and has a nearby resonance at ω_0 corresponding to the cavity length L_0. The intracavity power is a maximum at the length $L = \omega_0 L_0/\omega_d$, corresponding to resonance with the driving field. The intracavity power has half-maxima at the cavity lengths $L = \omega_0 L_0/\left(\omega_d \pm \gamma/2\right)$.

The intracavity power essentially gives the steady-state radiation pressure force on the mirror. If the mirror is on the left-hand-side of the peak, then as the mirror approaches resonance, the force is smaller than expected due to the time lag associated with the cavity lifetime, and larger than expected when the mirror retreats. Thus $\oint F\,dx < 0$, and the mirror does work on the field, such that it is damped. The opposite is true if the mirror is on the right-hand-side of the peak; net work will be done on the resonator, and its motion will be amplified.

6.2.4 Radiation Pressure Back-Action Cooling: Quantum Picture

A quantum description of the cooling process is more easily discussed in the frequency domain. Classically, modulation of the cavity resonance frequency by mechanical motion (with an amplitude x_0) is described by the evolution of the cavity mode amplitude as $\dot{\alpha} = -i(\omega_c + \kappa x_0 \cos\omega_m t)\alpha$. This equation integrates to

$$\alpha(t) = \exp\left[-i\left(\omega_c t + \frac{\kappa x_0}{\omega_m}\sin\omega_m t\right)\right] = e^{-i\omega_c t}\sum_{k=-\infty}^{+\infty} J_k\left[\frac{\kappa x_0}{\omega_m}\right]e^{-ik\omega_m t}, \tag{6.5}$$

where the second equality follows from the Jacobi-Anger expansion. Thus the cavity spectrum acquires sidebands spaced by ω_m, with strength $\left|J_k\left(\kappa x_0/\omega_m\right)\right|^2$. It is usually suffiient to consider just the lower and upper sidebands, known as the red (or "Stokes") and blue (or "anti-Stokes") sidebands, respectively. The presence of asymmetric sidebands, due to one sideband being closer to the cavity resonance than the other, implies a net energy transfer between the optical and mechanical modes. This sideband asymmetry is achieved by driving the cavity below or above resonance. A large asymmetry, and so a large energy transfer, is achieved in the resolved-sideband regime, with cooling achieved by driving below the resonance frequency. In fact, optimal cooling in the resolved-sideband regime is achieved by tuning the driving frequency

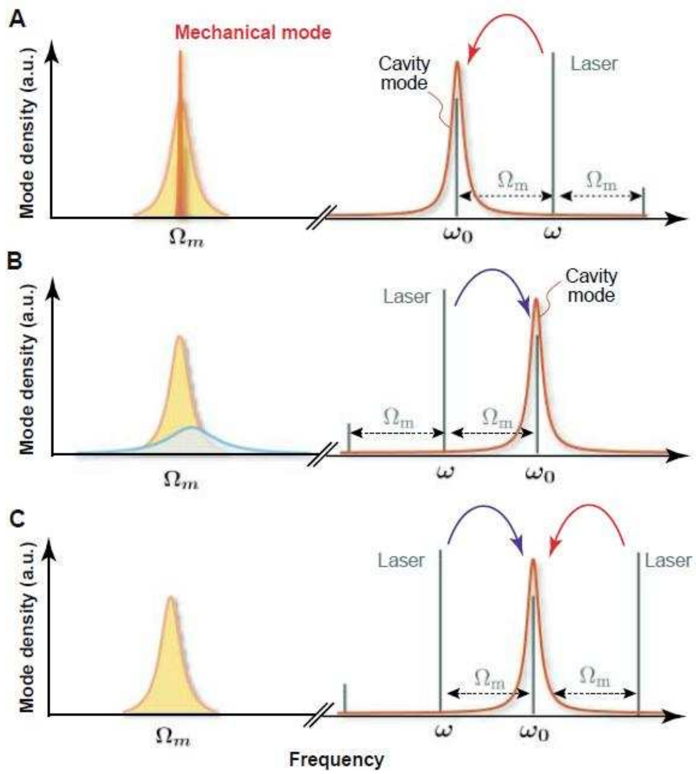

Fig. 6.2. Density of states in optomechanical systems, as a function of frequency, in the resolved-sideband regime ($\omega_m >> \gamma_c$). These are shown for: (a) blue-detuned driving of the cavity; (b) red-detuned driving of the cavity; and (c) blue- and red-detuned driving of the cavity. The dominant Raman scattering processes are indicated by arrows. Figure adapted from [187]. Reprinted with permission from AAAS.

to the red sideband of the cavity by an amount corresponding to the mechanical resonance frequency. In this case, the Raman process that involves a quantum being emitted by the mechanical mode is favoured. These considerations are depicted in the plot of mode density as a function of frequency in Fig. 6.2.

The quantum theory of radiation-pressure back-action cooling of mechanical systems has been developed by a number of authors [271, 272]. The key result is that ground-state cooling is only possible in the resolved-sideband regime. It is assumed that the Hamiltonian coupling takes the form of Eq. (4.3), and that the cavity is driven with some power P_{in} at a detuning Δ_d (including a radiation-pressure-induced frequency shift). Then it may be shown, by adiabatically eliminating the cavity modes, that, in the weak coupling regime, the mechanical resonator experiences a cooling rate (A_-) and a heating rate (A_+), given by [272]

$$A_{\mp} = 16\kappa^2 \left(\Delta x\right)^2 \frac{P_{in}}{\hbar\omega_d} \frac{\gamma_c}{4\Delta_d^2 + \gamma_c^2} \frac{\gamma_c}{4\left(\Delta_d \pm \omega_m\right)^2 + \gamma_c^2}. \tag{6.6}$$

The dynamical radiation pressure back-action thus provides a damping rate Γ, and a frequency shift $\Delta\omega_m$ to the mechanical resonator. These are given by

$$\begin{aligned}\Gamma &= A_- - A_+ \\ &= 16\kappa^2 \left(\Delta x\right)^2 \frac{P_{in}}{\hbar\omega_d} \frac{\gamma_c}{4\Delta_d^2 + \gamma_c^2} \left[\frac{\gamma_c}{\gamma_c^2 + 4\left(\Delta_d + \omega_m\right)^2} - \frac{\gamma_c}{\gamma_c^2 + 4\left(\Delta_d - \omega_m\right)^2} \right], \quad (6.7) \\ \Delta\omega_m &= 16\kappa^2 \left(\Delta x\right)^2 \frac{P_{in}}{\hbar\omega_d} \frac{\gamma_c}{4\Delta_d^2 + \gamma_c^2} \left[\frac{\Delta_d + \omega_m}{\gamma_c^2 + 4\left(\Delta_d + \omega_m\right)^2} + \frac{\Delta_d - \omega_m}{\gamma_c^2 + 4\left(\Delta_d - \omega_m\right)^2} \right]. \quad (6.8)\end{aligned}$$

Solution of the corresponding master equation yields the steady-state occupation of the mechanical mode, which is, neglecting a small coherent shift,

$$n_f = \frac{\gamma_m n_i + A_+}{\gamma_m + \Gamma}. \tag{6.9}$$

Assuming that the cooling rate is large compared with the intrinsic mechanical damping rate, $\Gamma \gg \gamma_m$, we have

$$n_f = \frac{\gamma_m}{\Gamma} n_i + \tilde{n}_f \quad \text{where} \quad \tilde{n}_f = -\frac{4\left(\Delta_d + \omega_m\right)^2 + \gamma_c^2}{16\omega_m \Delta_d}. \tag{6.10}$$

Now we consider the limit to cooling associated with the back-action; that is, the second term in Eq. (6.10). It is important to note that the first term may impose a limit to cooling, but this cannot be optimized further by simply varying the drive detuning. Now we seek to minimize the final occupation, n_f, with respect to this drive detuning, Δ_d. The appropriate limit is $\tilde{n}_L = \frac{1}{2}\left(\sqrt{1 + \gamma_c^2/4\omega_m^2} - 1\right)$, corresponding to the detuning $\Delta_d = -\frac{1}{2}\sqrt{\gamma_c^2 + 4\omega_m^2}$. In the adiabatic regime, $\omega_m \ll \gamma$, the optimal detuning is $\Delta_d = -\gamma_c/2$, with the lowest occupation achievable being

$$\tilde{n}_L \approx \frac{\gamma_c}{4\omega_m} \gg 1, \tag{6.11}$$

analogous to the Doppler limit of atomic physics. In the resolved-sideband regime, where the the cavity field cannot respond instantaneously to the mechanical motion, the asymmetry in the cooling and heating rates is more pronounced. For $4\omega_m^2 \gg \gamma_c^2$, the optimal detuning is $\Delta_d = -\omega_m$, and the lowest occupation achievable is

$$\tilde{n}_L = \frac{\gamma_c^2}{16\omega_m^2} \ll 1. \tag{6.12}$$

That is, the regime $\omega_m \gg \gamma_c$ allows ground-state cooling of the mechanical mode. However, different practical limitations may arise in different physical systems. The effects of pump noise with some finite correlation time [274] and of thermal occupation of the cavity and strong optomechanical coupling [275] have been considered. Indeed, a mechanical resonator in an optomechanical system has yet to be cooled to its quantum ground state.

6.3 Cooling in Electromechanical Systems

Cooling of the mechanical resonator of an electromechanical system may be achieved using feedback cooling or back-action cooling. There are proposals for feedback cooling of a nanomechanical resonator using a coupled single-electron transistor [276] or microwave cavity [277], though such proposals have proven difficult to implement. However, electromechanical feedback cooling of a resonant-mass gravitational wave detector has been demonstrated [204].

Back-action cooling has proven somewhat more successful. It has been demonstrated using a microwave cavity coupled to a resonant-mass gravitational wave detector [196], and more recently, using radio-frequency electrical circuits coupled to micromechanical resonators [249] and superconducting microwave cavities with embedded nanomechanical resonators [265, 266]. The first ground state cooling using this technique used a micromechanical membrane as one electrode of a capacitor in a lumped-element superconducting resonant cavity. Following demonstrations of strong coupling and normal-mode splitting [278], cooling to the ground state was achieved [59]. Transduction in the latter case was performed using a Josephson parametric amplifier.

The principle in all these experiments is the red-detuned driving of the circuit or cavity. Optimal cooling is achieved by driving the cavity at its full-width at half-maximum of its resonance (in the bad-cavity or adiabatic limit, where the mechanical resonance is less than the cavity damping), or at a sideband corresponding to the mechanical resonance (in the good-cavity limit, also known as the resolved-sideband regime, where the mechanical resonace is greater than the cavity damping). Preparation and detection of mechanical resonators in their quantum ground states has recently been achieved [59, 58]. Here, the cooling was limited by thermal excitation of the microwave cavity, heating due to the dissipative mechanical bath, and non-thermal force noise. These back-action cooling experiments are compared in Table 6.4.

Back-action cooling of a nanomechanical resonator was also demonstrated by coupling to an appropriately biased superconducting single-electron transistor [229]. A variety of other proposals for back-action cooling exist: examples include via coupling to a double-dot carbon nanotube [279], via laser cooling of an embedded quantum dot [280], via electron-phonon coupling in metallic nanowires [281], via current flow through a superconducting nanowire [282], or via

System	Micromechanical resonator	Cryogenic resonant-mass GWD	Ultracryogenic nanomechanical resonator	Ultracryogenic nanomechanical resonator	Ultracryogenic micromechanical membrane
Ref.	[249]	[196]	[265]	[266]	[59]
m	2.45μg	1500kg	6.2pg	2pg	48pg
$\omega_m/2\pi$	7kHz	713Hz	1.525MHz	6.37MHz	10.56MHz
ω_m/γ_c	0.02	0.01	6.6	12.9	52.8
n_f	10^8	10^5	140	4	0.34

Tab. 6.4. Comparison of experiments demonstrating back-action cooling via a radio-frequency or microwave circuit. The ratio ω_m/γ_c determines whether or not the system is in the resolved-sideband regime. Note that n_f denotes the final thermal occupation of the mechanical mode.

coupling to a superconducting qubit [283, 284, 285].

6.4 Resolved Sideband Cooling in Optomechanics

The theory of ground state cooling of a mechanical oscillator has been developed in a number of contexts, including resolved sideband cooling in optomechanics [286]. We will adopt a simpler approach using the quantum stochastic differential equations and focusing on the physics of the anti-Stokes process given in the scheme of Fig. 4.4. We first define the electromagnetic cavity mode operators $a, a^\dagger$ to be distinguished from the mechanical resonator's operators $b, b^\dagger$. In Sec. 4.1.3 we derived the linearised optomechanical coupling Hamiltonian in an interaction picture

$$H = \hbar g(ab^\dagger + a^\dagger b). \tag{6.13}$$

The equations of motion, in such a picture and with dissipation and fluctuations included, are

$$\frac{da}{dt} = -\frac{\kappa}{2}a - igb + \sqrt{\kappa}a_{in}, \tag{6.14}$$

$$\frac{db}{dt} = -\frac{\gamma}{2}b - iga + \sqrt{\gamma}b_{in}, \tag{6.15}$$

where γ is the mechanical resonator's linewidth and κ is the electromagnetic resonator's linewidth.

We need to ensure that the photon emitted into the cavity mode is lost to the zero temperature heat bath in the multimode field outside the cavity. In this limit, we may perform an adiabatic elimination of the cavity field. Assuming that $\kappa >> \gamma, g$ we regard the electromagnetic mode as *slaved* to the mechanical mode, so that on the time-scale of the mechanical dynamics, the cavity field amplitude is stationary. Accordingly, we solve for the cavity amplitude operator,

$$a \to -\frac{2ig}{\kappa}b + \frac{2}{\sqrt{\kappa}}a_{in}. \tag{6.16}$$

Substituting the cavity field from Eq. (6.16) into the equation of motion for the mechanical mode, Eq. (6.15),

$$\frac{db}{dt} = -\frac{\Gamma}{2}b - i\sqrt{\gamma_{om}}a_{in} + \sqrt{\gamma}b_{in}, \tag{6.17}$$

where the optomechanical and total damping rates are, respectively,

$$\gamma_{om} = \frac{4g^2}{\kappa}, \tag{6.18}$$

$$\Gamma = \gamma + \gamma_{om}. \tag{6.19}$$

Assuming that the optomechanical damping is into a bath with thermal occupation $\bar{n}_p$, and that the intrinsic damping is into a bath with thermal occupation $\bar{n}_m$, then it is easy to show that the steady-state mean phonon number in the mechanical system is given by

$$\langle b^\dagger b\rangle_{ss} = \frac{\gamma_{om}}{\Gamma}\bar{n}_p + \frac{\gamma}{\Gamma}\bar{n}_m. \tag{6.20}$$

For optical frequencies at room temperature, or for microwaves at mK temperatures, we may set $\bar{n}_p = 0$,

$$\langle a_m^\dagger a_m \rangle_{ss} = \frac{\gamma}{\Gamma} \bar{n}_m. \tag{6.21}$$

Clearly, cooling requires $\Gamma >> \gamma$. The full theory shows there is heating due to residual Stokes scattering (the blue sideband coupling).

A number of groups have reported cooling to very close to the quantum ground state using sideband cooling. In optics, the Kippenberg group reported $\bar{n} = 9$ [287], while the Painter group reported $\bar{n} = 0.85$ of a 3.68 GHz resonator. In the microwave domain, the Schwab group has reported $\bar{n} = 3.8$ [288], and Teufel *et al.* [289] has reported $\bar{n} = 0.34$.

7 Coherent Control

Along with state preparation the next key element for quantum technology is the ability to coherently control the system. Coherent control is described by unitary evolution. Imperfections arise from dissipation and dephasing in the system to be controlled, as well as from noise in the classical control lines. How serious a problem these pose is really question of time-scales. Often we can couple a classical control signal so strongly to the quantum target that the coherent control is so fast that we need not concern ourselves with non-unitary effects. There are a variety of ways we can coherently control the quantum state of macroscopic mechanical resonators, including harmonic and parametric driving, and control via single photons.

7.1 Harmonic Driving

We begin with the case of harmonic driving. The potential energy contribution of a classical driving force on a mechanical resonator is

$$H_{drive} = \mathcal{F}(t)x = \hbar f(t)(b + b^\dagger), \tag{7.1}$$

where we have introduced the notation

$$f(t) = \frac{\mathcal{F}(t)}{\sqrt{2\hbar m\omega_0}}. \tag{7.2}$$

Usually the force has a carrier frequency near the oscillator resonance, $\mathcal{F}(t) = f(t)\sin(\omega_D t)$, where $f(t)$ is a slowly-changing envelope on average with a stochastic component. That is, $f(t) = f_0(t) + \eta(t)$ where $\eta(t)$ is a zero mean noise. Including the driving term gives the equation of motion

$$\frac{db}{dt} = -i\omega_0 b(t) - \frac{\gamma}{2}b(t) - if(t)\sin(\omega_D t) + \sqrt{\gamma}b_{in}(t). \tag{7.3}$$

We now go to an interaction picture defined by $b_I(t) = b(t)e^{i\omega_D t}$, giving

$$\frac{db_I}{dt} = -i\delta b_I(t) - \frac{\gamma}{2}b_I(t) - if(t)\sin(\omega_D t)e^{i\omega_D t} + \sqrt{\gamma}b_{I,in}(t), \tag{7.4}$$

where $\delta = \omega_0 - \omega_D$. Typically we are interested in times such that $\omega_D t >> 1$. Then we can drop the rapidly rotating terms (the rotating wave approximation again), to find

$$\frac{db_I}{dt} = -i\delta b_I(t) - \frac{\gamma}{2}b_I(t) + \frac{f(t)}{2} + \sqrt{\gamma}b_{I,in}(t). \tag{7.5}$$

We now work exclusively in the interaction picture, so we drop the subscript I. The quantum stochastic differential equation for a driven, damped harmonic oscillator is generically of the form

$$\frac{db}{dt} = -i\delta b(t) - \frac{\gamma}{2}b(t) + \epsilon(t) + \sqrt{\gamma}b_{in}(t), \tag{7.6}$$

where $\epsilon(t)$ has the units of frequency. Now suppose that the drive is intended to be constant in this picture, but is subject to zero-mean noise. Then we can take the classical average and auto-correlation as

$$\begin{aligned} \overline{\epsilon(t)} &= \epsilon_0, & (7.7)\\ \overline{\epsilon(t), \epsilon(t+\tau)} &= G(\tau), & (7.8) \end{aligned}$$

where $\overline{A, B} \equiv \overline{AB} - \overline{A}\,\overline{B}$. Note that these quantities are independent of t, a condition known as stationarity. The steady-state amplitude is

$$\langle b \rangle_{ss} = \frac{-\epsilon_0}{i\delta + \gamma/2}. \tag{7.9}$$

The steady-state response to the force can be most easily calculated in the frequency domain:

$$\tilde{b}(\omega) = \frac{\sqrt{\gamma}\tilde{b}_{in}(\omega) + \tilde{\epsilon}(\omega)}{\gamma/2 + i(\delta - \omega)}, \tag{7.10}$$

where $\tilde{\epsilon}(\omega)$ is the Fourier transform of $\epsilon(t)$. Assuming that $\epsilon_0 = 0$, so that the oscillator is subject only to a classical fluctuating force, the steady-state photon number is

$$\langle \tilde{b}^\dagger(\omega)\tilde{b}(\omega) \rangle = \frac{1}{2\pi} \int_{-\infty}^{\infty} d\omega \frac{\gamma N + 2\pi S_f(\omega)}{\gamma^2/4 + (\delta - \omega)^2}, \tag{7.11}$$

where $S_f(\omega)$ is the spectrum of the driving force.

7.2 Parametric Driving

Parametric driving of a mechanical resonator is driving such that the mechanical resonance frequency is periodically modulated, typically via modulation of the spring constant. The Hamiltonian becomes explicitly time-dependent,

$$H(t) = \frac{\hat{p}^2}{2m} + \frac{m\omega_m(t)^2}{2}\hat{x}^2. \tag{7.12}$$

If we write $\omega_m(t) = \omega_m(1 + \epsilon \sin(2\Omega t + \phi))$, and assume the modulation depth ϵ is small we can use the approximate Hamiltonian,

$$H(t) = \frac{\hat{p}^2}{2m} + \frac{m\omega_m^2}{2}\hat{x}^2 + m\omega_m^2 \epsilon \sin(2\Omega t + \phi)\hat{x}^2. \tag{7.13}$$

Writing this in terms of mechanical annihilation and creation operators,

$$H = \hbar\omega_m b^\dagger b + \hbar r \sin(2\Omega t + \phi)(b + b^\dagger)^2, \tag{7.14}$$

where $r = \omega_m \epsilon/2$. If we now move to an interaction picture at frequency Ω and keep only time-independent terms (a rotating wave approximation), we find

$$H = \hbar\Delta b^\dagger b - i\hbar \left(\frac{\chi}{2} b^2 - \frac{\chi^*}{2} b^{\dagger 2} \right) \tag{7.15}$$

where $\chi = re^{i\phi}$ and $\Delta = \omega_m - \Omega$.

This Hamiltonian leads to an amplification of one quadrature and a deamplification of the other quadrature, and so produces squeezed states. On resonance, the Heisenberg equation of motion is

$$\frac{db}{dt} = \chi^* b^\dagger. \tag{7.16}$$

If we fix the phase so that χ is real, and define the quadrature operators, $\hat{X} = b + b^\dagger$ and $\hat{Y} = -i(b - b^\dagger)$, the solution to Eq. (7.16) and its hermitian conjugate may be written as

$$\hat{X}(t) = \hat{X}(0)e^{\chi t}, \tag{7.17}$$
$$\hat{Y}(t) = \hat{X}(0)e^{-\chi t}. \tag{7.18}$$

Note that the canonical commutation relations, $[\hat{X}(t), \hat{Y}(t)] = 2i$, are preserved. The X-quadrature is amplified while the Y-quadrature is attenuated. The variances are likewise amplified and attenuated,

$$\langle \Delta\hat{X}^2(t)\rangle = e^{\chi t}, \tag{7.19}$$
$$\langle \Delta\hat{Y}^2(t)\rangle = e^{-\chi t}, \tag{7.20}$$

where we have assumed that the system starts in the ground state, $\left\langle \Delta\hat{X}^2(0)\right\rangle = \left\langle \Delta\hat{Y}^2(0)\right\rangle \equiv 1$. The variance in the Y-quadrature is reduced below unity, producing a squeezed state [291]. Such a device is known as a degenerate parametric amplifier (DPA). Note that the ground state level is determined by $\chi = 0$; it is then conventional to subtract off this level to define the normally-ordered variances

$$\langle :\ \Delta\hat{X}^2\ :\rangle = \langle \Delta\hat{X}^2\rangle - 1, \tag{7.21}$$
$$\langle :\ \Delta\hat{Y}^2\ :\rangle = \langle \Delta\hat{Y}^2\rangle - 1. \tag{7.22}$$

One then easily sees that, assuming $\left\langle \Delta\hat{X}\right\rangle = \left\langle \Delta\hat{Y}\right\rangle = 0$,

$$\langle :\ \Delta\hat{X}^2\ :\rangle = \langle b^2 + b^{\dagger\,2} + 2b^\dagger b\rangle, \tag{7.23}$$

and similarly for the Y-quadrature. Since the creation operators appear to the left of the annihilation operators in this expression, it is referred to as a normally-ordered moment. While it may seem purely conventional to define normally-ordered moments, the motivation comes from the nature of homodyne detection in quantum optics, where all measurements ultimately become photon counting measurements. The statistics of these measurements are determined completely by normally-ordered moments. A similar situation can arise in microwave quantum circuits where linear amplifiers and IQ mixers are used in place of beam splitters and photodetectors [292].

The dynamics as it stands is unbounded and cannot reach a steady state. When dissipation is included a steady state is possible provided that the parametric driving does not exceed the critical value of $\kappa_c = \mu$ where μ is the damping rate for energy in the mechanical resonator. This is known as the “below threshold” condition.

The calculation of the quadrature variances is the first step in understanding how parametric driving is manifest as noise reduction. The next step is to compute how this translates into the statistics of the displacement transducer signals. If the mechanical resonator is coupled to a transducer it is necessarily an open system and we need to include dissipation and the associated quantum noise in the calculation. We will assume that the optomechanical cavity is also driven coherently on either the red, blue or simultaneously both sidebands [293]. The cavity field, or more precisely, the field leaking from the cavity will be used to transduce the mechanical squeezing.

Suppose that the cavity is driven on *one sideband*. Then setting $\Omega = 2\nu$ and transforming to an interaction picture with respect to $H_0^1 = \hbar\omega_{d1} a^\dagger a + \hbar\nu b^\dagger b$, using the rotating wave approximation, leads to

$$H_I^1 = \hbar\delta_1 a^\dagger a + \hbar g X\left(t\right) a^\dagger a + \hbar\left(\mathcal{E}_1^* a + \mathcal{E}_1 a^\dagger\right) + \hbar\left(\chi^* b^2 + \chi b^{\dagger 2}\right), \tag{7.24}$$

where $\delta_1 = \omega_c - \omega_{d1}$ is the detuning between the cavity resonance and the drive, and $X\left(t\right) = be^{-i\nu t} + b^\dagger e^{i\nu t}$.

Alternatively, following Clerk *et al.* [114], suppose the cavity is driven on two sidebands. This allows a back-action evading measurement of one quadrature of the nanoresonator's motion. Now transforming to an interaction picture with respect to $H_0^2 = \hbar\omega_c a^\dagger a + \hbar\nu b^\dagger b$, and again setting $\Omega = 2\nu$ and using the rotating wave approximation,

$$\begin{aligned} H_I^2 \;=\; & \hbar g X\left(t\right) a^\dagger a + \hbar(\mathcal{E}_1^* a e^{-i\delta_1 t} \\ & + \mathcal{E}_1 a^\dagger e^{i\delta_1 t}) + \hbar(\mathcal{E}_2^* a e^{-i\delta_2 t} + \mathcal{E}_2 a^\dagger e^{i\delta_2 t}) + \hbar\left(\chi^* b^2 + \chi b^{\dagger 2}\right), \end{aligned} \tag{7.25}$$

where $\delta_2 = \omega_c - \omega_{d2}$.

The last terms in both Eqs. (7.24) and (7.25) are the same form as the DPA below threshold. By driving the cavity on these sidebands, the cavity field on resonance couples to the slowly-varying quadratures of the mechanical resonator motion. For the cavity driven on one sideband, the Hamiltonian (7.24) leads to the quantum Langevin equations,

$$\dot{a}(t) \;=\; -i\delta_1 a(t) - i\mathcal{E}_1 - \frac{\mu}{2}a(t) + \sqrt{\mu}a_{in}(t) - ig\left[b(t)e^{-i\nu t} + b^\dagger(t)e^{i\nu t}\right]a(t), \tag{7.26}$$

$$\dot{b}(t) \;=\; -2i\chi b^\dagger(t) - iga^\dagger(t)a(t)e^{i\nu t} - \frac{\gamma}{2}b(t) + \sqrt{\gamma}b_{in}(t). \tag{7.27}$$

where

$$\left\langle a_{in}^\dagger\left(t\right), a_{in}\left(t'\right)\right\rangle \;=\; \delta\left(t - t'\right), \tag{7.28}$$

$$\left\langle b_{in}^\dagger\left(t\right), b_{in}\left(t'\right)\right\rangle \;=\; N_m\delta\left(t - t'\right), \tag{7.29}$$

with N_m as the thermal occupancy of the mechanical bath mode at the mechanical resonance frequency,

$$N_m = \left[\exp\left(\frac{\hbar\nu}{kT_m}\right) - 1\right]^{-1}, \tag{7.30}$$

and T_m being the effective mechanical bath temperature.

Assuming the condition for resolved sidebands,

$$|\delta_1| >> \mu, \tag{7.31}$$

solutions to (7.26)-(7.27) can be approximated by

$$\begin{aligned} a(t) &= a_0(t) + a_+(t)e^{-i\nu t} + a_-(t)e^{i\nu t}, && (7.32)\\ b(t) &= b_0(t), && (7.33) \end{aligned}$$

where the subscripts $+$ and $-$ denote sidebands above and below, respectively, the cavity drive frequency. Substituting this into Eqs. (7.26)-(7.27) and equating frequencies,

$$\begin{aligned} \dot{a}_0(t) &= -i\delta_1 a_0(t) - i\mathcal{E}_1 - ig\left[a_+(t)b_0^\dagger(t) + a_-(t)b_0(t)\right] - \frac{\mu}{2}a_0(t) + \sqrt{\mu}a_{o,in}(t), && (7.34)\\ \dot{a}_+(t) &= -i(\delta_1 - \nu)a_+(t) - iga_0(t)b_0(t) - \frac{\mu}{2}a_+(t) + \sqrt{\mu}a_{+,in}(t), && (7.35)\\ \dot{a}_-(t) &= -i(\delta_1 + \nu)a_-(t) - iga_0(t)b_0^\dagger(t) - \frac{\mu}{2}a_-(t) + \sqrt{\mu}a_{-,in}(t), && (7.36)\\ \dot{b}_0(t) &= -2i\chi b_0^\dagger(t) - ig\left[a_0^\dagger(t)a_+(t) + a_0(t)a_-^\dagger(t)\right] - \frac{\gamma}{2}b_0(t) + \sqrt{\gamma}b_{o,in}(t). && (7.37) \end{aligned}$$

Driving the cavity on either on the first blue or the first red sideband means the other sideband will be far from resonance. We may then neglect the off-resonant sideband. If the cavity is driven on its first blue sideband,

$$\omega_d = \omega_c + \nu, \qquad (i.e. \quad \delta_1 = -\nu), \tag{7.38}$$

We now neglect $a_+(t)$ and assuming $g << \mu, |\delta_1|, |\mathcal{E}_1|$ and, without loss of generality, that $\mathcal{E}_1$ is real and positive, the steady-state of the blue sideband component s $\langle a_0^b(t\to\infty)\rangle = \mathcal{E}_1/\nu$. Then Eqs. (7.36) and (7.37), (dropping sideband subscripts) gives

$$\begin{aligned} \dot{a}(t) &= -\frac{\mu}{2}a(t) - igb^\dagger(t) + \sqrt{\mu}a_{in}(t), && (7.39)\\ \dot{a}^\dagger(t) &= -\frac{\mu}{2}a^\dagger(t) + igb(t) + \sqrt{\mu}a_{in}^\dagger(t), && (7.40)\\ \dot{b}(t) &= -\frac{\gamma}{2}b(t) - 2i\chi b^\dagger(t) - iga^\dagger(t) + \sqrt{\gamma}b_{in}(t), && (7.41)\\ \dot{b}^\dagger(t) &= -\frac{\gamma}{2}b^\dagger(t) + 2i\chi^* b(t) + iga(t) + \sqrt{\gamma}b_{in}^\dagger(t), && (7.42) \end{aligned}$$

where the linearised coupling is $g = \left|g\langle a_0^b(t\to\infty)\rangle\right|$. This can be described by the effective Hamiltonian

$$H_b = \hbar\left(\chi^* b^2 + \chi b^{\dagger 2}\right) + \hbar g\left(ab + a^\dagger b^\dagger\right). \tag{7.43}$$

Assuming stability, the steady-state is a Gaussian state of zero amplitude with fluctuations fully characterised by its correlation matrix. The system is stable provided that

$$|\chi| < -\frac{g^2}{\mu} + \frac{\gamma}{4}. \tag{7.44}$$

We now Fourier transform the system to obtain

$$-\mathbf{D}\begin{bmatrix} a_{in}(\omega) \\ a_{in}^{\dagger}(-\omega) \\ b_{in}(\omega) \\ b_{in}^{\dagger}(-\omega) \end{bmatrix} = \mathbf{A}_b \begin{bmatrix} a(\omega) \\ a^{\dagger}(-\omega) \\ b(\omega) \\ b^{\dagger}(-\omega) \end{bmatrix}, \tag{7.45}$$

where **D** denotes the damping matrix

$$\mathbf{D} = \begin{bmatrix} \sqrt{\mu} & 0 & 0 & 0 \\ 0 & \sqrt{\mu} & 0 & 0 \\ 0 & 0 & \sqrt{\gamma} & 0 \\ 0 & 0 & 0 & \sqrt{\gamma} \end{bmatrix}, \tag{7.46}$$

and the dynamical matrix in the frequency domain is

$$\mathbf{A}_b = \begin{bmatrix} i\omega - \frac{\mu}{2} & 0 & 0 & -ig \\ 0 & i\omega - \frac{\mu}{2} & ig & 0 \\ 0 & -ig & i\omega - \frac{\gamma}{2} & -2i\chi \\ ig & 0 & 2i\chi^* & i\omega - \frac{\gamma}{2} \end{bmatrix}. \tag{7.47}$$

The column vectors in (7.45) will be denoted by $\mathbf{a}_{in}^b(\omega)$ and $\mathbf{a}^b(\omega)$, respectively.

The output field from the cavity is related to the intracavity field by

$$a_{out}(\omega) = \sqrt{\mu}a(\omega) + a_{in}(\omega), \tag{7.48}$$
$$b_{out}(\omega) = \sqrt{\gamma}b(\omega) + b_{in}(\omega). \tag{7.49}$$

This may be written, using Eq. (7.45), as

$$\mathbf{a}_{out}^b(\omega) = \mathbf{D}\mathbf{a}^b(\omega) - \mathbf{a}_{in}^b(\omega) = -\left(\mathbf{D}\mathbf{A}_b^{-1}\mathbf{D} + \mathbf{1}\right)\mathbf{a}_{in}^b(\omega). \tag{7.50}$$

To incorporate the effects of internal losses in the cavity, the total damping due to both internal losses and out-coupling of the field would be included in Eqs. (7.39)-(7.42), but only the component due to out-coupling of the field would be included in the boundary condition of Eq. (7.50). This would lead to a slight reduction in the magnitude of the squeezing attainable.

In a similar way we can treat red sideband driving,

$$\omega_d = \omega_c - \nu, \qquad (i.e. \quad \delta_1 = +\nu). \tag{7.51}$$

The oscillation of the red sideband of the driving field is off-resonance and accordingly we neglect $a_-(t)$. Assuming $g << \mu, |\delta_1|, |\mathcal{E}_1|$ and $\mathcal{E}_1$ real and positive, we solve Eq. (7.34) for the steady-state amplitude at the red sideband drive frequency, $\langle a_o^r(t \to \infty)\rangle = -\mathcal{E}_1/\nu$. From Eqs. (7.35) and (7.37), (again dropping sideband subscripts),

$$\dot{a}(t) = -\frac{\mu}{2}a(t) + igb(t) + \sqrt{\mu}a_{in}(t), \tag{7.52}$$
$$\dot{a}^{\dagger}(t) = -\frac{\mu}{2}a^{\dagger}(t) - igb^{\dagger}(t) + \sqrt{\mu}a_{in}^{\dagger}(t), \tag{7.53}$$
$$\dot{b}(t) = -\frac{\gamma}{2}b(t) - 2i\chi b^{\dagger}(t) + iga(t) + \sqrt{\gamma}b_{in}(t), \tag{7.54}$$
$$\dot{b}^{\dagger}(t) = -\frac{\gamma}{2}b^{\dagger}(t) + 2i\chi^* b(t) - iga^{\dagger}(t) + \sqrt{\gamma}b_{in}^{\dagger}(t), \tag{7.55}$$

where, equivalently to above, $g = -g \langle a_o^r(t \to \infty) \rangle$. The effective Hamiltonian is

$$H_r = \hbar \left(\chi^* b^2 + \chi b^{\dagger 2} \right) + \hbar g \left(a^\dagger b + a b^\dagger \right). \tag{7.56}$$

The stability conditions are now

$$|\chi| < \frac{g^2}{\mu} + \frac{\gamma}{4}, \quad |\chi| < \frac{\gamma + \mu}{4}, \tag{7.57}$$

We have,

$$\mathbf{a}_{out}^r(\omega) = \mathbf{D}\mathbf{a}^r(\omega) - \mathbf{a}_{in}^r(\omega) = -\left(\mathbf{D}\mathbf{A}_r^{-1}\mathbf{D} + \mathbf{1} \right) \mathbf{a}_{in}^r(\omega), \tag{7.58}$$

where

$$\mathbf{A}_r = \begin{bmatrix} i\omega - \frac{\mu}{2} & 0 & ig & 0 \\ 0 & i\omega - \frac{\mu}{2} & 0 & -ig \\ ig & 0 & i\omega - \frac{\gamma}{2} & -2i\chi \\ 0 & -ig & 2i\chi^* & i\omega - \frac{\gamma}{2} \end{bmatrix}. \tag{7.59}$$

Driving on the red and the blue sidebands the Hamiltonian of Eq. (7.25) gives

$$\begin{aligned} \dot{a}(t) &= -i\mathcal{E}_1 e^{i\delta_1 t} - i\mathcal{E}_2 e^{i\delta_2 t} - \frac{\mu}{2} a(t) + \sqrt{\mu} a_{in}(t) \\ &- ig \left[b(t) e^{-i\nu t} + b^\dagger(t) e^{i\nu t} \right] a(t), \end{aligned} \tag{7.60}$$

$$\dot{b}(t) = -2i\chi b^\dagger(t) - iga^\dagger(t)a(t)e^{i\nu t} - \frac{\gamma}{2} b(t) + \sqrt{\gamma} b_{in}(t), \tag{7.61}$$

with the input noise correlation functions (7.28)-(7.29). Assuming that we are in the resolved sideband regime,

$$|\delta_1|, |\delta_2| >> \mu, \tag{7.62}$$

the same assumption, (7.32)-(7.33), should solve Eqs. (7.60)-(7.61). Substituting, equating frequency components and also assuming $\delta_1 = -\nu$ and $\delta_2 = +\nu$ (corresponding to driving on both the red and blue sidebands), we have

$$\dot{a}_0(t) = -ig \left[b(t) a_-(t) + b^\dagger(t) a_+(t) \right] - \frac{\mu}{2} a_0(t) + \sqrt{\mu} a_{0,in}(t), \tag{7.63}$$

$$\dot{a}_+(t) = -igb(t)a_0(t) - i\mathcal{E}_1 + \left(i\nu - \frac{\mu}{2} \right) a_+(t) + \sqrt{\mu} a_{+,in}(t), \tag{7.64}$$

$$\dot{a}_-(t) = -igb^\dagger(t)a_0(t) - i\mathcal{E}_2 - \left(i\nu + \frac{\mu}{2} \right) a_-(t) + \sqrt{\mu} a_{-,in}(t), \tag{7.65}$$

$$\dot{b}_0(t) = -2i\chi b^\dagger(t) - ig \left[a_0^\dagger(t) a_+(t) + a_-^\dagger(t) a_0(t) \right] - \frac{\gamma}{2} b(t) + \sqrt{\gamma} b_{in}(t). \tag{7.66}$$

Setting $\mathcal{E}_1 = \mathcal{E} e^{-i\psi}$ and $\mathcal{E}_2 = -\mathcal{E} e^{i\psi}$ where $\mathcal{E}$ is real, and assuming $g << \mu, \mathcal{E}$, we have the steady-state amplitudes at the drive frequencies $\left\langle a_+^{br}(t \to \infty) \right\rangle = \mathcal{E} e^{i\psi}/\nu$ and $\left\langle a_-^{br}(t \to \infty) \right\rangle = \mathcal{E} e^{-i\psi}/\nu$. The phase variable ψ is the relative phase between the two cavity driving amplitudes.

Then Eqs. (7.63) and (7.66), with the corresponding Hermitian conjugate equations and again dropping sideband subscripts, lead to

$$\dot{a}(t) = -ig\left[b(t)e^{-i\psi} + b^\dagger(t)e^{i\psi}\right] - \frac{\mu}{2}a(t) + \sqrt{\mu}a_{in}(t), \tag{7.67}$$

$$\dot{a}^\dagger(t) = ig\left[b(t)e^{-i\psi} + b^\dagger(t)e^{i\psi}\right] - \frac{\mu}{2}a^\dagger(t) + \sqrt{\mu}a_{in}^\dagger(t), \tag{7.68}$$

$$\dot{b}(t) = -2i\chi b^\dagger(t) - ige^{i\psi}\left[a(t) + a^\dagger(t)\right] - \frac{\gamma}{2}b(t) + \sqrt{\gamma}b_{in}(t), \tag{7.69}$$

$$\dot{b}^\dagger(t) = 2i\chi^* b(t) + ige^{-i\psi}\left[a(t) + a^\dagger(t)\right] - \frac{\gamma}{2}b^\dagger(t) + \sqrt{\gamma}b_{in}^\dagger(t), \tag{7.70}$$

where the optomechanical coupling is $g = G_0\left|\left\langle a_+^{br}(t\to\infty)\right\rangle\right| = G_0\left|\left\langle a_+^{br}(t\to\infty)\right\rangle\right|$. The system is stable provided that

$$\chi < \frac{\gamma}{4}. \tag{7.71}$$

Note that this stability threshold is more stringent than that, Eq. (7.44), for the red sideband drive, but less stringent than that, Eq. (7.71), for the blue sideband drive. The effective Hamiltonian is

$$H_{br} = \hbar\left(\chi^* b^2 + \chi b^{\dagger 2}\right) + \hbar g\left(a + a^\dagger\right)\left(be^{-i\psi} + b^\dagger e^{i\psi}\right). \tag{7.72}$$

The second term has the form of a back-action evading measurement of a quadrature of the mechanical resonator motion; which quadrature is measured depends on the relative phase of the two cavity drives (and ultimately, on the local oscillator phase of the output microwave field homodyne detection). Physically, the Raman processes corresponding to the injection of a photon at the cavity resonance and the absorption or emission of a phonon by the mechanical resonator are both possible and occur at the same rate.

Given the system is stable, we may Fourier transform Eqs. (7.67)-(7.70) and apply the usual boundary conditions to find

$$\mathbf{a}_{out}^{br}(\omega) = \mathbf{D}\mathbf{a}^{br}(\omega) - \mathbf{a}_{in}^{br}(\omega) = -\left(\mathbf{D}\mathbf{A}_{br}^{-1}\mathbf{D} + \mathbf{1}\right)\mathbf{a}_{in}^{br}(\omega), \tag{7.73}$$

where the dynamical matrix is now

$$\mathbf{A}_{br} = \begin{bmatrix} i\omega - \frac{\mu}{2} & 0 & -ige^{-i\psi} & -ige^{i\psi} \\ 0 & i\omega - \frac{\mu}{2} & ige^{-i\psi} & ige^{i\psi} \\ -ige^{i\psi} & -ige^{i\psi} & i\omega - \frac{\gamma}{2} & -2i\chi \\ ige^{-i\psi} & ige^{-i\psi} & 2i\chi^* & i\omega - \frac{\gamma}{2} \end{bmatrix}. \tag{7.74}$$

We now calculate the variances in the quadrature phase amplitudes of the mechanical resonator,

$$X_m' = be^{-i\phi} + b^\dagger e^{i\phi}, \tag{7.75}$$

$$Y_m' = -i(be^{-i\phi} - b^\dagger e^{i\phi}), \tag{7.76}$$

where ϕ is a variable phase reference. The normally ordered variances are,

$$\begin{aligned} S_{X'_m} &= \langle : X'_m, X'_m : \rangle \\ &= e^{-2i\phi} \left\langle b^2 \right\rangle + e^{2i\phi} \left\langle b^{\dagger 2} \right\rangle + 2 \left\langle b^\dagger b \right\rangle, \quad (7.77) \\ S_{Y'_m} &= \langle : Y'_m, Y'_m : \rangle \\ &= -e^{-2i\phi} \left\langle b^2 \right\rangle - e^{2i\phi} \left\langle b^{\dagger 2} \right\rangle + 2 \left\langle b^\dagger b \right\rangle. \quad (7.78) \end{aligned}$$

These may be calculated by writing quantum Langevin equations for all second moments of the nanoresonator and cavity operators, and solving for their expectations in the steady-state.

With χ real, the optimally squeezed quadrature is Y'_m with $\phi = -\pi/4$, irrespective of the driving conditions, provided that we set $\psi = \pi/4$ for the two sideband drive case. Any quadrature may be optimally squeezed through suitable choice of the phase of the parametric driving; with $\mathrm{Arg}\,[\chi] = -\pi/2 \quad (+\pi/2)$ the position (momentum) quadrature is squeezed. We will give the results for χ real and the squeezed (Y'_m) quadrature. For driving on the blue, red, and blue and red sidebands we find that,

$$S^b_{Y'_m} = \frac{2\left[\mu(N_m\gamma - 2\chi)(\gamma + \mu + 4\chi) - 4g^2(N_m\gamma - \mu - 2\chi)\right]}{[(\gamma + \mu + 4\chi)(\mu\gamma + 4\mu\chi - 4g^2)]}, \quad (7.79)$$

$$S^r_{Y'_m} = \frac{2(N_m\gamma - 2\chi)(4g^2 + \mu\gamma + \mu^2 + 4\mu\chi)}{(\gamma + \mu + 4\chi)\,(4g^2 + \mu\gamma + 4\mu\chi)}, \quad (7.80)$$

$$S^{br}_{Y'_m} = \frac{2N_m\gamma - 4\chi}{\gamma + 4\chi}. \quad (7.81)$$

At the threshold of Eq. (7.57), assuming $4g^2 < \mu^2$, for the red sideband drive,

$$S^r_{Y'_m} = -\frac{1}{2}\frac{8g^2 + 2\gamma\mu + \mu^2}{4g^2 + 2\gamma\mu + \mu^2} + N_m \frac{\gamma\mu(8g^2 + 2\gamma\mu + \mu^2)}{(4g^2 + \gamma\mu)(4g^2 + 2\gamma\mu + \mu^2)}. \quad (7.82)$$

For all driving conditions, at threshold and in the adiabatic limit, $S_{Y'_m} \to -\frac{1}{2} + N_m$ and the noise in the conjugate quadrature (X'_m) diverges, as expected [291] .

The squeezing of a quadrature of the cavity field ($S_{X'_c}$ or $S_{Y'_c}$) is given by Eq. (7.77) or (7.78) with the replacement $b \to a$. Here we quote the results for the red sideband driving,

$$S^r_{Y'_m} = S^r_{X'_c} + \frac{2\mu(n^0_m\gamma - 2\chi)}{4g^2 + \gamma\mu + 4\mu\chi}, \quad (7.83)$$

such that at the threshold (7.57), assuming $4g^2 < \mu^2$,

$$S^r_{Y'_m} = S^r_{X'_c} - \frac{1}{2} + \frac{\gamma\mu}{4g^2 + \gamma\mu} N_m. \quad (7.84)$$

Thus squeezing of the internal cavity field implies squeezing of a mechanical resonator quadrature provided that

$$N_m < \frac{4g^2 + \gamma\mu}{2\gamma\mu}. \quad (7.85)$$

In an experiment we are primarily interested in how the output field from the cavity reflects the squeezing of the mechanical resonator. As discussed in Sec. 8.2, this requires that the cavity field act as a good transducer for the mechanical resonator, and that requires that the cavity field is rapidly damped, for in that case the output field responds immediately to changes in the mechanical displacement. Then we can perform an adiabatic elimination of the intracavity field. The details for the parametrically driven mechanical resonator discussed in this section are given in [293].

7.3 Single Photon Driving

Thus far we have been exclusively concerned with driving the optical system with a coherent laser source. however the ongoing development of single photon sources for quantum information processing [294] suggests these sources will soon be available for optomechanics. In the case of microwave nanomechanics, intracavity single photons sources are already well developed for experiments in circuit quantum electrodynamics [295, 296]. In fact one can coherently generate some very non classical states of a microwave cavity, such as cat states, and these can be used to control the mechanical resonator directly.

We begin with a short review of single photon states. In the continuum limit we define the positive frequency operator for the multi-mode field input to the cavity mode (a), at the input mirror, as

$$a_i(t) = e^{-i\Omega_a t}\frac{1}{\sqrt{2\pi}}\int_{-\infty}^{\infty} d\omega a_i(\omega)e^{-i\omega t} \tag{7.86}$$

where

$$[a_i(\omega_1), a_i^\dagger(\omega_2)] = \delta(\omega_1 - \omega_2) \tag{7.87}$$

Only some finite bandwidth, B, of these modes are excited around the carrier frequency Ω_a. The multi-mode single photon state is then defined by [297]

$$|1\rangle = \int_{-\infty}^{\infty} \nu(\omega)a_i^\dagger(\omega)|0\rangle. \tag{7.88}$$

Normalisation requires that $\int_{-\infty}^{\infty} d\omega|\nu(\omega)|^2 = 1$. This state has zero average field amplitude $\langle a(t)\rangle = 0$, but

$$\langle a^\dagger(t)a(t)\rangle \equiv n(t) = |\nu(t)|^2, \tag{7.89}$$

where $\nu(t)$ is the Fourier transform of $\nu(\omega)$. For example, if a single photon is prepared in a single-sided cavity at time $t = t_0$ with cavity decay rate γ, the mode function $\nu(t)$ is given by the exponential

$$\nu(t) = \begin{cases} \sqrt{\gamma}e^{-\gamma(t-t_0)/2} & t \geq t_0, \\ 0 & t < t_0. \end{cases} \tag{7.90}$$

Let us now consider an optomechanical cavity driven on the red sideband in the linearised regime; see Eq. (6.13). If we now add an extra single photon pulse on top of the coherent driving field, how does the system respond? If we assume that before the single photon pulse is added the system has reached a steady state, then the single photon pulse will push it way from the steady state, but it will eventually relax. Interesting dynamics will result, however, if the optomechanical

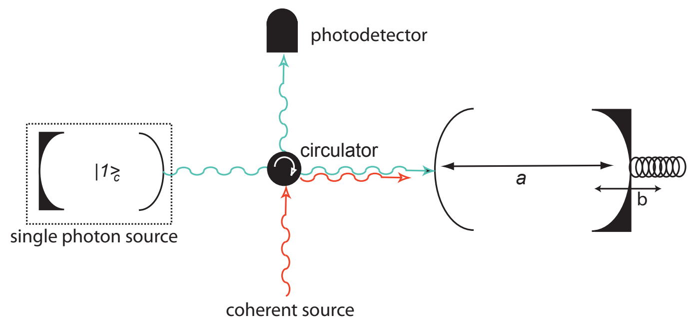

Fig. 7.1. A single photon optomechanical system. A single-sided opto-mechanical cavity of (right; depicted as a FabryPerot cavity with a moving end mirror) is driven by both a single-photon pulse and a continuous wave (CW) coherent pump source. Reproduced from [298].

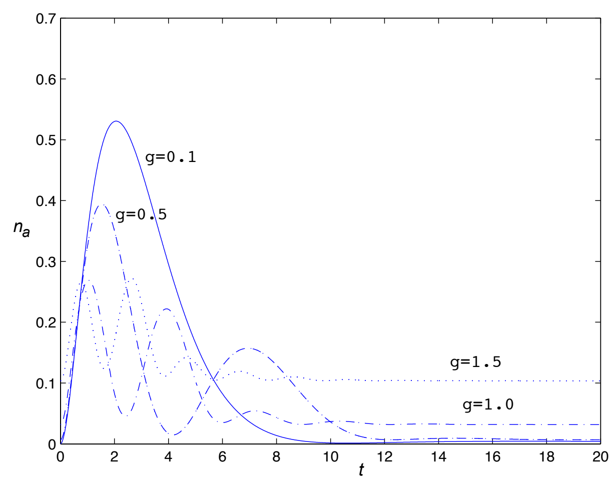

Fig. 7.2. The response of the intracvity mean photon number, above the coherent steady state value, versus time of a single optomechanical cavity driven near the first red sideband, for different values of the linearised coupling rate g. Reproduced from [298].

coupling over this time is big enough to enable the coherent exchange between cavity photon and mechanical phonon.

This question was addressed by Akram *et al.* [298]. The approach taken was to include the actual single photon source, and treat the optomechanical cavity as a cascaded system [299,300]. The source was modelled as a one-sided cavity that, at $t = 0$, is prepared in a single photon state using one of the intracavity methods currently used [301], see Fig. 7.1. The emission rate of the single added photon from the cavity is proportional to the photon number in the cavity in the displaced picture, so one needs to compute $\langle a^\dagger a \rangle$ as a function of time.

The results are shown in Fig. 7.2. As the linearised optomechanical coupling strength is increased we begin to see oscillations in the intracavity photon number. The minima corresponds to times when the excitation resides in the mechanical resonator as a phonon. The experimental signature of coherent photon-phonon exchange would thus be oscillations in the single photon detection rate outside the cavity. of course in order see this the large coherent amplitude at the driving laser frequency would first need to be filtered out. Note that as the optomechanical coupling increases the system does not return to a zero photon state as the residual excitation on the blue sideband heats the optomechanical system.

8 Quantum Measurement

8.1 A Quick Introduction

The problem of measurement of an individual quantum system lies at the heart of quantum mechanics. Quantum mechanics introduces into measurement the concepts of probabilistic measurement outcomes [302] and the projection postulate (or "wavefunction collapse") [303]. However, the lack of experimentally accessible individual quantum systems prohibited the experimental study of this problem until relatively recently [304].

The projection postulate states that an ideal measurement of an observable will project the state of the system being measured onto an eigenstate of the measured observable. Thus one may speak of the conditional dynamics of a system, being conditioned on some known measurement record. This may be expressed in terms of a model for a system interacting with a meter [305], in the more abstract language of measurement operators, operations and effects [306], or as a sum over histories using a path integral approach [307, 83]. However, the key point is that all of these formulations reproduce the same correlation functions for system observables [308].

Suppose that one seeks to measure an observable X having a continuous spectrum x, and particular measurement outcomes are denoted by r. Recall that measurement operators M_r are defined such that the probability of the measurement outcome r and the post-measurement conditional state of the system are given by

$$P(r) = \mathrm{Tr}\left[\rho(\mathrm{t})\mathrm{M}^{\dagger}(\mathrm{r})\mathrm{M}(\mathrm{r})\right], \qquad \rho_{\mathrm{r}}(\mathrm{t}^{+}) = \frac{\mathrm{M}(\mathrm{r})\rho(\mathrm{t})\mathrm{M}^{\dagger}(\mathrm{r})}{\mathrm{P_r}}, \tag{8.1}$$

respectively. The unconditional (non-selective) evolution is

$$\rho(t^{+}) = \int_{-\infty}^{+\infty} P(r)\rho_r(t^{+})dr = \int_{-\infty}^{+\infty} M(r)\rho(t)M^{\dagger}(r)dr. \tag{8.2}$$

Through Heisenberg's uncertainty principle, quantum mechanics also demands the necessity of measurement back-action on the measured system [309, 310]. It also places limits on the variances of conjugate variables for any quantum state [311], and places limits on the certainty with which canonically conjugate variables can be simultaneously known [312]. For the uncertainty in the position and momentum of a particle,

$$\Delta x \cdot \Delta p \geq \frac{\hbar}{2}. \tag{8.3}$$

This is a straightforward consequence of the lack of commutativity of the position and momentum operators in quantum mechanics.

In the context of measurement, an observable that is canonically conjugate to the measured observable must be perturbed by the measurement. Quantitatively, the added position noise spectral density due to a position measurement (or "imprecision") $S_x^{\mathrm{imp}}(\omega)$ and the associated back-action force noise spectral density $S_F^{\mathrm{ba}}(\omega)$ are constrained by

$$S_x^{\mathrm{imp}}(\omega) S_F^{\mathrm{ba}}(\omega) \geq \frac{\hbar^2}{4}. \tag{8.4}$$

It may be readily derived for simple physical systems, though a rigorous derivation is possible by considering conditional dynamics under a sequence of measurements [304]. Using Eq. (2.12) on resonance, we have

$$S_x^{\mathrm{imp}}(\omega_m) S_x^{\mathrm{ba}}(\omega_m) \geq \frac{\hbar^2}{4m^2\gamma^2\omega_m}. \tag{8.5}$$

The total added noise of the measurement is a minimum when there is an equal uncertainty arising from the measurement imprecision and from the added noise due to the back-action of the detector; that is, when $S_x^{\mathrm{imp}}(\omega_m) = S_x^{\mathrm{ba}}(\omega_m)$. Then the so-called standard quantum limit on the noise added by the measurement is

$$S_x^{\mathrm{SQL}}(\omega_m) = \frac{\hbar}{m\gamma\omega_m}. \tag{8.6}$$

The uncertainty due to the detector imprecision is then half of Eq. (8.6), multiplied by the mechanical bandwidth (γ). The result is the standard quantum limit [313],

$$\Delta x_{\mathrm{SQL}} = \sqrt{\frac{\hbar}{2m\omega_m}}. \tag{8.7}$$

It is important to note, however, that this limit is not really fundamental; it can, at least in principle, be circumvented via coherent quantum noise cancellation [314]. It is also worth noting that this limit is numerically equivalent to the zero-point uncertainty quoted earlier in Eq. (3.25).

8.1.1 Conditional Dynamics

The conditional dynamics of a measured system may be described by specifying appropriate measurement operators, as in Eq. (8.1). Continuous measurement may be formulated as the limit of a sequence of discrete measurements [315]. Consider small time intervals of length Δt, with a weak measurement in each such interval having a strength proportional to the time interval. Now define the Gaussian measurement operator corresponding to the measurement outcome r, a Gaussian-weighted sum of projectors onto the eigenstates of X, describing an unbiased measurement subject to Gaussian noise, by

$$M(r) = \sqrt[4]{\frac{4k\Delta t}{\pi}} \int_{-\infty}^{+\infty} \exp\left[-2k\Delta t(x-r)^2\right] |x\rangle \langle x| \, dx, \tag{8.8}$$

where k is the "strength" of the measurement. If Δt is sufficiently small then this Gaussian is broader than the system state, $\psi(x)$, and the measurement outcome has the probability distribution,

$$P(r) = \sqrt{\frac{4k\Delta t}{\pi}} \exp\left[-4k\Delta t \left(r - \langle X\rangle\right)^2\right]. \tag{8.9}$$

Taking the continuous limit, $\Delta t \to 0$, substituting Eqs. (8.8) and (8.9) into Eq. (8.1), and normalizing, one obtains the stochastic Schrödinger equation,

$$\begin{aligned} |\psi(t+dt)\rangle = \Big[1 - &\frac{i}{\hbar} H\, dt - k\left(X - \langle X\rangle\right)^2 dt \\ &+ 4k\left(X - \langle X\rangle\right)\left(dy - \langle X\rangle\, dt\right)\Big] |\psi(t)\rangle, \end{aligned} \tag{8.10}$$

where the measurement record increment is given by $dr = \langle X \rangle\, dt + dW/\sqrt{8k}$, with dW being the infinitesimal increment of a Wiener process. As the observer integrates dr, the state progressively collapses. Now $|\psi(t)\rangle$ corresponding to a particular realization of the Wiener process is referred to as a quantum trajectory [316]. One may also write down the corresponding (stochastic) conditional master equation [317],

$$d\rho = -\frac{i}{\hbar}[H,\rho] - k\,[X,[X,\rho]]\,dt + \sqrt{2k}\,(X\rho + \rho X - 2\langle X \rangle \rho)\,dW. \tag{8.11}$$

A generalized Lindblad form of diffusive measurement master equation under Gaussian noise with detection efficiency η, is

$$d\rho = -\frac{i}{\hbar}[H,\rho]\,dt + 2k\mathcal{D}[X]\,\rho\,dt + \sqrt{2\eta k}\mathcal{H}\left[Xe^{i\phi}\right]\rho\,dW, \tag{8.12}$$

where the dissipative superoperator is defined as

$$\mathcal{D}[X]\,\rho \equiv X\rho X^\dagger - \frac{1}{2}X^\dagger X\rho - \frac{1}{2}\rho X^\dagger X, \tag{8.13}$$

and the so-called measurement superoperator is

$$\mathcal{H}[X]\,\rho = X\rho + \rho X^\dagger - \left\langle X + X^\dagger \right\rangle \rho. \tag{8.14}$$

The associated measurement record increment is

$$dr = \left\langle X + X^\dagger \right\rangle dt + \frac{dW}{\sqrt{2\eta k}}. \tag{8.15}$$

If X is Hermitian, then Eq. (8.12) is equivalent to Eq. (8.11). In quantum optics, such a diffusive measurement master equation may be derived as the limit of a conditional master equation describing quantum counting on a field mixed with a strong coherent local oscillator [42]. Then Eq. (8.12) is the homodyne detection master equation.

From Eq. (8.12), the conditional dynamics of any system operator A may be evaluated as

$$\begin{aligned} d\langle A \rangle \;&=\; -\frac{i}{\hbar}\langle [A,H] \rangle\,dt + k\left\langle 2X^\dagger A X - X^\dagger X A - A X^\dagger X \right\rangle dt \\ &\qquad + \sqrt{2\eta k}\left\langle X^\dagger A + A X - \langle A \rangle \left\langle X + X^\dagger \right\rangle \right\rangle dW. \end{aligned} \tag{8.16}$$

In particular, if X is Hermitian,

$$d\langle A \rangle = -\frac{i}{\hbar}\langle [A,H] \rangle\,dt - k\,\langle [X,[X,A]] \rangle\,dt + \sqrt{2\eta k}\,[\langle \{X,A\} \rangle - 2\langle X \rangle \langle A \rangle]\,dW. \tag{8.17}$$

Further, if the system under consideration is a harmonic oscillator, the initial state is Gaussian, and one considers the measurement of position, $X \equiv \hat{x}$, then the system evolution is fully specified by quantum stochastic differential equations for the first and second moments [318]. The result is damping of the position variance, and a corresponding diffusion of the momentum at a rate required by the uncertainty principle. In the case of a dissipative measurement of a harmonic oscillator, $X \equiv a$, as defined in Eq. (3.8), the measurement record is related to a quadrature of the harmonic oscillator, and the measurement is referred to as homodyne detection. Both measurements select coherent states, though the system relaxes to the ground state in the case of a dissipative measurement.

8.1.2 Quantum Non-Demolition Measurement

Heisenberg's uncertainty principle states that canonically conjugate observables cannot be known simultaneously with arbitrary precision, but this does not exclude the possibility that one observable may be known with arbitrary precision [319]. For the case of continuous measurement, however, only particular observables can be monitored with arbitrary precision due to the effect of measurement back-action feeding back into the measured observable. Observables on which no perturbing measurement back-action acts are termed quantum non-demolition (QND) observables, and the corresponding measurements are called QND measurements [320]. Some progress has been made towards their implementation [321], particularly in the field of optics [322] and more recently in cavity QED [323].

A sufficient condition for a QND measurement is [304]

$$[X, H] = 0, \tag{8.18}$$

where X is the observable to be measured and H is the composite system-meter Hamiltonian. In the Heisenberg picture a QND observable obeys $[X(t), X(t')] = 0$. Generally, any constant of the motion of the system is a QND observable, and Eq. (8.18) reduces to $[X, H_I] = 0$ where H_I is the system-meter interaction Hamiltonian.

For a free mass, the QND observables are momentum and energy. Energy and phase are one pair of QND observables for the harmonic oscillator, while another pair of QND observables for the harmonic oscillator are the slowly-varying quadratures defined by Eqs. (3.12) and (3.16). For a harmonic oscillator, the standard quantum limit is applicable when one seeks to monitor the position of a resonator, that is, when one monitors the amplitude and phase of the oscillation simultaneously. A sensitivity better than the standard quantum limit is achievable if one monitors only one quadrature.

A QND measurement of the energy of a harmonic oscillator can be achieved by the Unruh-Braginsky interaction [324], $H_I = K\hat{Q}\hat{x}^2$, where $\hat{Q}$ is a meter coordinate. A number of schemes may be considered to measure a slowly-varying quadrature of an oscillator [325]. In one, the transducer must be coupled to both its position and momentum and both couplings must be modulated sinusoidally, such as

$$H_I = K\hat{X}(t)\hat{Q} = K\sqrt{\frac{2m\omega_m}{\hbar}}\cos\omega_m t\;\hat{x}\;\hat{Q} - K\sqrt{\frac{2}{\hbar m\omega_m}}\sin\omega_m t\;\hat{p}\;\hat{Q}. \tag{8.19}$$

In principle, a two-transducer measurement could be avoided by making a stroboscopic measurement, though experimental imperfections in such a scheme would be problematic. Another alternative is to modulate the coupling of a single weakly-coupled position or momentum transducer and filter the output [326]. For a position transducer, the required interaction is

$$H_I = K\hat{Q}\hat{x}\cos\omega_m t = \frac{1}{2}K\sqrt{\frac{\hbar}{2m\omega_m}}\hat{Q}\left[\hat{X}(t) + \cos 2\omega_m t\;\hat{X}(t) + \sin\omega_m t\;\hat{P}(t)\right], \tag{8.20}$$

while for a momentum transducer, the required interaction is

$$\begin{aligned} H_I &= \frac{K}{m\omega_m}\hat{Q}\hat{p}\sin\omega_m t \\ &= \frac{K}{2}\sqrt{\frac{\hbar}{2m\omega_m}}\hat{Q}\left[\hat{X}(t) - \cos 2\omega_m t\;\hat{X}(t) - \sin 2\omega_m t\;\hat{P}(t)\right]. \end{aligned} \tag{8.21}$$

Averaging over a measurement time $\tau >> 2\pi/\omega_m$, and ensuring that the back-action forces have negligible frequency components at $\pm 2\omega_m$, the achievable uncertainty is $\Delta x/\sqrt{\omega_m \tau}$, where Δx is the standard quantum limit of Eq. (8.7).

8.1.3 Quantum-limited Measurement

Given that the standard quantum limit exists for a continuous position measurement, the question remains as to how one attains it. Most measurement systems include an amplifier, and so the quantum limit to amplification is also relevant.

A linear, phase-insensitive amplifier must, by the laws of quantum mechanics, add noise to any signal that it amplifies [327]. Loosely speaking, this is due to the zero-point fluctuations associated with the uncorrelated internal modes of the amplifier. For a phase-insensitive linear amplifier, whose input and output are single bosonic modes, the added noise referred to the input A, in units of number of quanta, must obey the inequality

$$A \geq \frac{1}{2}\left|1 \mp G^{-1}\right|, \tag{8.22}$$

where G is the amplifier gain in units of number of quanta and the upper (lower) sign refers to a phase-preserving (-conjugating) amplifier. Thus a high-gain, phase-insensitive linear amplifier must add at least a half-quantum of noise at the input. For a phase-sensitive amplifier we have an uncertainty principle for the noise added to each quadrature. The noise temperature of an amplifier is defined as $T_n \equiv \hbar\omega/\left[k_B \ln\left(1 + A^{-1}\right)\right]$, such that, for a high-gain amplifier, $T_N \to \hbar\omega/k_B \ln 3$.

The criteria that must be met in order to achieve quantum-limited detection (that is, at the standard quantum limit) may be obtained by considering a general linear coupling to a detector [328]. One considers a linear detector with an input characterized by the operator $\hat{F}$ that interacts with the system position coordinate as $H_I = -A\hat{F} \cdot \hat{x}$, and with an output characterized by the operator $\hat{I}$. The detector output noise spectrum is given by $\delta I_{tot}(\omega) = \delta I_0(\omega) + A\lambda(\omega)x(\omega)$, where the first term describes intrinsic fluctuations in the detector output and the second term describes the amplified fluctuations of the oscillator. The quantum constraint on the detector noise is [329]

$$\bar{S}_I(\omega)\bar{S}_F(\omega) \geq \frac{\hbar^2}{4}\left\{\mathrm{Re}\left[\lambda(\omega) - \lambda'(\omega)\right]\right\}^2 + \left\{\mathrm{Re}\left[\bar{S}_{IF}(\omega)\right]\right\}^2, \tag{8.23}$$

where $\lambda(\omega)$ and $\lambda(\omega')$ are the forward and reverse gain of the detector, respectively, and $\bar{S}_I(\omega)$, $\bar{S}_F(\omega)$ and $\bar{S}_{IF}(\omega)$ are the symmetrized noise spectra of the detector output, input and correlation. Thus, if the detector has non-zero gain and no positive feedback, there must be a minimum amount of back-action and output noise.

A quantum-limited detector with no reverse gain, $\lambda'(\omega) \equiv 0$, then satisfies

$$\bar{S}_I(\omega)\bar{S}_F(\omega) = \frac{\hbar^2}{4}\left\{\mathrm{Re}\left[\lambda(\omega)\right]\right\}^2 + \left\{\mathrm{Re}\left[\bar{S}_{IF}(\omega)\right]\right\}^2, \tag{8.24}$$

the minimum amount of back-action and output noise. This implies a tight connection between the detector input and output. Using spectral decompositions of the noise, it may be shown that Eq. (8.24) leads to the ideal noise condition

$$\langle f\left|I\right|i\rangle = \alpha\left\langle f\left|F\right|i\right\rangle, \tag{8.25}$$

for some complex α for each pair of detector eigenstates $|i\rangle$ and $|f\rangle$ contributing to the noise spectra. Then Eq. (8.24) and (8.25) lead to the requirements

$$|\alpha(\omega)|^2 = \frac{\bar{S}_I(\omega)}{\bar{S}_F(\omega)}, \quad \tan\left[\mathrm{Arg}\,\alpha(\omega)\right] = -\frac{\hbar}{2}\frac{\mathrm{Re}\,\lambda(\omega)}{\mathrm{Re}\,\bar{S}_{IF}(\omega)}. \tag{8.26}$$

A non-vanishing gain implies $\mathrm{Im}\,\alpha \neq 0$ such that the set of all $|i\rangle$ contributing to the noise has no overlap with the set of all final $|f\rangle$, and a quantum-limited detector cannot be in equilibrium.

The total noise in the detector output, referred back to the oscillator, may be calculated from a quantum Langevin equation analogous to Eq. (2.10) as

$$S_{x,tot}(\omega) \equiv \frac{S_{I,tot}(\omega)}{A^2\lambda^2} = S_{x,d}(\omega) + \frac{\gamma_m}{\gamma_m + A^2\gamma} S_{x,t}, \tag{8.27}$$

where $S_{x,t}$ is the intrinsic position noise of Eq. (3.53) evaluated on resonance, and the detector contribution to the noise is

$$\begin{aligned} S_{x,d}(\omega) &= \frac{\bar{S}_I}{|\lambda|^2 A^2} + A^2 |\chi(\omega)|^2 \bar{S}_F - \frac{2\mathrm{Re}\left[-\lambda^* \chi^*(\omega)\bar{S}_{IF}\right]}{|\lambda|^2} \\ &\geq 2|\chi(\omega)| \left[\sqrt{\bar{S}_I \bar{S}_F / |\lambda|^2} - \frac{\mathrm{Re}\left[\lambda^* e^{-i\phi(\omega)}\bar{S}_{IF}\right]}{|\lambda|^2}\right], \end{aligned} \tag{8.28}$$

where the arguments of the noise spectra and gain have been dropped on the right-hand-side for the sake of brevity, $\chi(\omega)$ is the mechanical susceptibility of Eq. (2.12) with the total damping $\gamma \equiv \gamma_m + \gamma(\omega)$, and $\phi(\omega) = \mathrm{Arg}\ [-\chi(\omega)]$. The bound is achieved by balancing the intrinsic and back-action noises at the coupling strength,

$$A_{opt}^2 = \sqrt{\frac{\bar{S}_I(\omega)}{|\lambda(\omega)\chi(\omega)|^2 \bar{S}_F(\omega)}}. \tag{8.29}$$

Reaching the quantum limit also requires a detector with ideal noise properties as given by Eq. (8.24), where for a detector with a large power gain,

$$S_x(\omega) \geq 2|\chi(\omega)| \left[\sqrt{\left(\frac{\hbar}{2}\right)^2 + \left[\frac{\bar{S}_{IF}}{\lambda}\right]^2} - \frac{\cos\left[\phi(\omega)\right]\bar{S}_{IF}}{\lambda}\right]. \tag{8.30}$$

This is minimized via the cross-correlation

$$\frac{\bar{S}_{IF}(\omega)}{\lambda(\omega)} = \frac{\hbar}{2}\cot\phi(\omega), \tag{8.31}$$

with the resulting noise

$$S_{x,d}(\omega)\,|_{\min} = \lim_{T\to 0} S_{x,t}. \tag{8.32}$$

That is, the minimum displacement noise due to the detector is the noise due to a zero-temperature bath. This result is compatible with the linear amplifier constraint of Eq. (8.22).

It is now possible to clearly state that the requirements to reach the quantum limit are: a quantum-limited detector as per Eq. (8.25), the optimal coupling of Eq (8.29), and the optimized detector cross-correlator of Eq. (8.31). Optimizing the coupling at the oscillator resonance, it may be shown that the detector raises the oscillator temperature by half the zero-point energy.

8.2 The Transducer Problem

How do we measure the temperature of a mechanical resonator? In Sec. 3.3 we saw that if we had access to the noise power spectrum of the displacement amplitude we could find the temperature though its area. So the question becomes, how do we transduce the mechanical displacement? We have already discussed the optomechanical and electromechanical systems designed for this purpose, and now describe one such measurement quantitatively, being a phase-dependent measurement of the field leaking out of an optomechanical cavity.

The key to answering this question is to realise that the radiation pressure interaction leads to a phase modulation of the field due to the oscillating displacement of the mechanical resonator. This suggests that a displacement transducer can be based on a phase dependent measurement, such as homodyne or heterodyne detection, of the field amplitude leaving the optical or microwave resonator. For a good measurement of the mechanical displacement we need to ensure that minimal noise are added by the phase measurement of the field. This is much easier for optical fields than for microwave fields.

The quantum theory of homodyne and heterodyne detection is given in [330]. In the optical case homodyne detection is done by coherently adding the output field from the cavity with a strong local oscillator field having a carrier frequency equal to the cavity resonance. This is easily done using a beam splitter. The two output fields from the beam splitter then fall on photodetectors which produce a photocurrent proportional to the intensity of the field. This "square-law" detector does the multiplying of amplitudes required for homodyne detection. The appropriately normalised photocurrent is then a classical stochastic process given by the stochastic differential equation

$$J(t) \propto \kappa\sqrt{\eta}\langle ae^{i\theta} + a^\dagger e^{-i\theta}\rangle_c + \sqrt{\kappa}\xi(t) \tag{8.33}$$

where θ is the phase difference between the local oscillator and the signal, and $0 < \eta \leq 1$ is the quantum efficiency. It is a measure of the fraction of the signal intensity that actually contributes to the current due to imperfections in the detection scheme.

The simplest model of a mechanical transducer is obtained by considering the linearised radiation pressure interaction in the resolved sideband limit with homodyne detection of the output field. For simplicity we will neglect mechanical damping here although it is easily included. Red sideband excitation, with a damped field is the same situation that we need for good cooling and the quantum stochastic differential equations are given by (see Sec. 6.4),

$$\frac{da}{dt} = -\frac{\kappa}{2}a - igb + \sqrt{\kappa}a_{in}, \tag{8.34}$$

$$\frac{db}{dt} = -iga. \tag{8.35}$$

Assuming that $\kappa \gg g$ we solve for the cavity amplitude operator in terms of the mechanical amplitude,

$$a = -\frac{2ig}{\kappa}b + \frac{2}{\sqrt{\kappa}}a_{in}, \tag{8.36}$$

and substituting into Eq. (8.35), we have

$$\frac{db}{dt} = -\frac{\Gamma}{2}b - i\sqrt{\Gamma}a_{in}, \tag{8.37}$$

where the optomechanical damping rate is

$$\Gamma = \frac{4g^2}{\kappa}. \tag{8.38}$$

The homodyne current optical field in the adiabatic limit is obtained by the replacement of Eq.(8.36),

$$J(t) = -2ig\sqrt{\eta}\langle be^{i\theta} - b^\dagger e^{-i\theta}\rangle_c + \sqrt{\kappa}\xi(t), \tag{8.39}$$

where $\xi(t)$ is white noise and the subscript c is to remind us that this particular increment is a conditional dynamics and depends on the entire history of the observed process up to this point. If we choose $\theta = \pi/2$, we find that the normalised current, $\bar{J} \equiv J/(2g\sqrt{\eta})$, is

$$\bar{J}(t) = \langle b + b^\dagger\rangle_c + \frac{1}{\sqrt{\Gamma\eta}}\xi(t). \tag{8.40}$$

The ideal transducer limit then corresponds to $\eta \to 1$ and $\Gamma \to \infty$. In this limit the noise power spectrum of the homodyne current faithfully reflects that quantum dynamics of the mechanical resonator. In the case of optical homodyne detection, the quantum efficiency can be as high as $\eta = 0.9$. The measurement rate, Γ, is in fact the laser cooling rate for the resolved sideband cooling scheme. The transducer thus adds a white noise floor to the noise power spectrum of the mechanical displacement.

In the case of microwave systems, phase-dependent detection of the field is done quite differently due to the lack of photon counting devices at microwave frequencies. In this case a nonlinear mixing element called an IQ mixer is used. An IQ mixer is better described, using the quantum theory, as heterodyne detection [331]. IQ mixers cannot function with the low powers that must be measured, and a phase-insensitive preamplifier must be added. This effectively degrades the quantum efficiency of detection by adding a significant level of thermal noise to the input signal to the IQ mixer. A possible solution is to use phase-dependent amplifiers such as Josephson parametric amplifiers [332, 333].

8.3 Weak Force Detection

One of the primary applications of nanomechanical systems (or indeed, macromechanical systems in the case of gravitational wave detectors) is weak force detection. The weak force itself may arise from many things, including an electronic or nuclear spin, or a single electronic charge. The fundamental problem is to determine how big the force must be in order to see its effect on the displacement of the resonator from equilibrium in the presence of noise.

What is the minimum detectable force? We can get an idea of the problem by considering a single simple harmonic oscillator subject to a constant impulsive force. The situation is illustrated in Fig. 8.1. Here we sketch a phase space representation of an oscillator initially prepared in a thermal state. The circles are intended to indicate contours of a phase space probability distribution. Of course, no such distribution exists for quantum systems, but we can define various quasi-probability densities such as the Wigner function. In the figure, an impulsive force displaces the state in the momentum direction. If this displacement is at least as big as the uncertainty in momentum then in principle the force can be detected. If the oscillator is in a thermal

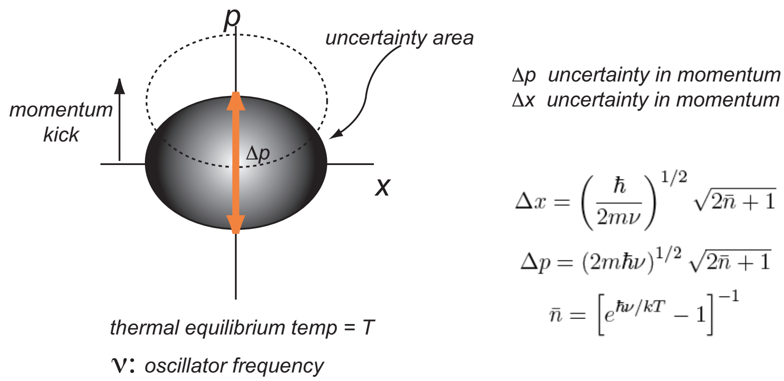

Fig. 8.1. An oscillator is subject to an impulsive force which displaces the state in the momentum direction in phase space. For this to be detectable it must displace the state by more than the uncertainty in the momentum direction. Reproduced from [351].

state with mean excitation number $\bar{n}$, the variance in momentum and position are, respectively,

$$\Delta x = \left(\frac{\hbar}{2m\omega_m}\right)^{1/2}\sqrt{2\bar{n}+1}, \tag{8.41}$$

$$\Delta p = (2m\hbar\omega_m)^{1/2}\sqrt{2\bar{n}+1}. \tag{8.42}$$

If the a constant force f_0 acts for a time $\tau \ll \omega_m$, much less than the resonator frequency, we find a condition on the minimum detectable force,

$$f_0 \geq \frac{\Delta p}{\tau}\sqrt{2\bar{n}+1}. \tag{8.43}$$

Clearly, it is advantageous to cool the resonator, but a fundamental limit is imposed by the zero point noise.

In practice we do not usually have an impulsive force, but rather a time-varying force with some stochastic component. Thus we need to consider a damped, continuously-driven mechanical resonator. Recall that the two-time correlation function for the displacement signal is

$$G_x(\tau) = \langle x(t)x(t+\tau)\rangle_{t\to\infty}, \tag{8.44}$$

and the noise power spectrum of this signal

$$S_x(\omega) = \frac{1}{2\pi}\int_{-\infty}^{\infty} d\tau e^{-i\omega\tau}G_x(\tau), \tag{8.45}$$

The steady state uncertainty in the position is

$$\langle x^2\rangle_{ss} = \int_{-\infty}^{\infty} d\omega S_x(\omega), \tag{8.46}$$

that is to say, the total noise power. Note that $S_x(\omega)$ has units of $\mathrm{m}^2\mathrm{Hz}^{-1}$.

In Sec. 8.2 we consider phase sensitive detection schemes that correspond to a measurement of

$$\langle \tilde{x}(\omega) \rangle = \int_{-\infty}^{\infty} dt \langle x(t) \rangle e^{-i\omega t} \tag{8.47}$$

The sensitivity of the measurement will then depend on noise at frequency ω. For a sensitive measurement of displacement we need

$$|\langle \tilde{x}(\omega) \rangle|^2 \geq S_X(\omega) \tag{8.48}$$

We are thus led to define a fine force sensitivity in terms of $\sqrt{S_x(\omega)}$,

$$\mathcal{S}_f(\omega_m) = k\sqrt{S_x(\omega_m)} \tag{8.49}$$

which has units of $\mathrm{N.Hz}^{-1/2}$ where k is the spring constant. Very good atomic force microscopy can achieve a room temperature sensitivity of a few hundred $\mathrm{aNHz}^{-1/2}$ [334]. Rugar *et al.* [335] achieved a landmark detection of a single electron spin using a magnetic force microscopy method with an equivalent force sensitivity of 0.8 $\mathrm{aNHz}^{-1/2}$ at a temperature of 1.6K. In the microwave domain 0.5 $\mathrm{aNHz}^{-1/2}$ was achieved at 15mK [336].

8.4 Nonlinear metrology.

One of the main applications of micromechanical resonators is as inertial sensors where the objective is to detect a small acceleration [337]. A typical device uses a silicon piezoelectric transducer. Another approach might be based on the Duffing nonlinearity. If a beam is stressed it can shift to a higher or lower fundamental resonance frequency. If this frequency shift can be transduced the weak stresses can be detected. In this section we consider the possibility of high-precision metrology using nanomechanical resonators [338].

The measurement objective is to estimate a single parameter of the Hamiltonian of a system [339]. The precision with which the parameter can be determined depends on the initial state of the system, the nature of the Hamiltonian describing the system's evolution, and the measurements to be performed on the system. Usually one assumes that system quanta are coupled independently to the parameter leading to equations of motion that are linear in the field variables. In that case, the optimal precision in a parameter estimate scales as $1/n$, where n is the number of system quanta used in the measurement, a scaling known as the Heisenberg limit [340]. To reach this with linear coupling requires an entangled initial state [341]. If one does not use entangled states, a linear coupling can only reach a $1/n^{1/2}$ scaling, the so-called shot-noise limit or the standard quantum limit. Boixo *et al.* [338] have shown that that quantum parameter estimation with scaling better than $1/n$ can be attained by using a coupling to the parameter that is *nonlinear* in field variables.

Woolley *et al.* [342] consider two parallel, flexural nanomechanical resonators, each with an intrinsic Duffing nonlinearity and with a switchable, electrostatically-actuated beamsplitter-like coupling between them. The measurement proceeds as follows: one mechanical resonator is excited into a large-amplitude coherent state, the beamsplitter interaction is pulsed on so that the coherent-state excitation is split equally between the two resonators, the mechanical resonators

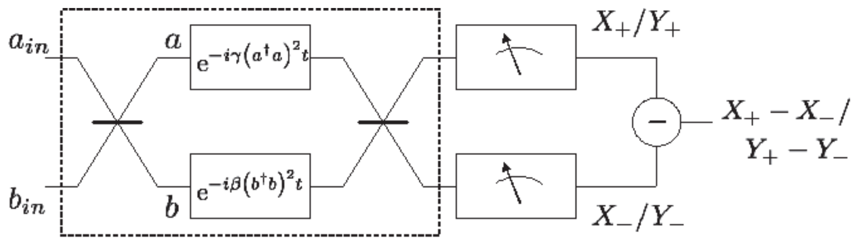

Fig. 8.2. Quantum circuit representation of nonlinear mechanical resonator interferometer. The input mechanical resonator modes experience a pulsed beamsplitter-like interaction, evolve according to a nonlinear Hamiltonian, and the beamsplitter-like interaction is then pulsed on again. We assume that measurements can be made of either the X or the Y quadrature, of one or both output modes (denoted "+" and "−"). Though not shown in the circuit, we have also considered the effect of dissipation accompanying the nonlinear evolution. Reproduced from [342].

evolve independently under the nonlinearities (and standard linear dissipation), the beamsplitter interaction is pulsed in the same way again, and a homodyne measurement of the mechanical resonator quadratures is performed. As depicted in Fig. 8.2, this scheme effectively realizes a nonlinear interferometer [343].

Each mechanical resonator in the pair will be treated as a thin bar of length l and lateral width a, and we quantise the fundamental mode of vibration of each mechanical resonator in the lateral direction. Each fundamental mode is described by a position-momentum pair, x_i-p_i, where $i = a, b$ labels the resonators. With a time-dependent capacitive coupling dependent on the displacements from the equilibrium positions, $C(x_a, x_b)$, and Duffing nonlinearities characterized by coefficients χ_i $(i = a, b)$, the system can be described classically by a Hamiltonian

$$\begin{aligned} H_{cl} \;=&\; \frac{1}{2}m\omega^2 x_a^2 + \frac{p_a^2}{2m} + \frac{1}{2}m\omega^2 x_b^2 + \frac{p_b^2}{2m} \\ &+\; P(t)\frac{1}{2}C(x_a, x_b)V_0^2 + \frac{1}{4}\chi_a m\omega^2 x_a^4 + \frac{1}{4}\chi_b m\omega^2 x_b^4 \;, \end{aligned} \tag{8.50}$$

where $P(t)$ specifies the coupling voltage pulses.

We assume that the mechanical resonators are capacitively coupled to nearby bias conducting surfaces in such a way that for small displacements, the capacitance can be expanded as

$$C(x_a, x_b) = C_0\left(1 + \frac{f x_a^2 + f x_b^2 + 2x_a x_b}{d^2} + \cdots\right) \;. \tag{8.51}$$

Here C_0 is the capacitance when the oscillators are at their equilibrium positions. The capacitive coupling must be balanced so that there is no net force on the resonators when the coupling is switched on (i.e., no linear terms in the expansion). This leaves the quadratic terms as the dominant effect of the coupling. In the quadratic terms, $d \simeq 100\,\text{nm}$ is a characteristic lateral separation between the resonators and the other conducting surfaces and f is a factor of order unity. Both d and f depend on the specific design of the capacitive coupling. Provided

$$C_0 V_0^2/2m\omega d^2 \equiv \kappa \ll \omega \;, \tag{8.52}$$

we can neglect the renormalization of the resonator frequencies during the pulsing of the capacitive coupling, retaining only the coupling between the resonators. With these assumptions, the capacitive term in the Hamiltonian (8.50) can be replaced by $P(t)C_0V_0^2x_ax_b/d^2$, which gives rise to the desired beamsplitter coupling. The parameter κ, introduced in Eq. (8.52), characterizes the strength of the beamsplitter coupling.

Transforming to an interaction picture and using the rotating-wave approximation, we find the Hamiltonian

$$H = \hbar\gamma(a^\dagger a)^2 + \hbar\beta(b^\dagger b)^2 + \hbar\kappa P(t)(a^\dagger b + ab^\dagger) \, , \tag{8.53}$$

where a, b are the annihilation operators for the relevant mechanical modes,

$$\gamma \equiv \frac{3}{4}\omega\chi_a\Delta_0 \, , \qquad \beta \equiv \frac{3}{4}\omega\chi_b(\Delta x)^2 \, , \tag{8.54}$$

with $\Delta_0 = \sqrt{\hbar/2m\omega}$. Then the evolution of the density matrix describing the state of the two mechanical resonators is given by

$$\dot{\rho}(t) = -\frac{i}{\hbar}[H,\rho] + \frac{\Gamma_a}{2}(2a\rho a^\dagger - a^\dagger a\rho - \rho a^\dagger a) + \frac{\Gamma_b}{2}(2b\rho b^\dagger - b^\dagger b\rho - \rho b^\dagger b) \, . \tag{8.55}$$

We will use the scheme to estimate the nonlinear coefficient γ of oscillator a, assuming that oscillator b has no nonlinearity ($\beta = 0$). Other operating conditions are possible and yield similar results. We consider a fiducial evolution time $t = 10^{-3}$ s, so that $\Gamma_i t = 4.7$, meaning that the effects of dissipation are large, but not overwhelming, and we consider a fiducial initial phonon number $n = 10^7$, so that the nonlinear phase shift $n\gamma t$ is about 1 rad. We investigate values within about an order of magnitude of these fiducial values. Notice that a phonon number $n = 10^7$ corresponds to an oscillation amplitude $\Delta x\sqrt{2n} = 1$ nm. This amplitude is close to the value we assumed for a_c, not by accident, but because the two oscillation amplitudes quantify, one for free oscillations and one for forced oscillations, the same measure of the relative strengths of the nonlinearity and the damping.

We are thus estimating the nonlinear coefficient γ of oscillator a. Other operating conditions are possible, but we focus on this one as a representative possibility in this section.

We phrase our results in terms of the precision in estimating the related dimensionless parameter γt, with t regarded as fixed. The uncertainty in an estimate of γt based on multiple measurements of a quantity Z—in our case, Z is one of the output quadratures—can be calculated from

$$\delta(\gamma t) = t\delta\gamma = t\frac{\Delta Z}{|d\langle Z\rangle/d\gamma|} = \frac{\Delta Z}{|d\langle Z\rangle/d(\gamma t)|} \, , \tag{8.56}$$

where ΔZ is the uncertainty in Z. In the case of no damping and again making the short-time approximation, the quadrature variances all take on coherent-state values, i.e., $\Delta X_\pm, \Delta Y_\pm \to 1$. The precision of the estimate of γt thus becomes

$$\delta_{X_\pm}(\gamma t) = \frac{1}{n^{3/2}|\sin n\gamma t|} \, , \qquad \delta_{Y_\pm}(\gamma t) = \frac{1}{n^{3/2}|\cos n\gamma t|} \, . \tag{8.57}$$

These sensitivities oscillate with the fringes produced by the nonlinear phase shift $n\gamma t$, but they all have the same basic scaling of $1/n^{3/2}$ with phonon number. This scaling beats the $1/n$ scaling achievable with a linear Hamiltonian and is consistent with the general result [344] for nonlinear Hamiltonians and initial product states. The factor of n enhancement compared with the standard quantum limit for linear Hamiltonians is a consequence of the rapidly oscillating fringes in the expectation values of the output quadratures.

From an experimental perspective, the strong damping regime is most relevant. In this regime, the quadrature variances have coherent-state values, and the derivatives of the expectation values lead to sensitivities

$$\delta_{X_\pm}(\gamma t) = \frac{\Gamma_a t\, e^{\Gamma_a t/2}}{n^{3/2}(1-e^{-\Gamma_a t})|\sin[n\gamma(1-e^{-\Gamma_a t})/\Gamma_a]|} \tag{8.58}$$

$$\delta_{Y_\pm}(\gamma t) = \frac{\Gamma_a t\, e^{\Gamma_a t/2}}{n^{3/2}(1-e^{-\Gamma_a t})|\cos[n\gamma(1-e^{-\Gamma_a t})/\Gamma_a]|}\,. \tag{8.59}$$

The improved $1/n^{3/2}$ sensitivity scaling survives in the presence of dissipation, but the absolute sensitivity is degraded, and the fringes become more widely separated. For feasible damping rates, the sensitivity is worsened by less than an order of magnitude, but if the damping is further increased, the sensitivity diverges, reflecting the absence of signal in the quadrature expectation values.

Figure 8.3 shows the measurement precision for measurements of the X_+ and Y_+ quadratures

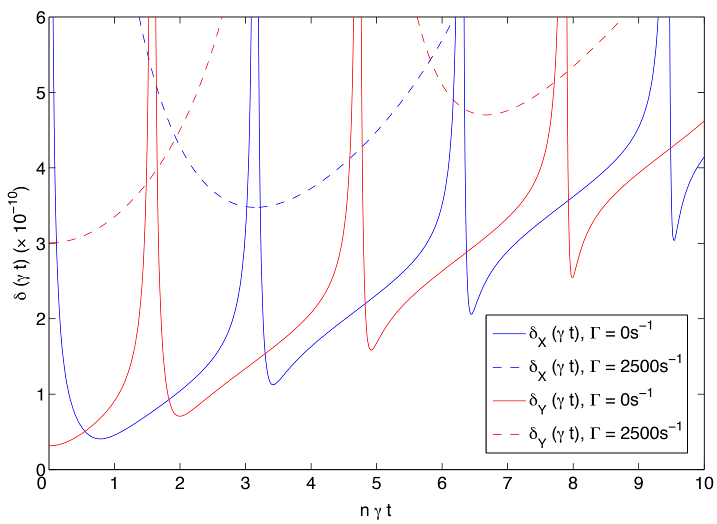

Fig. 8.3. Precision $\delta(\gamma t)$ for measurements of the X_+ and Y_+ quadratures as a function of the nonlinearity γ, expressed as the nonlinear phase shift $n\gamma t$, for the choices $n = 10^7$, $\beta = 0$, $t = 10^{-3}$ s, and $\Gamma_a = \Gamma_b = \Gamma$. Zero damping and moderate damping cases are shown for each quadrature. For zero damping, fringe boundaries are located at $n\gamma t = m\pi/2$, with the fringes based on measurements of conjugate quadratures displaced by $\pi/2$. Dissipation leads to an overall reduction in sensitivity, and the fringes become more widely spaced. Reproduced from [342].

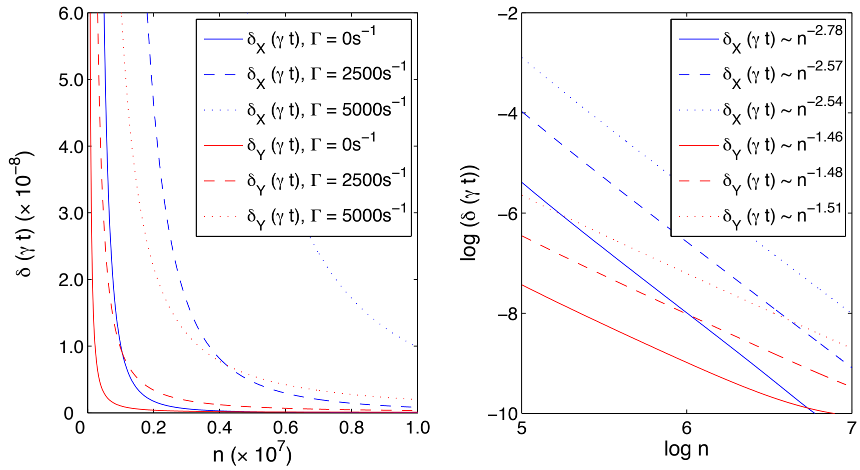

Fig. 8.4. Precision $\delta(\gamma t)$ for measurements of the X_+ and Y_+ quadratures as a function of mean phonon number n in the initial coherent state, for the choices $\gamma = 10^{-4}\,\mathrm{s}^{-1}$, $\beta = 0$, $t = 10^{-3}\,\mathrm{s}$, $\Gamma_a = \Gamma_b = \Gamma$. Plots for three values of the damping constant Γ are shown for each quadrature. These plots correspond to the regime $n\gamma t < 1$. From the log-log plots, we see that $\delta_{X_+} \propto n^{-5/2}$ and $\delta_{Y_+} \propto n^{-3/2}$. The extra n^{-1} factor for measurement of the X_+ quadrature is due to the precision improving as one moves away from the very poor sensitivity near the central fringe boundary. Reproduced from [342].

as a function of the nonlinearity γ and for two values of the damping rate $\Gamma = \Gamma_a = \Gamma_b$. Fringe boundaries are located at $n\gamma t = m\pi/2$; those based on measurement of the X_+ and Y_+ quadratures are displaced by $\pi/2$. As the damping rate increases, the overall sensitivity worsens, and the fringes become more widely spaced. These effects can be traced back to the reduced-amplitude and reduced-frequency oscillations of the quadrature expectations as a function of the nonlinear phase shift.

The scaling of the measurement precision as a function of n is plotted in Fig. 8.4. Here n is chosen so that $n\gamma t < 1$. The precision associated with measurement of the Y_+ quadrature is then near its optimal value, away from its first fringe boundary at $n\gamma t = \pi/2$, whereas the precision associated with measurement of the X_+ quadrature decreases rapidly as it falls from the very poor sensitivity near its central fringe boundary at $n\gamma t = 0$. From the log-log plot, we can calculate that $\delta_{X_+} \propto n^{-5/2}$ and $\delta_{Y_+} \propto n^{-3/2}$, though the extra n^{-1} in the $n^{-5/2}$ scaling is due to the sensitivity falling from the central fringe boundary, and the true scaling of the optimal sensitivity achievable is $n^{-3/2}$. The scaling behavior is maintained in the presence of feasible levels of dissipation, although there is a marked deterioration in sensitivity.

8.5 Phonon Number Measurements

We now describe a method to count individual quanta in a mechanical resonator using homodyne detection of the cavity field to which it is coupled [345]. Our model is based on the implementation of the Harris group in which a vibrating membrane is inserted into a Fabry-Pérot

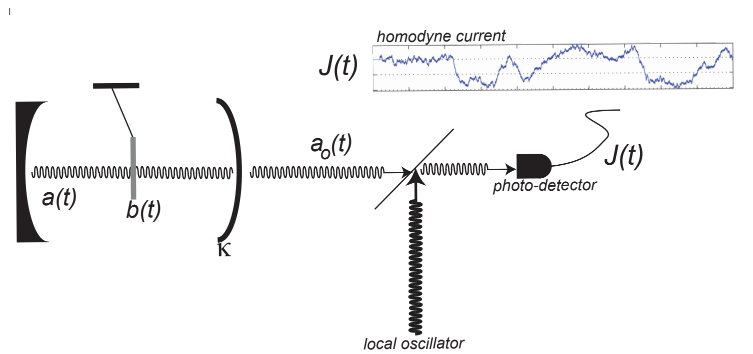

Fig. 8.5. A phonon number measurement scheme. The mechanical motion of the intracavity membrane modulates the phase of the field of a strongly driven cavity This is monitored using homodyne detection and the measurement record is the current from the homodyne detection scheme. Reproduced from [345].

cavity [110, 111]. As discussed in Sec. 4.1, if the membrane is located in an equilibrium position for which the variation of cavity frequency is quadratic in the mechanical displacement, a phase shift of the field proportional to the energy of the mechanical resonator can be engineered.

The measurement scheme is depicted in Fig. 8.5. The phonon number of the membrane modulates the phase of the intracavity field which is driven by a coherent source. This phase shift can be monitored using homodyne detection which gives a stochastic current as the measurement record; see Eq. (8.40)).

We assume that the cavity field is close to a coherent state in its steady state, and linearize the interaction Hamiltonian in Eq. (4.12),

$$H_I = \hbar\chi(\bar{a} + \bar{a}^\dagger)b^\dagger b. \tag{8.60}$$

This turns a phonon number dependent phase shift into a displacement of the cavity field. If $b^\dagger b$, is replaced by a classical stochastic 'birth-death' process, $n(t)$, representing phonons entering and exiting the mechanical resonator, the cavity will respond as if it were being driven by a fluctuating amplitude. In order to track this we need to monitor the field leaking out of the cavity via homodyne detection.

The quantum description is via a master equation that includes the damping of the cavity and the irreversible dynamics of the mechanical resonator,

$$\frac{d\rho}{dt} = -\frac{i}{\hbar}[H_I, \rho] + \kappa\mathcal{D}[a]\rho + \gamma(\bar{N}+1)\mathcal{D}[b]\rho + \gamma\bar{N}\mathcal{D}[b^\dagger]\rho, \tag{8.61}$$

where $\bar{N}$ is the mean thermal occupation of the mechanical resonator bath at frequency ω_m From the master equation we find the following equations of motion for the average field amplitude and phonon number,

$$\frac{d\langle a\rangle}{dt} = -i\chi\bar{n}_b - \frac{\kappa}{2}\langle a\rangle, \tag{8.62}$$

$$\frac{d\bar{n}_b}{dt} = -\gamma(\bar{n}_b - \bar{N}), \tag{8.63}$$

where $\bar{n}_b = \langle b^\dagger b \rangle$. The solution is

$$\bar{n}_b(t) = \bar{n}_b(0)e^{-\gamma t} + \bar{N}(1 - e^{-\gamma t}), \tag{8.64}$$

$$\langle a(t) \rangle = \langle a(0) \rangle e^{-\kappa t/2} - i\chi \left\{ \left[\bar{n}_b(0) - \bar{N}\right] \frac{e^{-\gamma t} - e^{-\kappa t/2}}{\kappa/2 - \gamma} + \bar{N} \frac{1 - e^{-\kappa t/2}}{\kappa/2} \right\}. \tag{8.65}$$

Thus the steady-state field in the cavity is $\langle a \rangle_{ss} = -2i\chi\bar{N}/\kappa$, in addition to the background field amplitude of α_0.

The mechanical damping rate, $\gamma \sim 1$Hz, is much less than the field damping rate, $\kappa \sim 10^7$ Hz. so we will set mechanical damping to zero. With this assumption we can solve the master equation for the *unconditional state*, with initial condition,

$$\rho(0) = \sum_{nm} P_{nm}(\alpha, \alpha')(|n\rangle\langle m|)_b \otimes (|\alpha\rangle\langle\alpha|)_a, \tag{8.66}$$

where $|\alpha\rangle$ is a coherent state for the cavity field. The solution is [113],

$$\begin{aligned}\rho(t) = & \sum_{nm\alpha\alpha'} P_{nm}(\alpha, \alpha') \exp\left[\frac{\chi^2}{\kappa^2}(n-m)^2(1 - \kappa t/2 - e^{-\kappa t/2})\right] \qquad (8.67)\\ & \times \exp\left[-i\frac{\chi}{\kappa}(n-m)(\alpha - \alpha^*)(1 - e^{-\kappa t/2})\right](|n\rangle\langle m|)_{(b)} \otimes \frac{(|\alpha_n(t)\rangle\langle\alpha_m(t)|)_{(a)}}{\langle\alpha_m(t)|\alpha_n(t)\rangle},\end{aligned}$$

where $\alpha_n(t)$ and $\alpha_m(t)$ are

$$\alpha_n(t) = -i\frac{\chi n}{\kappa}(1 - e^{-\kappa t/2}) + \alpha e^{-\kappa t/2}, \alpha_m(t) = -i\frac{\chi m}{\kappa}(1 - e^{-\kappa t/2}) + \alpha e^{-\kappa t/2}. \tag{8.68}$$

For short times this may be written,

$$\begin{aligned}\rho(t) = & \sum_{nm} P_{nm}(\alpha, \alpha') \exp\left[-\frac{\chi^2 t^2}{8}(n-m)^2\right]\\ & \times \exp\left[-i\frac{\chi t}{2}(n-m)(\alpha - \alpha^*)\right](|n\rangle\langle m|)_{(b)} \otimes \frac{(|\alpha_n(t)\rangle\langle\alpha_m(t)|)_{(a)}}{\langle\alpha_m(t)|\alpha_n(t)\rangle},\end{aligned} \tag{8.69}$$

We see that the mechanical resonator is rapidly diagonalised in its number basis, and the cavity is driven to a mixture of coherent states. This reflects the fact that the coherent states are the pointer basis states [346] for the cavity.

We now turn to the conditional dynamics of the system, conditioned on the stochastic homodyne current record. This is given by the conditional stochastic quantum dynamics [330]

$$\begin{aligned}d\rho = & -\frac{i}{\hbar}[H_I, \rho]dt + \gamma(\bar{N}+1)\mathcal{D}[b]\rho dt + \gamma\bar{N}\mathcal{D}[b^\dagger]\rho dt\\ & + \kappa\mathcal{D}[a]\rho dt + \sqrt{\kappa}dW\mathcal{H}[ae^{-i\frac{\pi}{2}}]\rho,\end{aligned} \tag{8.70}$$

where

$$\mathcal{H}[a]\rho = a\rho + \rho a^\dagger - \mathrm{Tr}(a\rho + \rho a^\dagger)\rho$$

is the measurement superoperator, and dW is the Wiener increment. This superoperator is zero when acting on coherent states

$$\mathcal{H}[a]\left(|\alpha\rangle\langle\alpha|\right) = 0 \tag{8.71}$$

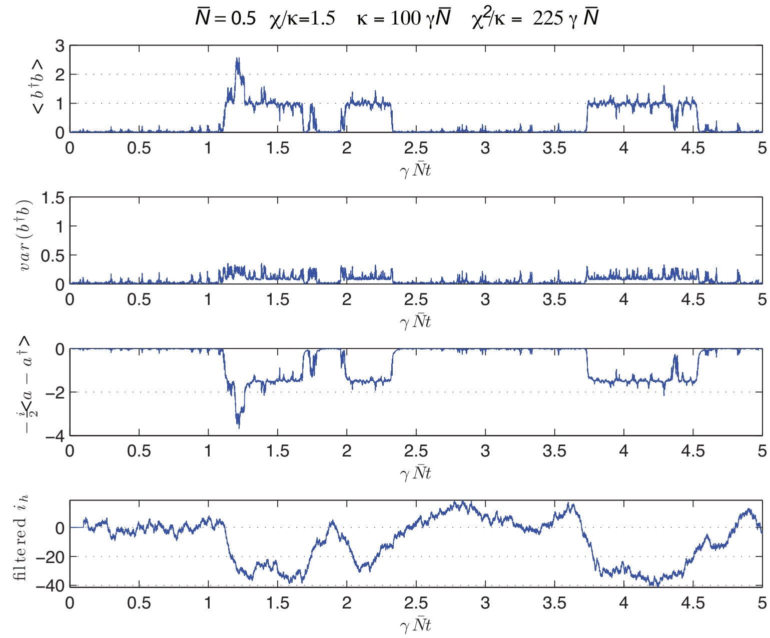

Fig. 8.6. The conditional moments and the corresponding conditional homodyne current versus time in the good measurement limit. The top plot shows the conditional mean phonon number exhibiting random telegram jumps as phonons enter and exist the resonator from the bath.

The effect of this is to localise the cavity field on coherent states, again reflecting the nature of the pointer basis.

Using the stochastic master equation we can simulate the homodyne current and simultaneously compute conditional moments of the mechanical resonator. The conditional moments in the good measurement limit, $\chi^2/\kappa \gg \gamma\bar{N}$, are shown in Fig. 8.6.

As typical for an optomechanical measurement, the best situation will result when the field is rapidly damped, and can be adiabatically eliminated. The resulting master equation for the mechanical resonator alone is

$$\begin{aligned} d\rho_b &= \gamma(\bar{N}+1)\mathcal{D}[b]\rho_b dt + \gamma\bar{N}\mathcal{D}[b^\dagger]\rho_b dt \\ &+ \Gamma\mathcal{D}[b^\dagger b]\rho_b dt + \sqrt{\Gamma}\mathcal{H}[b^\dagger b e^{-i(\theta+\pi/2)}]\rho_b dW, \end{aligned} \tag{8.72}$$

where $\Gamma \equiv 4\chi^2/\kappa$. The last term in this equation drives the system to a (random) eigenstate of phonon number. The corresponding homodyne current is given by

$$J(t) = -2\eta\chi\langle b^\dagger b\rangle + \sqrt{\eta\kappa}\xi(t), \tag{8.73}$$

which clearly indicates that the measurement record can track the fluctuating phonon number.

9 Nonlinear Optomechanics

The radiation pressure interaction is cubic in the amplitudes of the resonators involved which means the resulting Heisenberg equations of motion are nonlinear. Currently the quantum dynamics resulting from this is not readily observable due to the small size of the single photon coupling rate. This will change as new fabrication techniques are developed. In the optomechanical crystal devices of the Painter group for example the single photon optomechanical coupling rate is already around one MHz [107].

The inherent nonlinearity of the radiation pressure interaction can most easily be seen using a canonical transformation. The simplest way to see this is to make a canonical transformation on the original radiation pressure coupling Hamiltonian given in Eq. (4.5),

$$\bar{H} = e^{\beta a^\dagger a(b-b^\dagger)} H e^{-\beta a^\dagger a(b-b^\dagger)}. \tag{9.1}$$

This is a photon number dependent displacement amplitude,

$$e^{\beta a^\dagger a(b-b^\dagger)} b e^{-\beta a^\dagger a(b-b^\dagger)} = b + \beta a^\dagger a. \tag{9.2}$$

Applying Eq. (9.1) to the entire Hamiltonian, and writing $\beta = \kappa_0/\omega_m$, yields

$$\bar{H} = \hbar\omega_c a^\dagger a + \hbar\omega_m b^\dagger b - \hbar\frac{\kappa_0^2}{\omega_m}(a^\dagger a)^2 \tag{9.3}$$

In this new canonical picture, the interaction has been removed but the cavity field acquires a Kerr nonlinearity, i.e. an intensity-dependent detuning of the cavity field. This can lead to optical bistability if G_0/ω_m is large enough [291]. Typically, however, it is rather small.

Another route to nonlinearity is through the Duffing term in the elastic potential energy of a bulk mechanical resonator. Treating the mechanical mode as a simple harmonic oscillator by treating the elastic potential energy only to second-order in the displacement is a good approximation in most experiments, in which the resonator is not driven. However, for mechanical resonators subject to stress or strongly driven one may induce a significant quartic term in the elastic potential energy. The nonlinear response of nanomechnical systems is already used in classical sensing schemes [348, 347].

Kozinsky *et al.* [349] report an experiment that reveals the Duffing nonlinearity in a nanowire. As shown there, it is posible to relate the Duffing nonlinearity to the critical amplitude a_c. The equation of motion with the Duffing term included is

$$\ddot{x} + \frac{\omega_o}{Q}\dot{x} + \omega_0^2(x + \alpha x^3) = F\cos\Omega t, \tag{9.4}$$

where

$$\alpha = \frac{2\sqrt{3}}{9a_c^2 Q}, \tag{9.5}$$

with Q being the quality factor. An equation of motion of this form implies that the Duffing nonlinearity enters the Hamiltonian via a term like

$$H_D = \frac{m\alpha\omega_0^2}{4}x^4 \tag{9.6}$$

If we now write $x = \Delta x(b + b^\dagger)$ where $\Delta x = \hbar/(2m\omega_0)$, then the Hamiltonian takes the form

$$H_D = \frac{m\alpha\omega_0^2}{4}(\Delta x)^4(b + b^\dagger)^4. \tag{9.7}$$

Terms of the form $b^{\dagger k}b^{k'}$ $(k \neq k')$ will oscillate rapidly in the interaction picture and can be neglected. We can then write this using the highest-order normally-ordered term,

$$H_D = \hbar\chi b^{\dagger\, 2}b^2, \tag{9.8}$$

where

$$\chi = \frac{3\alpha\hbar}{8m}. \tag{9.9}$$

In this form the Duffing nonlinearity looks like the self-Kerr nonlinearity in nonlinear optics [291, 350]. For the platinum nanowire used by Kozinsky *et al.*, the critical amplitude was found to be $a_c = 2.68\mathrm{nm}$, with a quality factor of 1770 and a mass of approximately $5 \times 10^{-17}\mathrm{kg}$. These numbers give a nonlinearity of $\chi \sim 10^{-4}\mathrm{s}^{-1}$. This may appear small but the equivalent number for the optical Kerr effect is many orders of magnitude smaller.

A driven, nonlinear mechanical resonator, in an interaction picture at the pump frequency ω_p, and assuming that $\omega_0, \omega_p \gg \chi$ in order to neglect rapidly oscillating contributions from the quartic term, may be described by the Hamiltonian

$$H_I = \hbar\Delta b^\dagger b + \hbar\chi(b^\dagger)^2 b^2 + \hbar\epsilon_p(b + b^\dagger), \tag{9.10}$$

where $\Delta = \omega_m - \omega_p$ is the detuning of the resonator from the pump. Including dissipation, the master equation in the interaction picture for the system is then given by

$$\frac{d\rho}{dt} = -\frac{i}{\hbar}[H_I, \rho] + \frac{\gamma}{2}(\bar{n} + 1)(2b\rho b^\dagger - b^\dagger b\rho - \rho b^\dagger b) + \frac{\gamma}{2}\bar{n}(2b^\dagger\rho b - bb^\dagger\rho - \rho bb^\dagger), \tag{9.11}$$

where γ is the rate of energy loss from the resonator and $\bar{n}$ is the mean phonon number in a bath oscillator at frequency ω_0. We will usually assume low temperature operation so that $\bar{n} \to 0$. As discussed in Sec. 8.3, this is the limit in which quantum limited force detection is possible and should be achievable with new nanomechanical cooling techniques . The system has a steady state, or fixed point, which can change stability as the driving field is varied. It is this dependence of fixed point stability on driving field that can be used to amplify a weak driving signal.

Under certain conditions, the energy in the nanomechanical resonator as a function of the driving intensity can exhibit multiple stable fixed points and hysteresis [350]. In the semiclassical approximation, the equation of motion for the mean amplitude, $\alpha \equiv \langle a\rangle$, is given by

$$\dot{\alpha} = -i\epsilon_p - \left[\gamma/2 + i(\Delta + 2\chi|\alpha|^2)\right]\alpha. \tag{9.12}$$

The fixed point (or semiclassical steady state) is defined by $\dot{\alpha} = 0$, which corresponds to a complex amplitude α_0 must satisfy

$$I_p = n_0\left[\frac{\gamma^2}{4} + (\Delta + 2\chi n_0)^2\right], \tag{9.13}$$

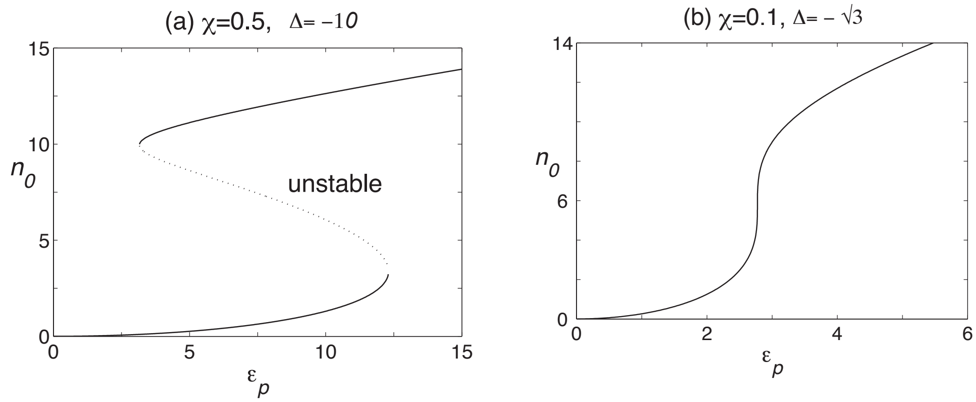

Fig. 9.1. Plots of the mean vibrational excitation number of the nanomechanical resonator, n_0 versus pump field intensity, ϵ_p for $\gamma = 2.0$. The unstable branch shown in (a) is absent from (b) due to different values of pump field detuning and dispersion. Reproduced from [351].

where $I_p = \epsilon_p^2$ is proportional to the pump power driving the nanomechanical resonator and $n_0 = |\alpha_0|^2$ determines the average energy in the nanomechanical resonator by $E = \hbar\omega_0 n_0$. Considered as a function of n_0, I_p is a cubic with turning points at the values of n_0 that satisfy

$$\frac{dI_p}{dn_0} = \frac{\gamma^2}{4} + (\Delta + 6\chi n_0)(\Delta + 2\chi n_0) = 0. \tag{9.14}$$

However, when we regard n_0 as a function of the pump power, it is multi-valued and Eq. (9.14) defines values at which the slope diverges, indicative of a change in stability.

In Fig. 9.1 we plot n_0 versus the pump intensity ϵ_p for various values of Δ. Clearly under some conditions n_0 becomes a multi valued function of ϵ_p. In fact it can be shown that this will occur for negative detuning, $\Delta < 0$. Not all the fixed point solutions are stable. To determine stability we linearise the equations of motion around the fixed points by writing $\alpha(t) = \alpha_0 + \delta\alpha(t)$. The equations of motion for the fluctuation field $\delta\alpha(t)$ are then given by

$$\frac{d}{dt}\begin{pmatrix} \delta\alpha \\ \delta\alpha^* \end{pmatrix} = M \begin{pmatrix} \delta\alpha \\ \delta\alpha^* \end{pmatrix}, \tag{9.15}$$

where

$$M = \begin{pmatrix} -\frac{\gamma}{2} - i(\Delta + 4\chi n_0) & -iG \\ iG^* & -\frac{\gamma}{2} + i(\Delta + 4\chi n_0) \end{pmatrix}, \tag{9.16}$$

with $G = 2\chi\alpha_0^2$ and α_0 being the solution to

$$\alpha_0 \left[\frac{\gamma}{2} + i(\Delta + 2\chi n_0)\right] = -i\epsilon_p. \tag{9.17}$$

Then we can write $\alpha_0 = \sqrt{n_0}e^{i\phi_0}$ where

$$\tan\phi_0 = \frac{\gamma}{2\Delta + 4\chi n_0}. \tag{9.18}$$

As we have taken ϵ_p as real, this is the phase shift of the resonator from the pump field.

The eigenvalues of the linearised motion determine stability. These are given by

$$\lambda^{\pm} = -\frac{\gamma}{2} \pm i\sqrt{(\Delta + 6\chi n_0)(\Delta + 2\chi n_0)} \tag{9.19}$$

For stability the real parts of these eigenvalues must be negative. The fixed points are unstable between the turning points of the state equation, Eq. (9.13). In Fig. 9.1(a) we show the unstable fixed points as a dashed line. Note that from Eq. (9.14),

$$\lambda^{+}\lambda^{-} \equiv \lambda^2 = \frac{dI_p}{dn_0}, \tag{9.20}$$

and one of the eigenvalues vanishes at the turning points. The linearised analysis thus breaks down at the bifurcation points.

This kind of nonlinear mechanical resonator can be used as a parametric amplifier. A detailed quantum noise analysis is given in [351]. However a simple approach will show how this works. We expect the effect of the quantum noise to be quite small unless the Duffing nonlinearity becomes comparable to the bare mechanical frequency as in that case the anharmonicity on the energy level spacing becomes very significant. Following a similar approach to that used in the case of the single photon radiation pressure coupling, we make a canonical transformation to a displaced resonator amplitude $\bar{b} = b - \beta_0$ where α_0 is the classical steady-state solution via

$$\bar{H}_I = e^{\beta_0 b^\dagger - \beta_0^* b} H_I e^{-\beta_0 b^\dagger + \beta_0^* b}. \tag{9.21}$$

The Hamiltonian in Eq. (9.10) is then approximated by the quadratic form,

$$\bar{H}_I = \hbar\Delta' \bar{b}^\dagger \bar{b} + \hbar\chi \left[(\beta_0^*)^2 \bar{b}^2 + \beta_0^2 (\bar{b}^\dagger)^2\right]. \tag{9.22}$$

This describes the nondegenerate parametric amplifier and produces squeezed states of the mechanical mode. The reduction in quadrature phase amplitude noise that characterises the nondegnerate parametric amplifier is very useful for quantum metrology. Note, however, that the strength of the parametric gain depends on where the steady-state is located on the curves shown in Fig. 9.1.

10 Many-Body Optomechanics

The integration of many nanomechanical systems into a single superconducting microwave cavity would be an obvious extension of current experiments. It may also be possible to couple many optomechanical resonators together using the optomechanical crystal structures pioneered by the Painter group [107]. In the case of nanomechanics, the common cavity mode leads to an all-to-all coupling, while in the optomechanical case one can have nearest neighbour coupling of distinct cavity modes via photon tunnelling. In both cases the inherent nonlinearity of the radiation pressure interaction leads to highly nonlinear many-body systems.

Holmes *et al.* [352] have considered the case of many nanomechanical resonators coupled to a common microwave cavity. The classical dynamics exhibits a rich bifurcation structure including Hopf bifurcations to multiple limit cycles and even synchronisation when the cavity is driven by a coherent driving field. The classical dynamical system is described by a complex field amplitude α which in the semiclassical limit may be regarded as the mean field $\alpha = \langle a \rangle$, and dimensionless displacement x_i and momentum y_i variables for each mechanical element. Assuming a coupling of the form $\sum_i g_i x_i |\alpha|^2$, we see that the equations of motion may be expressed in terms of collective variables,

$$\frac{d\alpha}{dt} = -i\delta\alpha - i\epsilon - i\alpha X - \kappa\alpha, \tag{10.1}$$

$$\frac{dX}{dt} = \omega Y - \gamma X, \tag{10.2}$$

$$\frac{dY}{dt} = -\omega X - \frac{G}{2}|\alpha|^2 - \gamma Y, \tag{10.3}$$

where ϵ is the coherent driving amplitude of the microwave cavity and X, Y and G are the collective variables

$$X = \frac{1}{N}\sum_j g_j x_j, \tag{10.4}$$

$$Y = \frac{1}{N}\sum_j g_j y_j, \tag{10.5}$$

$$G = \frac{1}{N}\sum_j g_j^2, \tag{10.6}$$

for a collection of N identical nanomechanical oscillators.

Although there are regions of the parameter space where stable critical points exist, periodic motion plays a major role in the dynamics for both the cases of identical and non-identical resonators. If the mechanical resonators are identical, even if their couplings are nonidentical, they will synchronize, in phase, to form a single effective mechanical mode. However, the synchronized motion exhibits multi-stable behaviour. synchronization of identical mechanical resonators may be described via amplitude equations. If, on the other hand, the mechanical resonators naturally oscillate at different frequencies, desynchronization can occur. To analyze this Holmes *et al.* consider the synchronization between different frequency groups. The resonators can then be attracted to out-of-phase solutions that oscillate at much greater amplitudes.

For all of the bifurcations that occur, a scaled version of the cavity forcing ϵ, which is tunable in an experiment, can be thought of as the bifurcation parameter. The natural time-scale of the system, given by the amplitude decay rate κ of the common cavity mode, provides the scaling and we introduce: a new time parameter $t' = \kappa t$; re-scaled nano-mechanical variables $X' = X/\kappa$ and $Y' = Y/\kappa$; and dimensionless coupling constants $\delta' = \delta/\kappa$, $\epsilon' = \epsilon/\kappa$, $\omega' = \omega/\kappa$, $\gamma' r = \gamma/\kappa$, $G' = G/\kappa^2$, and $\bar{\omega}' = \sqrt{\omega'^2 + \gamma'^2}$. If the uncoupled mechanical resonators are identical then the oscillators synchronize. This is a natural consequence of linear damping and the fact that each oscillator experiences the same forcing.

The synchronized motion can then be represented in collective variables which, suppressing the use of primes, gives the following equations of motion,

$$\frac{d\alpha}{dt} = -(1+i\delta)\alpha - i\alpha N X - i\epsilon, \tag{10.7}$$

$$\frac{d^2X}{dt^2} = -\bar{\omega}^2 X - \frac{G\omega}{2}|\alpha|^2 - 2\gamma\frac{dX}{dt}. \tag{10.8}$$

From a dynamical point of view $\epsilon\sqrt{NG}$ acts as one parameter and in fact both N and G could be removed by scaling. So if the number of resonators is increased, smaller values of the driving are necessary to achieve the same effect.

Periodic orbits and multiple periodic orbits can exist, if the weakly forced oscillators are sufficiently weakly damped. This multi-stable behaviour, resulting from the play-off between weak damping and cavity forcing, has been noted elsewhere [353, 354, 355]. Holmes *et al.* [352] used the method of “amplitude equations”. This relies on defining a slow time which is proportional to the weak damping, $\tau = \gamma t$, and on assuming that the forcing is on the order of the square root of the damping, $\epsilon = \sqrt{\gamma}\,\bar{\epsilon}$. Then the cavity amplitude is naturally of the same order as the forcing and we can obtain equations for the slowly varying amplitude $A(\tau)$ where,

$$X = X_0 + \left[A(\tau)e^{i\bar{\omega}\tau} + c.c.\right] = X_0 + 2|A(\tau)|\cos(\bar{\omega}\tau + \theta)\,, \tag{10.9}$$

with X_0 being the critical point of the system which is $O(\epsilon^2)$.

For blue detuning, $\delta < 0$, one can obtain a single equation for the amplitude,

$$\frac{dA}{d\tau} = -A + G\bar{\epsilon}^2 N A F(N|A|,\, \omega,\, \delta)\,, \tag{10.10}$$

where $F(Nr, \omega, \delta)$ is a complex function. This equation describes both nonlinear damping and a Kerr-like nonlinear detuning. Not surprisingly this leads to multistability and Hopf bifurcations to multiple limit cycles.

In the case of non-identical oscillators synchronisation can still occur for some parameter values. The model cannot be reduced to the standard Kuramoto model for synchronisation; nonetheless stable synchonized orbits do exist.

11 Conclusions

In this review we have been primarily concerned with the measurement and control of the quantised motion of bulk mechanical resonators via electromagnetic fields. While the discussion has focused on micron and sub-micron scale devices treated as a single unit, it is important to keep in mind that these systems involve the collective motion of a very large number of atoms. Experimental evidence shows that we can indeed prepare, control and measure the collective quantum dynamics of such systems.

Indeed, it is not essential to restrict the discussion to small mechanical resonators. In the LIGO experiments we potentially need to account for the quantum motion of kilogram scale mirrors separated by many kilometres [2]. It may soon be possible to cool to the quantum ground state the relative motion of two gram scale mirrors, in a LIGO like configuration separated by at least meters [124]. The traditional identification of the quantum-classical divide with the micro-macro divide is rapidly becoming invalid. Optomechanical systems may be the vanguard of a new approach to quantum mechanics in which large scale hybrid systems are engineered to perform a specific function that naturally occurring systems could never provide.

Now that ground-state cooling and near quantum-limited measurement of mechanical motion have been demonstrated in a few systems, the task remains to generalize these techniques to different and more versatile systems. Many fundamental tasks in quantum state engineering remain, and there are many interesting problems in nonlinear and many-body optomechanical systems. Of course, there is also potential for application in sensing and quantum information processing.

There is nothing in quantum mechanics to suggest that there is any limit to how large and complex a device can be before it fails to be described by quantum mechanics. Of course it will not be easy to develop the technology to control the quantum probability amplitudes of such systems. One thing will always remain the case: no matter how large and how complex a quantum system becomes, its quantum character will be revealed by comparing *classical* stochastic control signals with *classical* stochastic measurement records. The classical-quantum border will remain, but where we put it will be a function of our engineering capability alone.

References

[1] D. G. Blair, D. E. McClelland, H. A. Bachor, R. J. Sandeman: *The Detection of gravitational waves, Ed. D. G. Blair* (Cambridge University Press, 1991) 43

[2] B. C. Barish, C. Weiss: *Physics Today* **52** (1999) 44

[3] V. B. Braginsky, F. Ya. Khalilli and K. S. Thorne : *Quantum Measurement* **Cambridge University Press** (1995)

[4] C. M. Caves, K. S. Thorne, R. W. P. Drever, V. D. Sandberg and M. Zimmermann, : *Rev. Mod. Phys.* **52** (1980) 342-391

[5] T. Rocheleau, T. Ndukum, C. Macklin, J. B. Hertzberg, A. A. Clerk, K. C. Schwab: *Nature* **463** (2010) 72

[6] M. Eichenfield, J. Chan, R. M. Camacho, K. J. Vahala, O. Painter: *Nature* **462** (2009) 78

[7] A. Schliesser, T. J. Kippenberg : *Advances in Atomic, Molecular and Optical Physics* **58** (2010) 207

[8] S. Gröblacher, K. Hammerer, M. R. Vanner, M. Aspelmeyer: *Nature* **460** (2009) 724

[9] J. D. Teufel, D. Li, M. S. Allman, K. Cicak, A. J. Sirois, J. D. Whittaker, R. W. Simmonds: *Nature* **471** (2011) 204

[10] F. Marquardt and S. M. Girvin. Optomechanics. *Physics*, 2:40, 2009.

[11] M. P. Blencowe. Quantum electromechanical systems. *Physics Reports*, 395:159–222, 2004.

[12] K. C. Schwab and M. L. Roukes. Putting mechanics into quantum mechanics. *Physics Today*, July 2005.

[13] M. Poot and H. S. J. van der Zant. Mechanical systems in the quantum regime. arXiv:1106.2060.

[14] J. P. Dowling and G. J. Milburn. Quantum technology: the second quantum revolution. *Philosophical Transactions of the Royal Society of London*, 361:1809, 2003.

[15] A. J. Leggett. Testing the limits of quantum mechanics: motivation, state of play, prospects. *Journal of Physics: Condensed Matter*, 14:R415–R451, 2002.

[16] K. L. Ekinci and M. L. Roukes. Nanoelectromechanical systems. *Review of Scientific Instruments*, 76:061101, 2005.

[17] A. N. Cleland and M. L. Roukes. A nanometre-scale mechanical electrometer. *Nature*, 392:160, 1998.

[18] Y. T. Yang, C. Callegari, X. L. Feng, K. L. Ekinci, and M. L. Roukes. Zeptogram-scale nanomechanical mass sensing. *Nanotechnology Letters*, 6:583, 2006.

[19] A. K. Naik, M. S. Hanay, W. K. Hiebert, X. L. Feng, and M. L. Roukes. Towards single-molecule nanomechanical mass spectrometry. *Nature Nanotechnology*, 4:445–450, 2009.

[20] H.-Y. Chiu, P. Hung, H. W. Ch. Postma, and M. Bockrath. Atomic-scale mass sensing using carbon nanotube resonators. *Nano Letters*, 8:4342–4346, 2008.

[21] H. B. Peng, C. W. Chang, S. Aloni, T. D. Yuzvinsky, and A. Zettl. Ultrahigh frequency nanotube resonators. *Physical Review Letters*, 97:087203, 2006.

[22] B. Lassagne, D. Garcia-Sanchez, A. Aguasca, and A. Bachtold. Ultrasensitive mass sensing with a nanotube electromechanical resonator. *Nano Letters*, 8:3735–3738, 2008.

[23] P. Rabl, S. J. Kolkowitz, F. H. L. Koppens, J. G. E. Harris, P. Zoller, and M. D. Lukin. A quantum spin transducer based on nanoelectromechanical resonator arrays. *Nature Physics*, 6:602–608, 2010.

[24] K. Stannigel, P. Rabl, A. S. Sorenson, P. Zoller, and M. D. Lukin. Opto-mechanical transducers for long-distance quantum communication. arXiv:1006.4361v1 [quant-ph].

[25] D. Leibfried, R. Blatt, C. Monroe D. Wineland: *Rev. Modern Phys.* **75** (2003) 281

[26] A. J. Leggett: *Progress in Theor. Phys. (Suppl.)* **69** (1980) 80

[27] J. M. Martinis, M. H. Devoret, J. Clarke: *Phys. Rev. B* **35** (1987) 4682

[28] A. Wallraff, D. I. Schuster, A. Blais, L. Frunzio, R. -S. Huang, J. Majer, S. Kumar, S. M. Girvin, R. J. Schoelkopf: *Nature* **431** (1987) 162

[29] D. Hunger, S. Camerer, M. Korppi, A. Jöckel, T. W. Hänsch and P. Treutlein. Coupling ultracold atoms to mechanical oscillators. arXiv:1103.1820v1.

[30] D. Hunger, S. Camerer, T. W. Hänsch, D. König, J. P. Kotthaus, J. Reichel and P. Treutlein. Resonant Coupling of a Bose-Einstein Condensate to a Micromechanical Oscillator. *Physical Review Letters*, 104:143002, 2010.

[31] S. Camerer, M. Korppi, A. Jöckel, D. Hunger, T. W. Hänsch and P. Treutlein. Realization of an Optomechanical Interface Between Ultracold Atoms and a Membrane. *Physical Review Letters* 107:223001, 2011.

[32] A. N. Cleland: *Foundations of Nanomechanics* (Springer, Berlin, 2003)

[33] J. N. Reddy: *Theory and analysis of elastic plates* (Taylor and Francis, Philadelphia, 1999)

[34] A. J. Leggett, S. Chakravarty, A. T. Dorsey, M. P. A. Fisher, A. Garg, and W. Zwerger. Dynamics of the dissipative two-state system. *Reviews of Modern Physics*, 59:1–85, 1987.

[35] P. Mohanty, D. A. Harrington, K. L. Ekinci, Y. T. Yang, M. J. Murphy, and M. L. Roukes. Intrinsic dissipation in high-frequency micromechanical resonators. *Physical Review B*, 66:085416, 2002.

[36] M. Schlosshauer, A. P. Hines, and G. J. Milburn. Decoherence and dissipation of a quantum harmonic oscillator coupled to two-level systems. *Physical Review A*, 77:022111, 2008.

[37] L. G. Remus, M. P. Blencowe, and Y. Tanaka. Damping and decoherence of a nanomechanical resonator due to a few two level systems. *Physical Review B*, 80:174103, 2009.

[38] I. Wilson-Rae. Intrinsic dissipation in nanomechanical resonators due to phonon tunneling. *Physical Review B*, 77:245418, 2008.

[39] G. D. Cole, I. Wilson-Rae, K. Werbach, M. R. Vanner and M. Aspelmeyer. Minimization of phonon-tunneling dissipation in mechanical resonators. *Nature Communications*, 2:231, 2011.

[40] I. Wilson-Rae, R. A. Barton, S. S. Verbridge, D. R. Southworth, B. Ilic, H. G. Craighead and J. M. Parpia. High-Q Nanomechanics via Destructive Interference of Elastic Waves. *Physical Review Letters*, 106:047205, 2011.

[41] C. W. Gardiner. *Handbook of Stochastic Methods (2nd Ed.)*. Springer, Berlin, 1985.

[42] C. W. Gardiner and P. Zoller. *Quantum Noise (2nd Ed.)*. Springer, Berlin, 2000.

[43] H. W. Ch. Postma, I. Kozinsky, A. Husain, and M. L. Roukes. Dynamic range of nanotube- and nanowire-based electromechanical systems. *Applied Physics Letters*, 86:223105, 2005.

[44] S. I. Lee, S. W. Howell, A. Raman, and R. Reifenberger. Nonlinear dynamics of microcantilevers in tapping mode atomic force microscopy: A comparison between theory and experiment. *Physical Review B*, 66:115409, 2002.

[45] D. Rugar and P. Grutter. Mechanical parametric amplification and thermomechanical noise squeezing. *Physical Review Letters*, 67:699, 1991.

[46] B. Yurke, D. S. Greywall, A. N. Pargellis, and P. A. Busch. Theory of amplifier-noise evasion in an oscillator employing a nonlinear oscillator. *Physical Review A*, 51:4211–4229, 1995.

[47] A. H. Nayfeh and D. T. Mook. *Nonlinear Oscillations*. Wiley, Cambridge, 1979.

[48] D. F. Walls and G. J. Milburn. *Quantum Optics (2nd Ed.)*. Springer, Berlin, 2007.

[49] D. M. Meekhof, C. Monroe, B. E. King, W. M. Itano, and D. J. Wineland. Generation of nonclassical motional state of a trapped atom. *Physical Review Letters*, 76:1796–1799, 1996.

[50] C. Monroe, D. M. Meekhof, B. E. King, and D. J. Wineland. A “Schrödinger cat” superposition state of an atom. *Science*, 272:1131–1136, 1996.

[51] C. J. Hood, T. W. Lynn, A. C. Doherty, A. S. Parkins, and H. J. Kimble. The atom-cavity microscope: single atoms bound in orbit by single photons. *Science*, 287:1447–1453, 2000.

[52] J. D. Jost, J. P. Home, J. M. Amini, D. Hanneke, R. Ozeri, C. Langer, J. J. Bollinger, D. Leibfried, and D. J. Wineland. Entangled mechanical oscillators. *Nature*, 459:683–685, 2009.

[53] K. R. Brown, C. Ospelkaus, Y. Colombe, A. C. Wilson, D. Liebfried and D. J. Wineland. Coupled quantized mechanical oscillators. *Nature* 471:196-199, 2011.

[54] M. H. Anderson, J. H. Ensher, M. R. Matthews, C. E. Wieman, and E. A. Cornell. Observation of Bose-Einstein condensation in a dilute atomic vapour. *Science*, 269:198–201, 1995.

[55] C. Orzel, A. K. Tuchman, M. L. Fenselau, M. Yasuda, and M. A. Kasevich. Squeezed states in a Bose-Einstein condensate. *Science*, 291:2386–2389, 2001.

[56] K. W. Murch, K. L. Moore, S. Gupta, and D. M. Stamper-Kurn. Observation of quantum-measurement backaction with an ultracold atomic gas. *Nature Physics*, 4:561–564, 2008.

[57] A. D. O'Connell, M. Hofheinz, M. Ansmann, R. C. Bialczak, M. Lenander, E. Lucero, M. Neeley, D. Sank, H. Wang, M. Weides, J. Wenner, J. M. Martinis, and A. N. Cleland. Quantum ground state and single-phonon control of a mechanical resonator. *Nature*, 464:697–703, 2010.

[58] J. Chan, T. P. Mayer Alegre, A. H. Safavi-Naeini, J. T. Hill, A. Krause, S. Groöblacher, M. Aspelmeyer and O. Painter. Laser cooling of a nanomechanical oscillator into its quantum ground state. *Nature* 478:89-92, 2011.

[59] J. D. Teufel, T. Donner, D. Li, J. W. Harlow, M. S. Allman, K. Cicak, A. J. Sirois, J. D. Whittaker, K. W. Lehnert and R. W. Simmonds. Sideband cooling of micromechanical motion to the quantum ground state *Nature* 475:359-363, 2011.

[60] H.-W. Lee. Theory and application of the quantum phase-space distribution functions. *Physics Reports*, 259:147–211, 1995.

[61] E. P. Wigner. On the quantum correction for thermodynamic equilibrium. *Physical Review*, 40:749, 1932.

[62] R. J. Glauber. Coherent and incoherent states of the radiation field. *Physical Review*, 131:2766, 1963.

[63] E. C. G. Sudarshan. Equivalence of semiclassical and quantum mechanical descriptions of statistical light beams. *Physical Review Letters*, 10:277, 1963.

[64] K. Husimi. Some formal properties of the density matrix. *Proceedings of the Physical and Mathematical Society of Japan*, 22:264–314, 1940.

[65] R. J. Glauber. *Quantum Optics and Electronics: lectures delivered at Les Houches during the 1964 session of the Summer School of Theoretical Physics*, page 63. Gordon and Breach, 1965.

[66] H. P. Breuer and F. Petruccione. *The Theory of Open Quantum Systems (2nd Ed.)*. Oxford University Press, Oxford, 2002.

[67] M. Schlosshauer. *Decoherence: And the Quantum-to-Classical Transition*. Springer, Berlin, 2008.

[68] W. H. Zurek. Pointer basis of quantum apparatus: Into what mixture does the wave packet collapse? *Physical Review D*, 24:1516–1525, 1981.

[69] W. H. Zurek. Environment-induced superselection rules. *Physical Review D*, 26:1862–1880, 1982.

[70] H. M. Wiseman and G. J. Milburn. *Quantum Measurement and Control*. Cambridge University Press, Cambridge, 2009.

[71] E. Joos and H. D. Zeh. The emergence of classical properties through interaction with the environment. *Zeitschrift für Physik B: Condensed Matter*, 59:223–243, 1985.

[72] J. P. Paz, S. Habib, and W. H. Zurek. Reduction of the wave packet: Preferred observable and decoherence time scale. *Physical Review D*, 47:488–501, 1993.

[73] W. H. Zurek, S. Habib, and J. Paz. Coherent states via decoherence. *Physical Review Letters*, 70:1187, 1993.

[74] J. P. Paz and W. H. Zurek. Quantum limit of decoherence: Environment induced superselection of energy eigenstates. *Physical Review Letters*, 82:5181–5185, 1999.

[75] A. A. Clerk, M. H. Devoret, S. M. Girvin, F. Marquardt, and R. J. Schoelkopf. Introduction to Quantum Noise, Measurement and Amplification. *Review of Modern Physics*, 82:1155, 2010.

[76] G. W. Ford, M. Kac, and P. Mazur. Statistical mechanics of assemblies of coupled oscillators. *Journal of Mathematical Physics*, 6:504, 1965.

[77] M. J. Collett and C. W. Gardiner. Squeezing of intracavity and traveling-wave light fields produced in parametric amplification. *Physical Review A*, 30:1386–1391, 1984.

[78] C. W. Gardiner and M. J. Collett. Input and output in damped quantum systems: Quantum stochastic differential equations and the master equation. *Physical Review A*, 31:3761, 1985.

[79] U. Weiss. *Quantum Dissipative Systems*. World Scientific, Singapore, 1999.

[80] R. Feynman and F. L. Vernon. The theory of a general quantum system interacting with a linear dissipative system. *Annals of Physics (N.Y.)*, 24:118–173, 1963.

[81] A. O. Caldeira and A. J. Leggett. Path integral approach to quantum Brownian motion. *Physica (Amsterdam)*, 121A:587, 1983.

[82] A. O. Caldeira and A. J. Leggett. Quantum tunneling in a dissipative system. *Annals of Physics (N.Y.)*, 149:374, 1983.

[83] C. M. Caves. Quantum mechanics of measurements distributed in time. A path-integral formulation. *Physical Review D*, 33:1643–1665, 1986.

[84] V. Gorini, A. Frigerio, M. Verri, A. Kossokowski, and E. C. G. Sudarshan. Properties of quantum Markovian master equations. *Reports on Mathematical Physics*, 13:149–173, 1978.

[85] G. Lindblad. On the generators of quantum dynamical semigroups. *Communications in Mathematical Physics*, 48:119–130, 1976.

[86] A. O. Caldeira, H. A. Cerdeira, and R. Ramaswamy. Limits of weak damping of a quantum harmonic oscillator. *Physical Review A*, 40:3438, 1989.

[87] I. Wilson-Rae: *Phys. Rev. B* **77** (2008) 245418

[88] L. G. Remus, M. P. Blencowe, Y. Tanaka: *Phys. Rev. B* **80** (2009) 174103

[89] G D Cole, I Wilson-Rae, K Werbach, M R Vanner, M Aspelmeyer: *Nature Communications* **2** (2010) 231

[90] A. B. Matsko, E. A. Zubova, and S. P. Vyatchanin. The value of the force of radiative friction. *Optics Communications*, 131:107–113, 1996.

[91] K. Karrai, I. Favero, and C. Metzger. Doppler optomechanics of a photonic crystal. *Physical Review Letters*, 100:240801, 2010.

[92] J. Mertz, O. Marti, and J. Mlynek. Regulation of a microcantilever response by force feedback. *Applied Physics Letters*, 62:2344, 1993.

[93] E. F. Nichols and G. F. Hull. A Preliminary Communication on the Pressure of Heat and Light Radiation. *Physical Review (Series I)*, 13:307–320, 1901.

[94] P. Lebedev. Untersuchungen über die Druckkräfte des Lichtes. *Annalen der Physik (Leipzig)*, 6:433, 1901.

[95] A. Dorsel, J. D. McCullen, P. Meystre, E. Vignes, and H. Walther. Optical bistability and mirror confinement induced by radiation pressure. *Physical Review Letters*, 51:1550, 1983.

[96] V. B. Braginsky, A. B. Manukin, and M. Yu. Tikhonov. Investigation of dissipative ponderomotive effects of electromagnetic radiation. *Soviet Physics JETP*, 31:829, 1970.

[97] M. Dykman. Heating and cooling of local and quasilocal vibrations by a nonresonance field. *Soviet Physics Solid State*, 20:1306–1311, 1978.

[98] G. Bahl, J. Zehnpfennig, M. Tomes and T. Carmon. Stimulated optomechanical excitation of surface acoustic waves in a microdevice. *Nature Communications* 2:403, 2011.

[99] G. Bahl, M. Tomes, F. Marquardt and T. Carmon. Observation of Spontaneous Brillouin Cooling. arXiv:1109.2084.

[100] J. D. Thompson, B. M. Zwickl, A. M. Jayich, F. Marquardt, S. M. Girvin, and J. G. E. Harris. Strong dispersive coupling of a high-finesse cavity to a micromechanical membrane. *Nature*, 452:72–75, 2008.

[101] A. Ashkin. Acceleration and Trapping of Particles by Radiation Pressure. *Physical Review Letters*, 24:156–159, 1970.

[102] D. Van Thourhout and J. Roels. Optomechanical device actuation through the optical gradient force. *Nature Photonics*, 4:211–217, 2010.

[103] A. F. Pace, M. J. Collett, and D. F. Walls. Quantum limits in interferometric detection of gravitational radiation. *Physical Review A*, 47:3173–3189, 1993.

[104] G. J. Milburn, K. Jacobs, and D. F. Walls. Quantum-limited measurements with the atomic force microscope. *Physical Review A*, 50:5256, 1994.

[105] C. K. Law. Interaction between a moving mirror and radiation pressure: A Hamiltonian formulation. *Physical Review A*, 51:2537–2541, 2008.

[106] S. Gigan, H. R. Böhm, M. Paternostro, F. Blaser, G. Langer, J. B. Hertzberg, K. C. Schwab, D. Bäuerle, M. Aspelmeyer, A. Zeilinger: *Nature* **44** (2006) 67

[107] J. Chan, M. Eichenfield, R. Camacho, O. Painter: *Opt. Express* **17** (2009) 3802

[108] S. Gröblacher, K. Hammerer, M. R. Vanner, and M. Aspelmeyer. Observation of strong coupling between a micromechanical resonator and an optical cavity field. *Nature*, 460:724–727, 2009.

[109] A. M. Jayich, J. C. Sankey, B. M. Zwickl, C. Yang, J. D. Thompson, S. M. Girvin, A. A. Clerk, F. Marquardt, and J. G. E. Harris. Dispersive optomechanics: a membrane inside a cavity. *New Journal of Physics*, 10:095008, 2008.

[110] J. D. Thompson, B. M. Zwickl, A. M. Jayich1, F. Marquardt, S. M. Girvin, J. G. E. Harris: *Nature* **452** (2008) 72

[111] J. C Sankey, C Yang, B. M Zwickl, A. M Jayich, J. G. E Harris: *Nature Physics* **6** (2010) 707

[112] C. M. Caves, K, S. Thorne, R. W. P. Drever, M. Zimmermann, and V. D. Sandberg: *Rev. Mod. Phys.* **52** (1980) 341

[113] D.F.Walls, G.J.Milburn: *Phys. Rev. A* **31** (1985) 2403

[114] A. A. Clerk, F. Marquardt and K. Jacobs: *New J. Phys.* **10** (2008) 095010

[115] F. Elste, S. M. Girvin, and A. A. Clerk. Quantum noise interference and backaction cooling in cavity nanomechanics. *Physical Review Letters*, 102:207209, 2009.

[116] M. Li, W. H. P. Pernice, and H. X. Tang. Reactive cavity optical force on microdisk-coupled nanomechanical beam waveguides. *Physical Review Letters*, 103:223901, 2009.

[117] K. S. Thorne. Gravitational Waves. In *Proceedings of the Snowmass 95 Summer Study on Particle and Nuclear Astrophysics and Cosmology*, 1995.

[118] LIGO. LIGO: The Laser Interferometer Gravitational-wave Observatory. *Science*, 256:325, 1992.

[119] LIGO. LIGO: The Laser Interferometer Gravitational-Wave Observatory. *Reports of Progress in Physics*, 72:076901, 2009.

[120] LIGO. Observation of a kilogram-scale oscillator near its quantum ground state. *New Journal of Physics*, 11:073032, 2009.

[121] The LIGO Scientific Collaboration. A gravitational wave observatory operating beyond the quantum shot-noise limit. Published online 11 September, 2011.

[122] B. S. Sheard, M. B. Gray, C. M. Mow-Lowry, and D. E. McClelland. Observation and characterization of an optical spring. *Physical Review A*, 69:051801(R), 2004.

[123] T. Corbitt, Y. Chen, E. Innerhofer, H. Müller-Ebhardt, D. Ottaway, H. Rehbein, D. Sigg, S. Whitcomb, C. Wipf, and N. Mavalvala. An all-optical trap for a gram-scale mirror. *Physical Review Letters*, 98:150802, 2007.

[124] T. Corbitt, C. Wipf, T. Bodiya, D. Ottaway, D. Sigg, N. Smith, S. Whitcomb, and N. Mavalvala. Optical dilution and feedback cooling of a gram-scale oscillator to 6.9mK. *Physical Review Letters*, 99:160801, 2007.

[125] C. M. Mow-Lowry, A. J. Mullavey, S. Goβler, M. B. Gray, and D. E. McClelland. Cooling of a gram-scale cantilever flexure to 70 mK with a servo-modified optical spring. *Physical Review Letters*, 100:010801, 2008.

[126] P. F. Cohadon, A. Heidmann, and M. Pinard. Cooling of a mirror by radiation pressure. *Physical Review Letters*, 83:3174, 1999.

[127] O. Arcizet, P.-F. Cohadon, T. Briant, M. Pinard, and A. Heidmann. Radiation-pressure cooling and optomechanical instability of a micromirror. *Nature*, 444:71, 2006.

[128] D. Kleckner and D. Bouwmeester. Sub-Kelvin optical cooling of a micromechanical resonator. *Nature*, 444:71, 2006.

[129] S. Gigan, H. R. Böhm, M. Paternostro, F. Blaser, G. Langer, J. B. Hertzberg, K. C. Schwab, D. Bäuerle, M. Aspelmeyer, and A. Zeilinger. Self-cooling of a micromirror by radiation pressure. *Nature*, 444:67, 2006.

[130] S. Gröblacher, J. B. Hertzberg, M. R. Vanner, S. Gigan, K. C. Schwab, and M. Aspelmeyer. Demonstration of an ultracold micro-optomechanical oscillator in a cryogenic cavity. *Nature Physics*, 5:485–488, 2009.

[131] D. J. Wilson, C. A. Regal, S. B. Papp, and H. J. Kimble. Cavity optomechanics with stoichiometric SiN films. *Physical Review Letters*, 103:207204, 2009.

[132] M. Li, W. H. P. Pernice, C. Xiong, T. Baehr-Jones, M. Hochberg, and H. X. Tang. Harnessing optical forces in integrated photonic circuits. *Nature*, 456:480–484, 2008.

[133] M. Eichenfield, C. P. Michael, R. Perahia, and O. Painter. Actuation of micro-optomechanical systems via cavity-enhanced optical dipole forces. *Nature Photonics*, 1:416–422, 2007.

[134] M. Poggio, C. L. Degen, H. J. Mamin, and D. Rugar. Feedback cooling of a cantilever's fundamental mode below 5mK. *Physical Review Letters*, 99:017201, 2007.

[135] G. Anetsberger, O. Arcizet, Q. P. Unterreithmeier, E. M. Weig, J. P. Kotthaus, and T. J. Kippenberg. Near-field cavity optomechanics with nanomechanical oscillators. *Nature Physics*, 5:909–914, 2009.

[136] K. H. Lee, T. G. McRae, G. I. Harris, J. Knittel, and W. P. Bowen. Cooling and control of a cavity optoelectromechanical system. *Physical Review Letters*, 104:123604, 2010.

[137] Y. Hadjar, P. F. Cohadon, C. G. Aminoff, M. Pinard, and A. Heidmann. High-sensitivity optical measurement of mechanical Brownian motion. *Europhysics Letters*, 47:545, 1999.

[138] I. Tittonen, G. Breitenbach, T. Kalkbrenner, T. Müller, R. Conradt, and S. Schiller. Interferometric measurements of the position of a macroscopic body: Towards observation of quantum limits. *Physical Review A*, 59:1038–1044, 1999.

[139] O. Arcizet, P.-F. Cohadon, T. Briant, M. Pinard, A. Heidmann, J.-M. Mackowski, C. Michel, L. Pinard, O. Francais, and L. Rousseau. High-sensitivity optical monitoring of an optomechanical resonator with a quantum-limited optomechanical sensor. *Physical Review Letters*, 97:133601, 2006.

[140] C. Hohberger Metzger and K. Karrai. Cavity cooling of a microlever. *Nature*, 432:1002–1005, 2004.

[141] J. C. Sankey, C. Yang, B. M. Zwickl, A. M. Jayich, and J. G. E. Harris. Strong and tunable nonlinear optomechanical coupling in a low-loss system. *Nature Physics*, Advance Online Publication, 2010.

[142] T. P. Purdy, D. W. C. Brooks, T. Botter, N. Brahms, Z.-Y. Ma and D. M. Stamper-Kurn. Tunable Cavity Optomechanics with Ultracold Atoms. *Physical Review Letters* 105:133602, 2010.

[143] D. W. C. Brooks, T. Botter, N. Brahms, T. P. Purdy, S. Schreppler and D. M. Stamper-Kurn. Ponderomotive light squeezing with atomic cavity optomechanics. arXiv:1107.5609v1.

[144] N. Brahms, T. Botter, S. Schreppler, D. W. C. Brooks and D. M. Stamper-Kurn. Backaction-limited cavity-sideband spectroscopy of quantum collective motion. arXiv:1109.5233v1.

[145] O. Romero-Isart, A. C. Pflanzer, M. L. Juan, R. Quidant, N. Kiesel, M. Aspelmeyer, J. Ignacio Cirac. Optically Levitating Dielectrics in the Quantum Regime: Theory and Protocols. *Physical Review A* 83:013803 (2011).

[146] D. E. Chang, C. A. Regal, S. B. Papp, D. J. Wilson, J. Ye, O. Painter, H. J. Kimble and P. Zoller. Cavity opto-mechanics using an optically levitated nanosphere. *Proc. Natl. Acad. Sci.* 107:1005-1010 (2010).

[147] T. Li, S. Kheifets and M. Raizen. Millikelvin cooling of an optically trapped microsphere in vacuum. *Nature Physics* 7, 527-530, 2011.

[148] O. Romero-Isart, M. L. Juan, R. Quidant and J. I. Cirac. Toward quantum superposition of living organisms. *New Journal of Physics* 12:033015, 2011.

[149] T. Carmon, H. Rokhsari, L. Yang, T. J. Kippenberg, and K. J. Vahala. Temporal behaviour of radiation-pressure-induced vibrations of an optical microcavity phonon mode. *Physical Review Letters*, 94:223902, 2005.

[150] K. J. Vahala. Optical microcavities. *Nature*, 424:839, 2003.

[151] D. K. Armani, T. J. Kippenberg, S. M. Spillane, and K. J. Vahala. Ultra-high-Q toroid microcavity on a chip. *Nature*, 421:925, 2003.

[152] T. J. Kippenberg, H. Rokhsari, T. Carmon, A. Scherer, and K. J. Vahala. Analysis of radiation-pressure induced mechanical oscillation of an optical microcavity. *Physical Review Letters*, 95:033901, 2005.

[153] A. Schliesser, P. Del'Haye, N. Nooshi, K. J. Vahala, and T. J. Kippenberg. Radiaton pressure cooling of a micromechanical oscillator using dynamical backaction. *Physical Review Letters*, 97:243905, 2006.

[154] A. Schliesser, R. Riviere, G. Anetsberger, O. Arcizet, and T. J. Kippenberg. Resolved-sideband cooling of a micromechanical oscillator. *Nature Physics*, 4:415–419, 2008.

[155] R. Rivière, S. Deléglise, S. Weis, E. Gavartin, O. Arcizet, A. Schliesser and T. J. Kippenberg. Optomechanical sideband cooling of a micromechanical oscillator close to the quantum ground state. *Physical Review A* 83, 063835, 2011.

[156] A. Schliesser, O. Arcizet, R. Riviere, and T. J. Kippenberg. Resolved-sideband cooling and position measurement of a micromechanical oscillator close to the heisenberg uncertainty limit. *Nature Physics*, 5:509–514, 2009.

[157] G. Anetsberger, R. Rivière, A. Schliesser, O. Arcizet, and T. J. Kippenberg. Ultralow-dissipation optomechanical resonators on a chip. *Nature Photonics*, 2:627–633, 2008.

[158] S. Weis, R. Rivière, S. Deléglise, E. Gavartin, O. Arcizet, A. Schliesser, and T. J. Kippenberg. Optomechanically Induced Transparency. *Science*, 330:1520-1523, 2010.

[159] J. Hofer, A. Schliesser, and T. J. Kippenberg. Cavity optomechanics with ultra-high Q crystalline micro-resonators. arXiv:0911.1178v2 [physics.optics].

[160] Y.-S. Park and H. Wang. Resolved-sideband and cryogenic cooling of an optomechanical resonator. *Nature Physics*, 5:489–493, 2009.

[161] D. E. Chang, C. A. Regal, S. B. Papp, D. J. Wilson, J. Ye, O. Painter, H. J. Kimble, and P. Zoller. Cavity opto-mechanics using an optically levitated nanosphere. *Proceedings of the National Academy of Sciences*, 107:1005–1010, 2010.

[162] M. A. Taylor, A. Szorkovksy, J. Knittel, K. H. Lee, T. G. McRae and W. P. Bowen. Cavity optoelectromechanical regenerative amplification. arXiv:1107.0779v1.

[163] G. I. Harris, U. L. Andersen, J. Knittel and W. P. Bowen. Feedback Enhanced Sensitivity in Optomechanics: Surpassing the Parametric Instability Barrier. arXiv:1109.2381v1.

[164] T. G. McRae and W. P. Bowen. Near threshold all-optical backaction amplifier. arXiv:1109.2004v1.

[165] Q. Lin, J. Rosenberg, X. Jiang, K. J. Vahala, and O. Painter. Mechanical oscillation and cooling actuated by the optical gradient force. *Physical Review Letters*, 103:103601, 2009.

[166] I. S. Grudinin, O. Painter, and K. J. Vahala. Phonon laser action in a tunable two-level system. *Physical Review Letters*, 104:083901, 2010.

[167] M. Li, W. H. P. Pernice, and H. X. Tang. Broadband all-photonic transduction of nanocantilevers. *Nature Nanotechnology*, 4:377–382, 2009.

[168] M. Bagheri, M. Poot, M. Li, W. P. H. Pernice and H. X. Tang. Dynamic manipulation of mechanical resonators in the high-amplitude regime and non-volatile mechanical memory operation. *Nature Nanotechnology* 6:726-732, 2011.

[169] M. Li, W. H. P. Pernice, and H. X. Tang. Tunable bipolar optical interactions between guided lightwaves. *Nature Photonics*, 3:464–468, 2009.

[170] J. Roels, I. De Vlaminck, L. Lagae, B. Maes, D. Van Thorhaut, and R. Baets. Tunable optical forces between nanophotonic waveguides. *Nature Nanotechnology*, 4:510–513, 2009.

[171] G. S. Wiederhecker, L. Chen, A. Gondarenko, and M. Lipson. Controlling photonic structures using optical forces. *Nature*, 462:633–636, 2009.

[172] M. Eichenfield, R. Camacho, J. Chan, K. J. Vahala, and O. Painter. A picogram- and nanometre-scale photonic-crystal optomechanical cavity. *Nature*, 459:550–555, 2009.

[173] Q. Lin, J. Rosenberg, D. Chang, R. Camacho, M. Eichenfield, K. J. Vahala, and O. Painter. Coherent mixing of mechanical excitations in nano-optomechanical systems. *Nature Photonics*, 4:236–242, 2010.

[174] M. Eichenfield, J. Chan, R. M. Camacho, K. J. Vahala, and O. Painter. Optomechanical crystals. *Nature*, 462:78–82, 2009.

[175] Z. Liu, X. Zhang, Y. Mao, Y. Y. Zhu, Z. Yang, C. T. Chan and P. Sheng. Locally Resonant Sonic Materials. *Science* 289:1734-1736, 2000.

[176] A. H. Safavi-Naeini, T. P. Mayer Alegre, J. Chan, M. Eichenfield, M. Winger, Q. Lin, J. T. Hill, D. E. Chang and O. Painter. Electromagnetically induced transparency and slow light with optomechanics. *Nature* 472:69-73, 2011.

[177] A. H. Safavi-Naeini, J. Chan, J. T. Hill, T. P. Mayer Alegre, A. Krause and O. Painter. Measurement of the zero-point motion of a nanomechanical resonator. arXiv:1108.4680v1.

[178] T. P. Mayer Alegre, A. Safavi-Naeini, M. Winger and O. Painter. Quasi-two-dimensional optomechanical crystals with a complete phononic bandgap. *Optics Express* 19(6):5658-5669, 2011.

[179] O. Arcizet, V. Jacques, A. Siria, P. Poncharal, P. Vincent and S. Seidelin. A single nitrogen-vacancy defect coupled to a nanomechanical oscillator. *Nature Physics* 7:879-883, 2011.

[180] M. Winger, T. Blasius, T. P. Mayer Alegre, A. H. Safavi-Naeini, S. Meenahan, J. Cohen, S. Stobbe and O. Painter. A chip-scale integrated cavity-electro-optomechanics platform. arXiv:1111.4602v1.

[181] G. Anetsberger, E. Gavartin, O. Arcizet, Q. P. Unterreithmeier, E. M. Weig, M. L. Gorodetsky, J. P. Kotthaus, and T. J. Kippenberg. Measuring nanomechanical motion with an imprecision far below the standard quantum limit. arXiv:1003.3752v1 [quant-ph], 2010.

[182] E. D. Black. An introduction to Pound-Drever-Hall laser frequency stabilization. *American Journal of Physics*, 69:79–87, 2001.

[183] L. Conti, M. De Rosa, F. Marin, L. Taffarello, and M. Cerdonio. Room temperature gravitational wave bar detector with optomechanical readout. *Journal of Applied Physics*, 93:3589–3595, 2003.

[184] Q. P. Unterreithmeyer, T. Faust, S. Manus, and J. P. Kotthaus. On-chip interferometric detection of nanomechanical motion. *Nano Letters*, 10:887–890, 2010.

[185] J. M. Dobrindt and T. J. Kippenberg. Theoretical analysis of mechanical displacement measurement using a multiple cavity mode transducer. *Physical Review Letters*, 104:033901, 2010.

[186] C. M. Caves. Quantum-mechanical radiation-pressure fluctuations in an interferometer. *Physical Review Letters*, 45:75, 1980.

[187] T. J. Kippenberg and K. J. Vahala. Cavity optomechanics: Back-action at the mesoscale. *Science*, 321:1172–1176, 2008.

[188] A. Schliesser, G. Anetsberger, R. Rivière, O. Arcizet, and T. J. Kippenberg. High-sensitivity monitoring of micromechanical vibration using whispering gallery mode resonators. *New Journal of Physics*, 10:095015, 2008.

[189] W. G. Unruh. Quantum Noise in the Interferometer Detector. In *Quantum Optics, Experimental Gravitation and Measurement Theory*, pages 647–660. Plenum Press, 1983.

[190] J. Weber. Detection and generation of gravitational waves. *Physical Review*, 117:306, 1960.

[191] S. P. Boughn, W. M. Fairbank, R. P. Giffard, J. N. Hollenhorst, M. S. McAshen, H. J. Paik, and R. C. Taber. Observation of mechanical Nyquist noise in a cryogenic gravitational-wave antenna. *Physical Review Letters*, 38:454, 1977.

[192] NAUTILUS. First cooling below 0.1K of the new gravitational-wave antenna NAUTILUS of the Rome group. *Europhysics Letters*, 16:231–235, 1991.

[193] M. E. Tobar and D. G. Blair. Parametric transducers for resonant bar gravitational wave antennae. *Journal of Physics D: Applied Physics*, 26:2276, 1993.

[194] V. B. Braginsky, A. B. Manukin, E. I. Popov, V. N. Rudenko, and A. A. Khorev. An upper limit on the density of gravitational radiation of electromagnetic origin. *Soviet Physics JETP*, 39:387, 1974.

[195] K. Tsubono, S. Hiramatsu, and H. Hirakawa. Cavity transducer for subatomic mechanical vibration. *Japanese Journal of Applied Physics*, 16:1641–1645, 1977.

[196] D. G. Blair, E. N. Ivanov, M. E. Tobar, P. J. Turner, F. van Kann, and I. S. Heng. High sensitivity gravitational wave antenna with parametric transducer readout. *Physical Review Letters*, 74:1908, 1995.

[197] H. J. Paik. Superconducting tunable-diaphragm transducer for sensitive acceleration measurements. *Journal of Applied Physics*, 47:1168–1178, 1976.

[198] ROG. Long-term operation of the Rome "Explorer" cryogenic gravitational wave detector. *Physical Review D*, 47:362–375, 1993.

[199] AURIGA. Initial operation of the gravitational wave detector AURIGA. In *Gravitational Waves: Proceedings of the Second Edoardo Amaldi Conference*, pages 148–158, 1997.

[200] ALLEGRO. The ALLEGRO gravitational wave detector: Data acquisition and analysis. *Physical Review D*, 54:1264, 1996.

[201] W. W. Johnson and M. Bocko. Approaching the quantum "limit" for force detection. *Physical Review Letters*, 47:1184–1187, 1981.

[202] M. F. Bocko and W. W. Johnson. Phase-sensitive parametric motion transducer. *Physical Review A*, 30:2135, 1984.

[203] M. F. Bocko and W. W. Johnson. Surpassing the amplifier limit for force detection. *Physical Review Letters*, 48:1371–1374, 1982.

[204] AURIGA. Feedback cooling of the normal modes of a massive electromechanical system to submillikelvin temperature. *Physical Review Letters*, 101:033601, 2008.

[205] K. E. Petersen. Silicon as a mechanical material. *Proceedings of the IEEE*, 70:420, 1982.

[206] A. N. Cleland and M. L. Roukes. Fabrication of high frequency nanometer scale mechanical resonators from bulk Si crystals. *Applied Physics Letters*, 69:2653–2655, 1996.

[207] D. W. Carr and H. G. Craighead. Fabrication of nanoelectromechanical systems in single crystal silicon using silicon on insulator substrates and electron beam lithography. *Journal of Vacuum Science and Technology B*, 15:2760–2763, 1997.

[208] Y. T. Yang, K. L. Ekinci, X. M. H. Huang, L. M. Schiavone, M. L. Roukes, C. A. Zorman, and M. Mehregany. Monocrystalline silicon carbide nanoelectromechanical systems. *Applied Physics Letters*, 78:162–164, 2001.

[209] X. M. H. Huang, C. A. Zorman, M. Mehregany, and M. L. Roukes. Nanodevice motion at microwave frequencies. *Nature*, 421:496, 2003.

[210] A. N. Cleland, M. Pophristic, and I. Ferguson. Single-crystal aluminum nitride nanomechanical resonators. *Applied Physics Letters*, 79:2070–2072, 2001.

[211] L. Sekaric, D. W. Carr, S. Evoy, J. M. Parpia, and H. G. Craighead. Nanomechanical resonant structures in silicon nitride: fabrication, operation and dissipation issues. *Sensors and Actuators A - Physical*, 101:215–219, 2002.

[212] T. F. Li, Y. A. Pashkin, O. Astafiev, Y. Nakamura, J. S. Tsai, and H. Im. High-frequency metallic nanomechanical resonators. *Applied Physics Letters*, 92:043112, 2008.

[213] A. B. Hutchinson, P. A. Truitt, K. C. Schwab, L. Sekaric, J. M. Parpia, H. G. Craighead, and J. E. Butler. Dissipation in nanocrystalline-diamond nanomechanical resonators. *Applied Physics Letters*, 84:972–974, 2004.

[214] N. E. Flowers-Jacobs, D. R. Schmidt, and K. W. Lehnert. Intrinsic noise properties of atomic point contact displacement detectors. *Physical Review Letters*, 98:096804, 2007.

[215] X. L. Feng, R. R. He, P. D. Yang, and M. L. Roukes. Very high frequency silicon nanowire electromechanical resonators. *Nano Letters*, 7:1953–1959, 2007.

[216] I. Kozinsky, H. W. Ch. Postma, I. Bargatin, and M. L. Roukes. Tuning nonlinearity, dynamic range, and frequency of nanomechanical resonators. *Applied Physics Letters*, 88:253101, 2006.

[217] S. S. Verbridge, D. Finkelstein Shapiro, H. G. Craighead, and J. M. Parpia. Macroscopic tuning of nanomechanics: Substrate bending for reversible control of frequency and quality factor of nanostring resonators. *Nano Letters*, 7:1728–1735, 2007.

[218] B. Reulet, A. Yu. Kasumov, M. Kociak, R. Deblock, I. I. Khodos, Yu. B. Gorbatov, V. T. Volkov, C. Journet, and H. Bouchiat. Acoustoelectric effects in carbon nanotubes. *Physical Review Letters*, 85:2829–2832, 2000.

[219] V. Sazonova, Y. Yaish, H. Ustenel, D. Roundy, T. A. Arias, and P. L. McEuen. A tunable carbon nanotube electromechanical oscillator. *Nature*, 431:284–287, 2004.

[220] B. Witkamp, M. Poot, and H. S. J. van der Zant. Bending-mode vibration of a suspended nanotube resonator. *Nano Letters*, 6:2904–2908, 2006.

[221] A. K. Huettel, G. A. Steele, B. Witkamp, M. Poot, L. P. Kouwenhoven, and H. S. J. van der Zant. Carbon nanotubes as ultra-high quality factor mechanical resonators. *Nano Letters*, 9:2547–2552, 2009.

[222] J. S. Bunch, A. M. van der Zande, S. S. Verbridge, I. W. Frank, D. M. Tanenbaum, J. M. Parpia, H. G. Craighead, and P. L. McEuen. Electromechanical resonators from graphene sheets. *Science*, 315:490–493, 2007.

[223] J. C. Meyer, M. Paillet, and S. Roth. Single-molecule torsional pendulum. *Science*, 309:1539–1541, 2005.

[224] D. S. Greywall, B. Yurke, P. A. Busch, A. N. Pargellis, and R. L. Willett. Evading amplifier noise in nonlinear oscillators. *Physical Review Letters*, 72:2992–2995, 1994.

[225] D. W. Carr, S. Evoy, L. Sekaric, H. G. Craighead, and J. M. Parpia. Measurement of mechanical resonance and losses in nanometer scale silicon wires. *Applied Physics Letters*, 75:920–922, 1999.

[226] Q. P. Unterreithmeier, E. M. Weig, and J. P. Kotthaus. Universal transduction scheme for nanomechanical systems based on dielectric forces. *Nature*, 458:1001–1004, 2009.

[227] S. C. Masmanidis, R. B. Karabalin, I. De Vlaminck, G. Borghs, M. R. Freeman, and M. L. Roukes. Multifunctional nanomechanical systems via tunably coupled piezoelectric actuation. *Science*, 317:780–783, 2007.

[228] W. J. Venstra and H. S. J. van der Zant. Efficient readout of micromechanical resonator arrays in ambient conditions. *Applied Physics Letters*, 93:234106, 2008.

[229] A. Naik, O. Buu, M. D. LaHaye, A. D. Armour, A. A. Clerk, M. P. Blencowe, and K. C. Schwab. Cooling a nanomechanical resonator with quantum backaction. *Nature*, 443:193, 2006.

[230] S. Etaki, M. Poot, I. Mahboob, K. Onomitsu, H. Yamaguchi, and H. S. J. van der Zant. Motion detection of a micromechanical resonator embedded in a d.c. SQUID. *Nature Physics*, 4:785–788, 2008.

[231] M. Poggio, M. P. Jura, C. L. Degen, M. A. Topinka, H. J. Mamin, D. Goldhaber-Gordon, and D. Rugar. An off-board quantum point contact as a sensitive detector of cantilever motion. *Nature Physics*, 4:635–638, 2008.

[232] A. N. Cleland, J. S. Aldridge, D. C. Driscoll, and A. C. Gossard. Nanomechanical displacement sensing using a quantum point contact. *Applied Physics Letters*, 81:1699–1701, 2002.

[233] D. Garcia-Sanchez, A. San Paulo, M. J. Esplandiu, F. Perez-Murano, L. Forró, A. Aguasca, and A. Bachtold. Mechanical detection of carbon nanotube resonator vibrations. *Physical Review Letters*, 99:085501, 2007.

[234] U. Kemiktarak, T. Ndukum, K. C. Schwab, and K. L. Ekinci. Radio-frequency scanning tunnelling microscopy. *Nature*, 450:85–88, 2007.

[235] R. G. Knobel and A. N. Cleland. Nanometre-scale displacement sensing using a SET. *Nature*, 424:291, 2003.

[236] M. D. LaHaye, O. Buu, B. Camarota, and K. C. Schwab. Approaching the quantum limit of a nanomechanical resonator. *Science*, 304:74, 2004.

[237] G. A. Steele, A. K. Hüttel, B. Witkamp, M. Poot, H. B. Meerwaldt, L. P. Kouwenhoven, and H. S. J. van der Zant. Strong coupling between single-electron tunneling and nanomechanical motion. *Science*, 325:1103–1107, 2009.

[238] H. S. Solanki, S. Sengupta, S. Dhara, V. Singh, S. Patil, R. Dhall, J. Parpia, A. Bhattacharya, and M. M. Deshmukh. Tuning mechanical modes and influence of charge screening in nanowire resonators. *Physical Review B*, 81:115459, 2010.

[239] M. Tortonese, R. C. Barrett, and C. F. Quate. Atomic resolution with an atomic force microscope using piezoresistive detection. *Applied Physics Letters*, 62:834, 1993.

[240] T. Itoh and T. Suga. Scanning force microscope using a piezoelectric microcantilever. *Journal of Vacuum Science and Technology B*, 12:1581, 1994.

[241] I. Bargatin, E. B. Myers, J. Arlett, B. Gudlewski, and M. L. Roukes. Sensitive detection of nanomechanical motion using piezoresistive signal downmixing. *Applied Physics Letters*, 86:133109, 2005.

[242] R. He, X. L. Feng, M. L. Roukes, and P. Yang. Self-transducing silicon nanowire electromechanical systems at room temperature. *Nano Letters*, 8:1756–1761, 2008.

[243] R. G. Beck, M. A. Eriksson, M. A. Topinka, R. M. Westervelt, K. D. Marnowski, and A. C. Gossard. GaAs/AlGaAs self-sensing cantilevers for low temperature scanning probe microscopy. *Applied Physics Letters*, 73:1149–1151, 1998.

[244] J. Stettenheim, M. Thalakulam, F. Pan, M. Bal, Z. Jhi, W. Zhu, L. Pfeiffer, K. W. West, M. P. Blencowe, and A. J. Rimberg. A macroscopic mechanical resonator driven by mesoscopic electrical back-action. *Nature*, 466:86–90, 2010.

[245] C. A. Regal, J. D. Teufel, and K. W. Lehnert. Measuring nanomechanical motion with a microwave cavity interferometer. *Nature Physics*, 4:555–560, 2008.

[246] J. D. Teufel, T. Donner, M. A. Castellanos-Beltran, J. W. Harlow, and K. W. Lehnert. Nanomechanical motion measured with an imprecision below that at the standard quantum limit. *Nature Nanotechnology*, 4:820–823, 2009.

[247] J. B. Hertzberg, T. Rocheleau, T. Ndukum, M. Savva, A. A. Clerk, and K. C. Schwab. Back-action-evading measurements of nanomechanical motion. *Nature Physics*, 6:213–217, 2010.

[248] P. A. Truitt, J. B. Hertzberg, C. C. Huang, K. L. Ekinci, and K. C. Schwab. Efficient and sensitive capacitive readout of nanomechanical resonator arrays. *Nano Letters*, 7:120–126, 2007.

[249] K. R. Brown, J. Britton, R. J. Epstein, J. Chiaverini, D. Leibfried, and D. J. Wineland. Passive cooling of a micromechanical oscillator with a resonant electric circuit. *Physical Review Letters*, 99:137205, 2007.

[250] T. Faust, P. Krenn, S. Manus, J. P. Kotthaus and E. M. Weig. Microwave cavity-enhanced transduction for plug and play nanomechanics at room temperature. arXiv:1109.1156v1.

[251] F. Massel, T. T. Heikkilä, J. M. Pirkkalainen, S. U. Cho, H. Suloniemi, P. Hakonen and M. A. Sillanpää. Microwave amplification with nanomechanical resonators. arXiv:1107.4903v1.

[252] M. Poot, S. Etaki, I. Mahboob, K. Onomitsu, H. Yamaguchi, Ya. M. Blanter and H. S. J. van der Zant Tunable backaction of a DC SQUID on an integrated micromechanical resonator. *Physical Review Letters* 105:207203, 2010.

[253] M. D. LaHaye, J. Suh, P. M. Echternach, K. C. Schwab, and M. L. Roukes. Nanomechanical measurements of a superconducting qubit. *Nature*, 459:960–964, 2009.

[254] J. Suh, M. D. LaHaye, P. M. Echternach, K. C. Schwab and M. L. Roukes Parametric Amplification and Back-Action Noise Squeezing by a Qubit-Coupled Nanoresonator *Nano Letters* 10:3990-3994, 2010.

[255] A. Cho The First Quantum Machine *Science* 330:1604, 2010.

[256] A. D. O'Connell, M. Hofheinz, M. Ansmann, R. C. Bialczak, M. Lenander, E. Lucero, M. Neeley, D. Sank, H. Wang, M. Weides, J. Wenner, J. M. Martinis, A. N. Cleland: *Nature* **464** (2010) 697

[257] C. J. Pethick, H. Smith: *Bose-Einstein Condensation in DIlute Gases* (Cambridge University Press 2008)

[258] O. Arcizet, P. -F. Cohadon, T. Briant, M. Pinard, A. Heidmann: *Nature* **44** (2006) 71

[259] D. Kleckner, D. Bouwmeester: *Nature* **44** (2006) 75

[260] J. M. W. Milatz and J. J. van Zolingen. The Brownian motion of electrometers. *Physica (Amsterdam)*, 19:181, 1953.

[261] J. M. W. Milatz, J. J. van Zolingen, and B. B. van Iperen. The reduction of the Brownian motion of electrometers. *Physica (Amsterdam)*, 19:195, 1953.

[262] T. Hänsch and A. Schawlow. Cooling of gases by laser radiation. *Optics Communications*, 13:68, 1975.

[263] D. Wineland and H. Dehmelt. Proposed $10^{14}\Delta\nu < \nu$ Laser Fluorescence Spectroscopy Tl^{+} Mono-Ion Oscillator III . *Bulletin of the American Physical Society*, 20:637, 1975.

[264] W. Neuhauser, M. Hohenstatt, P. Toschek, and H. Dehmelt. Optical-sideband cooling of visible atom cloud confined in parabolic well. *Physical Review Letters*, 41:233–236, 1978.

[265] J. D. Teufel, J. W. Harlow, C. A. Regal, and K. W. Lehnert. Dynamical backaction of microwave fields on a nanomechanical oscillator. *Physical Review Letters*, 101:197203, 2008.

[266] T. Rocheleau, T. Ndukum, C. Macklin, J. B. Hertzberg, A. A. Clerk, and K. C. Schwab. Preparation and detection of a mechanical resonator near the ground state of motion. *Nature*, 463:72–75, 2010.

[267] V. B. Braginsky and S. P. Vyatchanin. Low quantum noise tranquilizer for Fabry-Pérot interferometer. *Physics Letters A*, 293:228, 2002.

[268] S. Mancini, D. Vitali, and P. Tombesi. Optomechanical cooling of a macroscopic oscillator by homodyne feedback. *Physical Review Letters*, 80:688, 1998.

[269] D. Vitali, S. Mancini, L. Ribichini, and P. Tombesi. Mirror quiescence and high-sensitivity position measurements with feedback. *Physical Review A*, 65:063803, 2002.

[270] C. Genes, D. Vitali, P. Tombesi, S. Gigan, and M. Aspelmeyer. Ground-state cooling of a micromechanical oscillator: Comparing cold damping and cavity-assisted cooling schemes. *Physical Review A*, 77:033804, 2008.

[271] F. Marquardt, J. P. Chen, A. A. Clerk, and S. M. Girvin. Quantum theory of cavity-assisted sideband cooling of mechanical motion. *Physical Review Letters*, 99:093902, 2007.

[272] I. Wilson-Rae, N. Nooshi, W. Zwerger, and T. J. Kippenberg. Theory of ground state cooling of a mechanical oscillator using dynamical back-action. *Physical Review Letters*, 99:093901, 2007.

[273] E. Verhagen, S. Deléglise, S. Weis, A. Schliesser and T. J. Kippenberg. Quantum-coherent coupling of a mechanical oscillator to an optical cavity mode. arXiv:1107.3761v1.

[274] P. Rabl, C. Genes, K. Hammerer, and M. Aspelmeyer. Phase-noise induced limitations in resolved-sideband cavity cooling of mechanical resonators. *Physical Review A*, 80:063819, 2009.

[275] I. Wilson-Rae, N. Nooshi, J. Dobrindt, T. J. Kippenberg, and W. Zwerger. Cavity-assisted back action cooling of mechanical resonators. *New Journal of Physics*, 10:095007, 2008.

[276] A. Hopkins, K. Jacobs, S. Habib, and K. Schwab. Feedback cooling of a nanomechanical resonator. *Physical Review B*, 68:235328, 2003.

[277] J. Zhang, Y. Liu, and F. Nori. Cooling and squeezing the fluctuations of a nanomechanical beam by indirect quantum feedback control. *Physical Review A*, 79:052102, 2009.

[278] J. D. Teufel, D. Li, M. S. Allman, K. Cicak, A. J. Sirois, J. D. Whittaker and R. W. Simmonds. Circuity cavity electromechanics in the stong-coupling regime *Nature* 471:204-208, 2011.

[279] S. Zippilli, G. Morigi, and A. Bachtold. Cooling carbon nanotubes to the phononic ground state with a constant electron current. *Physical Review Letters*, 102:096804, 2009.

[280] I. Wilson-Rae, P. Zoller, and A. Imamoglu. Laser cooling of a nanomechanical resonator mode to its quantum ground state. *Physical Review Letters*, 92:075507, 2004.

[281] F. W. J. Hekking, A. O Niskanen, and J. P. Pekola. Electron-phonon coupling and longitudinal mechanical-mode cooling in a metallic nanowire. *Physical Review B*, 77:033401, 2008.

[282] G. Sonne, M. E. Pena-Aza, L. Y. Gorelik, R. I. Shekhter, and M. Jonson. Cooling of a suspended nanowire by an ac Josephson current flow. *Physical Review Letters*, 104:226802, 2010.

[283] I. Martin, A. Shnirman, L. Tian, and P. Zoller. Ground-state cooling of mechanical resonators. *Physical Review B*, 69:125339, 2004.

[284] J. Hauss, A. Fedorov, S. André, V. Brosco, C. Hutter, R. Kothari, S. Yeshwanth, A. Shnirman, and G. Schön. Dissipation in circuit quantum electrodynamics: lasing and cooling of a low-frequency oscillator. *New Journal of Physics*, 10:095018, 2008.

[285] K. Jaehne, K. Hammerer, and M. Wallquist. Ground-state cooling of a nanomechanical resonator via a Cooper-pair box qubit. *New Journal of Physics*, 10:095019, 2008.

[286] I. Wilson-Rae, N. Nooshi, W. Zwerger, T. J. Kippenberg: *Phys. Rev. Lett.* **99** (2007) 093901

[287] R. Riviere, S. Deleglise, S. Weis, E. Gavartin, O. Arcizet, A. Schliesser, and T. J. Kippenberg: *Phys. Rev. A* **83** (2011) 063835

[288] T. Rocheleau, T. Ndukum, C. Macklin, J. B Hertzberg, A. A Clerk, K. C Schwab: *Nature* **463** (2010) 72

[289] J. D. Teufel, T. Donner, D. Li, J. W. Harlow, M. S. Allman, K. Cicak, A. J. Sirois, J. D. Whittaker, K. W. Lehnert, R. W. Simmonds: *Nature* **475** (2011) 359

[290] C. W. Gardiner and P. Zoller: *Quantum Noise* (Springer Berlin, 2010)

[291] D.F.Walls, G.J. Milburn: *Quantum Optics* (Springer Berlin 2008)

[292] D. Bozyigit, C. Lang, L. Steffen, J. M. Fink, M. Baur, R. Bianchetti, P. J. Leek, S. Filipp, M. P. da Silva, A. Blais, A. Wallraff *arxiv:*1002.3738 (2010)

[293] M. J. Woolley, A. C. Doherty, G. J. Milburn, K. C. Schwab: *Phys. Rev. A* **78** (2008) 062303

[294] M. D. Eisaman, J. Fan, A. Migdall, and S. V. Polyakov: *Rev.. Sci. Instr.* **82** (2011) 071101

[295] C Eichler, D Bozyigit, C Lang, L Steffen, J Fink, A Wallraff: *Phys. Rev. Letts.* **106** (2011) 220503

[296] M. Hofheinz, H. Wang, M. Ansmann, R. C. Bialczak, E. Lucero, M. Neeley, A. D. O'Connell, D. Sank, J. Wenner, J. M. Martinis, A. N. Cleland: *Nature* **459** (2009) 546

[297] G J Milburn: *Eur. Phys. J. Special Topics* **159** (2008) 113

[298] U. Akram, N Kiesel, M Aspelmeyer, G J Milburn: *New J. Physics* **12** (2010) 083030

[299] H. J. Carmichael: *Phys. Rev. Lett.* **70** (1993) 2273

[300] C. W. Gardiner—: *Phys. Rev. Lett.* **70** (1993) 2269

[301] H. P. Specht, J. Bochmann, M. Mücke, B. Weber, E. Figueroa, D. L. Moehring, G. Rempe: *Nature Photonics* **3** (2009) 469

[302] M. Born. Zur quantenmechanik der stoβvorgänge. *Zeitschrift für Physik*, 37:863–867, 1926.

[303] J. von Neumann. *Matematische Grundlagen der Quantenmechanik*. Verlag Julius Springer, Berlin, 1932 (reprinted as Mathematical Foundations of Quantum Mechanics, Princeton University Press, Princeton, 1983).

[304] V. B. Braginsky and F. Ya. Khalilli. *Quantum Measurement*. Cambridge University Press, Cambridge, 1992.

[305] C. M. Caves and G. J. Milburn. Quantum-mechanical model for continuous position measurements. *Physical Review A*, 36:5543, 1987.

[306] K. Krauss. *States, Effects and Operations: Fundamental Notions of Quantum Theory*. Springer-Verlag, Berlin, 1983.

[307] A. Barchielli, L. Lanz, and G. M. Prosperi. A model for the macroscopic description and continual observations in quantum mechanics. *Nuovo Cimento B*, 72:79, 1982.

[308] C. M. Caves. Quantum mechanics of measurements distributed in time. II. Connections among formulations. *Physical Review D*, 35:1815, 1987.

[309] W. Heisenberg. Über den anschulichen Inhalt der quantentheoretischen Kinematik und Mechanik. *Zeitschrift für Physik*, 43:172–198, 1927.

[310] W. Heisenberg. *Die physikalischen Prinzipien der Quantentheorie*. Bibliograph. Inst., Berlin, 1930 (reprinted as Physical Principles of Quantum Theory, Dover, New York, 1949).

[311] H. P. Robertson. The Uncertainty Principle. *Physical Review*, 34:163, 1929.

[312] E. Arthurs and M. S. Goodman. Quantum correlations: A generalized Heisenberg uncertainty relation. *Physical Review Letters*, 60:2447, 1988.

[313] V. B. Braginsky. Classical and quantum restrictions on the detection of weak disturbances of a macroscopic oscillator. *Soviet Physics JETP*, 26:831, 1968.

[314] M. Tsang and C. M. Caves. *Physical Review Letters*, 105:123601, 2010.

[315] K. Jacobs and D. A. Steck. A straightforward introduction to continuous quantum measurement. *Contemporary Physics*, 47:279, 2006.

[316] H. Carmichael. *An Open Systems Approach to Quantum Optics*. Springer, Berlin, 1993.

[317] V. P. Belavkin. *Information, Complexity and Control in Quantum Physics*, page 311. Springer-Verlag, Vienna, 1987.

[318] A. C. Doherty, S. M. Tan, A. S. Parkins, and D. F. Walls. State determination in continuous measurement. *Physical Review A*, 60:2380, 1999.

[319] V. B. Braginsky and Yu. I. Vorontsov. Quantum-mechanical limitations in macroscopic experiments and modern experimental technique. *Soviet Physics Uspekhi*, 17:644, 1975.

[320] V. Braginsky, Y. I. Vorontsov, and K. P. Thorne. Quantum nondemolition measurements. *Science*, 209:547, 1980.

[321] V. B. Braginsky and F. Ya. Khalili. Quantum nondemolition measurements: the route from toys to tools. *Reviews of Modern Physics*, 68:1–11, 1996.

[322] M. D. Levenson, R. M. Shelby, M. Reid, and D. F. Walls. Quantum nondemolition detection of optical quadrature amplitudes. *Physical Review Letters*, 57:2473, 1986.

[323] C. Guerlin, J. Bernu, S. Deliglise, C. Sayrin, S. Gleyzes, S. Kuhr, M. Brune, J. M. Raimond, and S. Haroche. Progressive field-state collapse and quantum non-demolition photon counting. *Nature*, 448:889–893, 2007.

[324] V. B. Braginsky, Yu. I. Vorontsov, and F. Ya. Khalili. Quantum singularities of a ponderomotive meter of electromagnetic energy. *Soviet Physics JETP*, 46:705, 1977.

[325] C. M. Caves, K. S. Thorne, R. W. P. Drever, V. D. Sandberg, and M. Zimmermann. On the measurement of a weak classical force coupled to a quantum-mechanical oscillator. I. Issues of principle. *Reviews of Modern Physics*, 52:341–392, 1980.

[326] K. S. Thorne, R. W. P. Drever, C. M. Caves, M. Zimmermann, and V. D. Sandberg. *Physical Review Letters*, 40:667–671, 1978.

[327] C. M. Caves. Quantum limits on noise in linear amplifiers. *Physical Review D*, 26:1817–1839, 1982.

[328] A. A. Clerk. Quantum-limited position detection and amplification: a linear response perspective. *Physical Review B*, 70:245306, 2004.

[329] A. A. Clerk, S. M. Girvin, and A. D. Stone. Quantum-limited measurement and information in mescoscopic detectors. *Physical Review B*, 67:165324, 2003.

[330] H M Wiseman, G.J.Milburn: *Quantum Measurement and Control* (Cambridge University Press, 2010)

[331] M. P. da Silva, D. Bozyigit, A. Wallraff, A. Blais: *Phys. Rev. A* **82** (2010) 043804 (2010).

[332] B. Abdo, F. Schackert, M. Hatridge, C.Rigetti, and M. Devoret: *Appl. Phys. Lett.* **99** (2011) 162506

[333] M. A. Castellanos-Beltran and K. W. Lehnert: *Appl. Phys. Lett.* **91** (2007) 083509

[334] J. L. Arlett, J. R. Maloney, B. Gudlewski, M. Muluneh, and M. L. Roukes: *Nano Letters* **6** (2006) 1000

[335] D. Rugar, R. Budakian, H. J. Mamin, B. Chui: *Nature* **430** (2004) 6997 (2004).

[336] J. D Teufel, T Donner, M. A Castellanos-Beltran, J. W Harlow, K. W Lehnert: *Nature Nanotechnology* **4** (2009) 820

[337] N. Yazdi, F. Ayazi, K. Najafi: *Proceedings of the IEEE* **86** (1998) 1640

[338] S. Boixo, S. T. Flammia, C. M. Caves, J. M. Geremia: *Phys. Rev. Lett.* **98** (2007) 090401

[339] C. W. Helstrom: *Quantum Detection and Estimation Theory* (Academic Press, 1976)

[340] V. Giovannetti, S. Lloyd, L. Maccone: *Phys. Rev. Lett.* **96** (2006) 010401

[341] V. Giovannetti, S. Lloyd, L. Maccone: *Science* **306** (2004) 1330

[342] M.J.Woolley, G J Milburn, C.M.Caves: *New J. Physics* **10** (2008) 12501

[343] M. Kitagawa, Y. Yamamoto: *Phys. Rev. A* **34** (1986) 3974

[344] S. Boixo, A. Datta, S. T. Flammia, A. Shaji, E. Bagan, C. M. Caves: *Phys. Rev. A* **77** (2008) 012317

[345] A. Gangat, G. J. Milburn: *New J.Phys.* **13** (2011) 043024

[346] W.H. Zurek: *Phys. Rev. D* **24** (1981) 1516

[347] J F Rhoads, S W Shaw, K L Turner: *Journal of Dynamic Systems, Measurement, and Control* **132** (2010) 034001

[348] N. Kacem, S. Hentz, D. Pinto, B. Reig and V. Nguyen: *Nanotechnology* **20** (2009) 275501

[349] I. Kozinsky, H. W. Ch. Postma, O. Kogan, A. Husain, M. L. Roukes: *Phys. Rev. Lett.* **99** (2007) 207201

[350] P. D. Drummond D. F. Walls: *J. Phys. A* **13** (1980) 725

[351] E. Babourina-Brooks, A Doherty and G J Milburn: *New J. Physics* **10** (2008) 105020

[352] C. A. Holmes, C. P. Meaney, G. J. Milburn, arXiv:1105.2086 (2011).

[353] F. Marquardt, J. G. E. Harris, S. M. Girvin, Phys. Rev. Lett., **96**, 103901, (2006).

[354] G. Heinrich, M. Ludwig, J. Qian, B. Kubala, F. Marquardt, arXiv:1007.4819, (2010).

[355] F. Mueller, S. Heugel, L. J. Wang, Phys. Rev. A,**77** 031802 (2008).

Gerard Milburn obtained a PhD in theoretical Physics from the University of Waikato in 1982 for work on squeezed states of light and quantum nondemolition measurements. He is currently an Australian Research Council Federation Fellow at the University of Queensland and Director of the Australian Research Council Centre of Excellence in Engineered Quantum Systems. Gerard Milburn is a Fellow of the Australian Academy of Science and The American Physical Society. He has worked in the fields of quantum optics, quantum measurement and stochastic processes, atom optics, quantum chaos, mesoscopic electronics, quantum information and quantum computation, and most recently in quantum nanomechanics and superconducting circuit QED. He has published four books. Together with Dan Walls he published one of the first texts on Quantum Optics (Springer 1994), recently updated with a new edition (Springer, 2008), and two non technical books on quantum technology and quantum computing (Schroedinger's Machines, Allen and Unwin, 1996; The Feynman Processor, Allen and Unwin 1998). He has just completed a book on quantum measurement and control with Howard Wiseman, Cambridge University Press, December, 2009.

Matthew Woolley received his PhD in physics from the University of Queensland in 2011. He is currently a postdoctoral research associate at McGill University and the Universite de Sherbrooke. His research interests are in quantum optomechanics, quantum electromechanics and superconducting circuits.